Identification of Putative Target Genes of miR-106b, miR-93, miR-25 in Medulloblastoma

NG, Hin Yi Winnie

A Thesis Submitted in Partial Fulfillment of

the Requirements for the Degree of

Master of Philosophy

in

Anatomical and Cellular Pathology

The Chinese University of Hong Kong

April 2011

ACKNOWLEDGEMENTS

First and foremost, I would like to express my sincere thanks to my supervisor, Dr. K. M. Lau for accepting me into his laboratory. In addition to his patient guidance and directions for my project, I truly thank for his understanding and constant trust through these past years.

I wish to express my gratitude to Prof. H. K. Ng for his professional supervision, sharing of vast knowledge, and giving me the opportunities to participate in departmental events & conferences through which I have gained a lot of invaluable experience.

I also have to thank the folks in 5/F Cancer Centre, and especially my teammates for their friendship. I will never forget the cheers we have shared.

Last but not least, I would like to express my deepest appreciation to my family for their endless love and support, all of which I will treasure forever.

LIST OF TABLES

Table 1.1 Aberrant miRNA expression in MB 14

Table 3.1 Primers used in real-time PCR amplification for potential target genes 39

Table 3.2 Cloning constructs of the potential target genes 40

Table 3.3 Primers sequences and specific annealing temperature for 3'UTR cloning 41

Table 3.4 Primers for site-directed mutagenesis 46

Table 3.5 Number of predicted target genes from different prediction programs 54

Table 3.6 Common predicted targets among the seven prediction programs 55

Table 4.1 Components of "1st-round"-reverse transcription buffer 81

Table 4.2 Components of "2nd-round"-reverse transcription buffer 83

Table 4.3 Sequences of adaptors and primers 85

Table 4.4 Reagents for PCR amplification 87

Table 4.5 PCR amplification condition 87

Table 4.6 Primers used in real-time PCR amplification for ZNF793 & CLN8 ... 92

Table 4.7 PCR primers for 3'UTR cloning 93

Table 4.8 Primers for site-directed mutagenesis of CLN8 94

Table 4.9 Statistical summary of the cDNA library 97

Table 4.10 Blast result for potential sequences 97

LIST OF FIGURES

Figure 3.1 Schematic flowchart for the computational approach 26

Figure 3.2 Taqman stemloop qRT-PCR analyses of miRNA expression levels in MB cell lines and normal cerebellum 50

Figure 3.3 Transfection efficiency using Lipofectamine 2000 51

Figure 3.4 Inhibitory effect of anti-miRNAs 53

Figure 3.5 Quantitative real-time PCR for candidate genes 56

Figure 3.6 Changes in target gene expression in DAOY 58

Figure 3.7 Relative luciferase activity of pMIR-ZNFX1 and pMIR-DNAJB12 ..60

Figure 3.8 Luciferase constructs with mutations at microRNA target sites 64

Figure 3.9 Site-directed mutagenesis of 3'UTR 65

Figure 3.10 Western Blotting of ZNFX1 66

Figure 4.1 Schematic diagram of the biochemical method 78

Figure 4.2 Preparation of cell extracts 80

Figure 4.3 Reverse transcription using endogenous miRNAs as primers 81

Figure 4.4 Second-strand cDNA synthesis 83

Figure 4.5 Restriction enzyme digestion 84

Figure 4.6 Ligation of adaptor 85

Figure 4.7 PCR amplification with biotin-labelled miRNA primers 87

Figure 4.8 Final round of PCR amplification 89

Figure 4.9 Cloning potential sequence into the pCR2.1 vector 90

Figure 4.10 Final construct of a cDNA clone 96

Figure 4.11 Blast result for ZNF793 and CLN8 99

Figure 4.12 Quantitative real-time PCR for candidate genes 101

Figure 4.13 Changes in mRNA level upon treatment with miRNA inhibitors 102

Figure 4.14 Relative luciferase activity of ZNF793-pMIR and CLN8-pMIR 103

Figure 4.15 Mutation construct for CLN8-pMIR 106
Figure 4.16 Site-directed mutagenesis of CLN8 3'UTR 106
Figure 5.1 Effects of inhibition of miR-106b-25 cluster on cell growth 120
Figure 5.2 Cell cycle progression profile 121
Figure 5.3 IC_{50} for cisplatin in DAOY 123
Figure 5.4 Cell growth after treatment with cisplatin 124
Figure 5.5 Effect of inhibition of miR-106b-25 cluster on cell proliferation 125
Figure 5.6 Wound healing assays 127
Figure 5.7 Efficiency of over-expression of miR-106b mimic on cell growth ... 129
Figure 5.8 Effects of miR-106b inhibition or over-expression on cell growth ... 130

ABSTRACT

Medulloblastoma (MB) is a brain malignancy with high incidence in childhood. It is often classified by its morphology and immunohistochemical features; however, the pathogenesis of MB still remains elusive. In the past decades, more emphasis has been put onto elucidating the molecular aspect contributing to the pathogenesis of MB, and in which microRNAs (miRNAs) are found to be key regulators involved. Therefore, investigating the relationships between microRNA and MB lay the basic groundwork for understanding tumour biology. MicroRNA expression analysis can lead to identification of candidate miRNAs that may play important roles in medulloblastoma carcinogenesis. It is also important to identify target genes that are associated with these known aberrant miRNA expression. Currently there are several approaches in identifying potential targets of miRNAs, which include a variety of bioinformatic prediction programs, as well as experimental techniques (Dalmay 2008). Bioinformatic prediction programs predict miRNA targets mainly based on the degree of complementarity between the miRNAs and their targets; as a consequence, they often result in extensive lists of putative target genes that include many false positives. On the other hand, experimental techniques usually involve series of complicated experimental procedures, and are time consuming. Therefore, identification of target genes still remains as a challenging task. My project focuses on the identification of

putative target genes that are associated with the aberrant expression of miR-106b-25 cluster in medulloblastoma. The project mainly consists of three parts: 1) target prediction of miR-106b-25 cluster using bioinformatics; 2) miR-106b-25 cluster target identification using experimental techniques; 3) functional studies on miR-106b-25 cluster in MB.

1) Target Prediction Using Bioinformatics:

In an attempt to narrow down the list of potential downstream targets for miR-106b-25 cluster, we have combined the prediction results from seven bioinformatic programs and have selected out only common genes that appeared in all of the seven prediction programs. This approach allowed us to narrow down to ZNFX1 as a candidate gene for miR-106b and miR-93. Validation of ZNFX1 was confirmed using luciferase reporter assay. Upon inhibition of miR-106b, and miR-93, significant decrease in luciferase activity was observed. Site-direct mutagenesis on the conserved recognition site at 484^{th}-491^{st} on the 3'UTR of ZNFX1 further confirmed specific interactions between miR-106b & miR-93 and ZNFX1. Collectively, these data suggest that ZNFX1 is a potential target gene for miR-106b and miR-93.

2) Experimental Technique in Identifying Target Genes:

Adopting the experimental approach of using miRNAs as endogenous primers in series of reverse transcription reactions, we hope to create a library of clones from

which we could isolate individual clones that possess partial sequence of potential target genes for miR-106b. By screening 96 clones from our library, we have identified ZNF793 and CLN8 as potential target genes for miR-106b. Through luciferase reporter assay and subsequent site-direct mutagenesis at the deduced miR-106b recognition site, we have successfully confirmed CLN8 as a target gene regulated by miR-106b.

3) Functional Studies on miR-106b-25 Cluster in Medulloblastoma:

MicroRNAs have been implicated in biological processes, including cell development, cell proliferation, apoptosis, and tumorigenesis. MTT assay revealed that silencing the activity of the miR-106b-25 cluster with specific inhibitors resulted in a decrease in cell growth in MB cell lines (ONS-76 & DAOY). However, there was no shift in cell cycle distribution observed. Upon inhibition of the miR-106b-25 cluster, decrease in cell proliferation and migration were observed in DAOY. These data suggest that the miR-106b-25 cluster may be involved in cellular pathways that are responsible for the tumorigenesis of MB.

In conclusion, using a combination of prediction programs and experimental techniques, we were able to identify potential target genes for the miR-106b-25 cluster. The deregulation of miRNA expression may contribute to the development of MB through modulation of their identified target genes.

中文摘要

髓母細胞瘤（MB）是一種常見於兒童的腦惡性腫瘤。它往往是按它們的形態和免疫組織化學特徵而分類，但其發病機制仍有待確定。而在過去的幾十年，MB的分子發病機制倍受重視。而其中小分子RNA(microRNA)被發現為癌症發病機制的主要調節子，因此，研究小分子RNA與髓母細胞瘤之間的關係可為了解MB腫瘤生物學奠定基礎。雖然小分子RNA的表達分析有助發現髓母細胞瘤的形成，但去確定與已知的小分子RNA異常表達有關的目標基因亦同樣重要。目前，有幾種方法去確定小分子RNA的潛在目標基因，其中包括各種生物信息學預測程式，與實制實驗。由於小分子RNA與目標基因是不完全互補，生物信息學預測程式往往列出廣泛的假定靶基因，其中包括許多偽陽性。另一方面，實制實驗亦涉及一系列複雜的實驗程序。為此，這個項目的重點是要識別出在髓母細胞瘤中已發現有異常表達的小分子 RNA(miR-106b-25 集群)的潛在目標基因 。此項目主要分為三部分：1）利用生物信息學去預測miR-106b-25集群的目標基因;2)應用實驗技術去識別miR-106b-25集群的目標基因;3)研究miR-106b-25集群在髓母細胞瘤的功能性。

1） 利用生物信息學去預測目標基因：

最近的研究指出，哺乳動物的小分子 RNA 每個可平均有 100-200 預測目標。為了縮窄範圍，我們結合了七個不同的生物信息學預測程式的結果，並篩選出在七個程式都共同出現的基因。最後我們篩選出 ZNFX1 為 miR-106b 和 miR-93 的候

選基因。在抑制 miR-106b 和 miR-93 後，在熒光素酶檢測中，ZNFX1 被驗證為 miR-106b 和 miR-93 的目標基因。在特定保存識別序列進行定點突變更確定了 miR-106b 和 miR-93 與 ZNFX1 3'UTR 的相互作用。這表明 ZNFX1 是 miR-106b 和 miR-93 的目標基因。

2） 應用實驗技術識別目標基因：

在採用內源性的小分子 RNA 作為引子而製作出的大量克隆中，我們希望能分出擁有 miR-106b 目標基因的克隆。通過篩選，我們發現 ZNF793 和 CLN8 為 miR-106b 的潛在靶基因。通過熒光素酶和定點突變測試後，我們已經成功證實 CLN8 作為 miR-106b 的目標基因。

3）miR-106b-25集群在髓母細胞瘤的功能性研究：

小分子RNA被證明在生物學過程中，包括細胞發育，細胞增殖，凋亡和腫瘤形成有重大的關係。MTT檢測顯示，在miR-106b-25集群被抑制後，MB細胞的生長減少。不過，細胞週期分佈和非固著依賴性細胞生長都不受影響。另外，細胞增生和細胞移動都輕微下降。這些數據反映了 miR-106b-25 集群是參與 MB 腫瘤形成的主要機制。

總括而言，結合預測程式和應用實驗技術，我們能夠識別出miR-106b-25集群的目標基因。通過小分子RNA的異常表達而導致目標基因的管制失調可引致MB腫瘤的形成。

TABLE OF CONTENTS

Acknowledgements ..... **ii**

List of Tables ..... **iii**

List of Figures ..... **iv**

Abstract in English ..... **vi**

Abstract in Chinese ..... **ix**

Table of Contents ..... **xi**

CHAPTER 1: INTRODUCTION **1**

1.1 Medulloblastoma (MB) **1**

1.1.1 Definition of Medulloblastoma 1

1.1.2 Pathological Classification 2

1.1.3 Current Treatment 3

1.1.4 Molecular Pathology 4

1.1.5 Molecular Classification of MB 7

1.2 MicroRNAs (miRNAs) **9**

1.2.1 Biogenesis 9

1.2.2 Functions 10

1.2.3 MicroRNAs & Cancers 10

1.2.4 Aberrant Expressions of MicroRNAs in Medulloblastoma 12

1.2.5 MiR-106b-25 Cluster in MB 13

1.2.6 miR-106b-25 Cluster in Regulating Target Genes 15

1.2.7 Application of Regulatory miRNAs 16

1.3 Target Gene Identification **18**

1.3.1 Recent Molecular Advances in Target Gene Identification 18

1.3.2 Importance of Target Gene Identification 19

CHAPTER 2: AIMS OF STUDY **21**

CHAPTER 3: COMPUTATIONAL TARGET PREDICTION **23**

3.1 Introduction- Computational Approach **23**

3.2 Methods **27**

3.2.1 Prediction Algorithms 27

3.2.1.1 EIMMo2 27

3.2.1.2 miRDB 27

3.2.1.3 miR-Tar-miRanda 28

3.2.1.4 miR-Tar-RNAhybrid 28

3.2.1.5 Diana-microT 29

3.2.1.6 Pic-Tar 29

3.2.1.7 TargetScan 4.2 29

3.2.2 Cell Culture 30

3.2.2.1 Cell Lines 30

3.2.2.2 Cell Counts 31

3.2.3 Transfections 31

3.2.3.1 Transfection of MicroRNA Inhibitors 31

3.2.3.1.1 Transfection Efficiency of Lipofectamine2000 32

3.2.3.1.2 Transfection of MicroRNA Inhibitors for Real-time PCR 32

3.2.3.1.3 Transfection of MicroRNA Inhibitors for Western Blotting 33

3.2.3.2 Co-transfection of Plasmid and MicroRNA Inhibitors 33

3.2.3.2.1 Blocking Efficiency of MicroRNA Inhibitors 33

3.2.3.2.2 Co-transfection of Target Gene Expression Vector and MicroRNA Inhibitors 34

3.2.4 Real-time PCR Amplification 35

3.2.4.1 Total RNA Extraction from Cell Lines 35

3.2.4.2 Stemloop miRNA Taqman qRT-PCR Analysis 36
3.2.4.3 Reverse Transcription 37
3.2.4.4 Real-time PCR Target Gene Expression 38
3.2.5 Cloning of Potential Target Genes into pMIR Luciferase Expression Vector 39
3.2.5.1 High-Fidelity PCR Amplification of 3'UTRs 41
3.2.5.2 PCR Purification of Amplified PCR Product 42
3.2.5.3 Restriction Enzyme Digestions 42
3.2.5.4 Ligation of 3'UTR to Expression Vector 43
3.2.5.5 Transformation 43
3.2.5.6 Preparation of the Cloned Plasmid 43
3.2.5.7 Sequencing of the Cloned Plasmid 44
3.2.6 Site-directed Mutagenesis 45
3.2.7 Dual-Luciferase Assay 47
3.2.8 Western Blot Analysis 47

3.3 Results 49
3.3.1 Expression Levels of miR-106b-25 Cluster in MB Cell Lines ... 49
3.3.2 Evaluation of Transfection Efficiency Using Lipofetamine200051
3.3.3 Blocking Efficiency of MicroRNA Inhibitors 52
3.3.4 Target Prediction List 53
3.3.5 Recognition Sites of Potential Targets 55
3.3.6 Expression Levels of ZNFX1 in MB Cell Lines 56
3.3.7 Transcriptional Regulation of ZNFX1 and DNAJB12 57
3.3.8 Verification of Potential Target Genes 59
3.3.9 Identification of Critical Target Sites 61
3.3.10 Effects of Anti-microRNA Inhibitors on ZNFX1 Protein Levels 66

3.4 Discussion 67

CHAPTER 4: EXPERIMENTAL APPROACH IN INDENTIFYING POTENTIAL TARGETS 77

4.1 Introduction- Experimental Approach 74

4.2 Methods 79

4.2.1 Isolation of cDNA Clone Library 79

4.2.1.1 Preparation of Cytoplasmic Extracts 79

4.2.1.2 Reverse Transcription Using Endogenous miRNA as Primers 81

4.2.1.3 Collection of Polynucleotides 82

4.2.1.4 Synthesis of Second-strand cDNAs 82

4.2.1.5 PCR Purification of Double-stranded cDNAs 83

4.2.1.6 Restriction Endonuclease Digestion 84

4.2.1.7 Ligation to Adaptor 85

4.2.1.8 PCR Amplification with Biotin-labelled miRNA PCR Primers 86

4.2.1.9 Capture of Biotin-labelled PCR Fragments 88

4.2.1.10 Introducing NotI Recognition Sequences 88

4.2.1.11 Cloning into the pCR2.1 Vector 89

4.2.1.12 Ligation of the cDNA Fragments and the pCR2.1 Vector... 90

4.2.1.13 Transformation 90

4.2.1.14 Preparation of Purified Plasmids 91

4.2.1.15 Sequencing Analysis of the cDNA Clone Library 91

4.2.2 Real-time PCR Target Gene Expression in Cell Lines 92

4.2.3 Real-time PCR Target Gene Expression Upon Inhibition of miR-106b 92

4.2.4 Cloning of Potential Target Genes into pMIR Luciferase Expression Vector 93

4.2.5 Site-directed Mutagenesis 94

4.2.6 Luciferase Reporter Assay 94

4.3 Results **95**

4.3.1 Sequencing Analysis of the cDNA Clone Library 95

4.3.2 Expression Levels of Candidate Genes in MB Cell Lines 100

4.3.3 Effects of Anti-miR-106b Inhibitors on 3'UTR of Target Genes 101

4.3.4 Verification of Candidate Genes 103

4.3.5 Verification of Target Sites with Site-directed Mutagenesis 104

4.4 Discussion **107**

CHAPTER 5: FUNCTIONAL ASSAYS **111**

5.1 Introduction- Functional Investigation of miR-106b-25 Cluster **111**

5.2 Methods **113**

5.2.1 Cell Culture 113

5.2.2 Over-expression of miR-106b Mimic 113

5.2.3 MTT Assay 114

5.2.4 IC_{50} of Cisplatin 115

5.2.5 MTT Assay with Cisplatin Treatment 115

5.2.6 Cell Cycle 116

5.2.7 BrdU Cell Proliferation Assay 117

5.2.8 Wound Healing Assay 117

5.3 Results **119**

5.3.1 Effects of Inhibition of miR-106b-25 Cluster on Cell Growth . 119

5.3.2 Cell Cycle Distribution Analysis 121

5.3.3 Sensitivity to Cisplatin 123

5.3.4 Cell Proliferation Assay 124

5.3.5 Cell Motility 126

5.3.6 Efficiency of Over-expression Using miR-106b Mimic 129
5.3.7 Effects of miR-106b on Cell Growth 130

5.4 Discussion 131

CHAPTER 6: CONCLUSION 135

REFERENCE 137

CHAPTER 1: INTRODUCTION

1.1 Medulloblastoma (MB)

1.1.1 Definition of Medulloblastoma

Medulloblastoma is the most common malignant brain tumour of childhood (Lee et al. 2001). It accounts for about 25% of all pediatric brain tumours, and there are approximately 500 cases diagnosed in the US each year (Hjalmars et al. 1999). It has a slightly higher incidence in boys than girls (Polkinghorn and Tarbell 2007). Patients often present with symptoms such as headaches, morning vomiting, and ataxia; MRI imaging typically reveals a well-defined enhancing mass locating at the posterior fossa (Polkinghorn and Tarbell 2007). The tumour usually arises from midline vermis and may invade into the fourth ventricle or through the floor of the ventricle to the brainstem (Halperin 1986). Medulloblastoma has the propensity to metastasize and disseminate through the subarachnoid space with approximately 30% of patients diagnosed with cerebrospinal fluid (CSF) metastasis (Fouladi et al. 1999). Patients with medulloblastoma are generally stratified into two risk categories, "standard-risk" and "high-risk". Stratification is mainly based on three criteria: 1) age at diagnosis; 2) degree of surgical resection; and 3) disease spread (Dhall 2009). Long-term survival

rate reaches approximately 85% for standard-risk patients who are above the age of 3, and for high-risk patients, the survival rate is lowered to approximately 70% (Dhall 2009). However, patients who are below the age of 3, particularly infants, are at significantly higher risk for suffering severe side-effects from treatments (Dhall 2009).

1.1.2 Pathological Classification

According to the WHO classification, medulloblastoma is classified as one of the five embryonal tumours (Polkinghorn and Tarbell 2007). For years, classification based on morphological features has caused great controversy due to the fact that medulloblastoma is histogenetically indistinguishable from other central nervous system (CNS) embryonal tumors; as a consequence, they were collectively called peripheral neuroectodermal tumours (PNETs) (Polkinghorn and Tarbell 2007). Despite the controversy, morphological classification forms the foundation on which current pathological diagnosis still rest (Huse and Holland 2010). On the basis of their histopathological features, medulloblastomas are separated into the classic tumours and four variants, which include medulloblastoma with extensive nodularity (MBEN), desmoplastic/nodular (D/N), anaplastic, and large cell medulloblastoma (Ellison 2010). This scheme of classification proves to have clinical utility. For instance, MBENs and D/N medulloblastomas have better outcome in infants than classic tumours, while

anaplastic and large cell medulloblastomas are more aggressive (Ellison 2010). As there are increasing recognitions of medulloblastoma as a heterogeneous disease, researchers are shifting their approach to develop a classification system based on molecular classification. Many reports have demonstrated that medulloblastoma has molecular phenotypes distinct from other brain tumours, such as primitive neuroectodermal tumours, atypical teratoid/rhabdoid tumours, and malignant gliomas (Pomeroy et al. 2002).

1.1.3 Current Treatment

Medulloblastoma was once thought a fatal disease; it was only following the introduction of intensive craniospinal irradiation in 1969 that the 5-year survival rate improved to approximately 32% (Bloom et al. 1969). Nowadays, treatment usually involves a combination of surgery, radiation therapy, and chemotherapy depending on the risk stratification of individual patients (Polkinghorn and Tarbell 2007). As a result, today approximately 60% of patients with medulloblastomas are free of progressive disease 5 years after diagnosis (Lee et al. 2001). Relatively speaking, compared to malignant glioma, radiation and chemotherapy are generally more successful in combating medulloblastoma; however, these conventional treatment are often accompanied with long-term side effects (Huse and Holland 2010). Of those

who survived, nearly all patients suffer side effects from radiation to different extent, which include cognitive impairment, psychiatric disorders, endocrine dysfunction, and skeletal growth retardation (Polkinghorn and Tarbell 2007). Despite the seemingly favourable survival rates, the adverse therapeutic effects from treatment still remain a serious concern. There is no doubt that clinical and morphological classification has laid the groundwork for standard treatment regimens, yet risk stratification for treatment merely based on clinical parameters proves to have shortcomings. Perhaps the new challenge lies towards compiling a "tailor-made" treatment for individual patients as influential factors such as the aggressiveness of the tumour and the sensitivity to treatment varies from different individuals (Ellison 2010). To better improve the treatment outcome and ameliorating adverse effects caused by standard treatments, more emphasis is needed to put onto the molecular pathogenesis of medulloblastoma. In other words, the ultimate goal is to provide molecular definition to medulloblastoma in addition to morphological classification.

1.1.4 Molecular Pathology

To improve upon the current clinical risk stratification and aiming at minimizing side effects from treatments, scientists have worked on unraveling the molecular basis of medulloblastoma in order to better understand the pathogenesis of

this tumour. In fact, an extensive literature now exists on the molecular biology of medulloblastoma. Aberrant activation of several cell-signaling pathways has been implicated in MB development: 1) the Sonic hedgehog cascade (Shh), accounting for approximately 25% of medulloblastoma, 2) the Wingless signaling pathway (Wnt), accounting for approximately 15% of the tumours (Polkinghorn and Tarbell 2007), and 3) ERBB signaling (Gilbertson 2004).

Shh signaling has been found to have critical roles in the development of the CNS such as driving the proliferation in the granule neuron precursors of the cerebellum (Huse and Holland 2010). As various murine models have demonstrated that medulloblastoma tumours are resulted from perturbation of granule cells (Marino 2005), granule cell progenitors (GCPs) remain as the main focus for the source of medulloblastomas. During normal development, granule cells undergo massive expansion in the external granule layer shortly after birth (Polkinghorn and Tarbell 2007); however, dysregulated granule cell development is observed to be associated with overactive SHH signaling in GCPs. PTCH1, SMO, and SUFU mutations together resulted in the aberrant activation of the Shh pathway, thereby re-initiate proliferation of the GCPs (Polkinghorn and Tarbell 2007). These expanding cells would exit the cell cycle, migrate into the inner zone of the external granule layer, and eventually differentiate in the internal granule layer forming the tumour mass

(Polkinghorn and Tarbell 2007).

Another mechanism by which Shh signaling contributes to medulloblastoma formation is via the upregulation of MYCN expression (Kenney et al. 2003). Upregulation of MYCN activates D-type cyclins, while represses the expression of other cyclin-dependent kinase inhibitors, and thus disrupting cell-cycle control (Knoepfler and Kenney 2006). Degradation of MYCN is accomplished via phosphorylation by glycogen synthase kinase-3 beta (GSK3β); in other words, inhibition of GSK3β results in increased MYCN levels and thus eventually contributes to the formation of medulloblastoma.

Other pathways involved in medulloblastoma pathogenesis include the Wnt pathway (Huse and Holland 2010). It is associated with defects in APC, a tumor suppressor gene which keeps the Wnt signaling pathway in check (Pfister et al. 2010). In fact, activating point mutations in CTNNB1 which encodes for β-catenin result in preventing GSK3-β to phosphorylate β-catenin (Pfister et al. 2010). As a result, upon such activation, β-catenin accumulates in the nucleus and activates series of transcription factors, and subsequent downstream targets including MYC and cyclin D1 (Polkinghorn and Tarbell 2007).

Members of ERBB can trigger the cell-signal pathways of mitogen-activated protein kinase (MAPK), AKT, and STAT, which in turns regulate cell proliferation,

apoptosis, migration, and differentiation (Gilbertson 2004). In fact, ERBB2 might have a role in MB formation, in a study with more than 150 pediatric MB patients, ERBB2 protein expression was shown in 80% of the tumour samples, whereas healthy cells in the cerebellum do not express ERBB2 at any stage during development (Gilbertson 2004). High expression of ERBB2 is likely contributing to tumor development by interacting through the complex network of homodimers and heterodimers, activating ERK1/2 and AKT signals, as well as upregulating prometastic genes when overexpressed in MB (Gilbertson 2004). Taken together, aberrant molecular alterations in critical pathways (either through excess signaling or absence of appropriate inhibitory signals) play an important part in medulloblastoma tumorigenesis. These tremendous progresses in the field of molecular biology of medulloblastoma are of great help in forming the basis of molecular risk stratification in the near future.

1.1.5 Molecular Classification of MB

As mention previously, better molecular understanding may benefit clinical classification and prognostication of MB; in fact, there are increasing number of studies that use gene expression data to identify distinct molecular subgroups in MB (Thompson et al. 2006). Based on their transcriptome, WNT- and SHH-driven MB

was demonstrated to be comprised of two very distinct biological subgroups with distinctive expression signatures (Pfister et al. 2010). More specifically, CTNNB1 mutation and monosomy 6 were found to be associated with the WNT-driven tumours, while PTCH/SUFU mutation, and 9q deletion were found to be associated with the SHH-driven tumours (Pfister et al. 2010). Five molecular subtypes were identified by Kool et al. using mRNA expression data of MB: the two most distinct subtypes (WNT or SHH signaling), as well as Kool type C, D, and E (Kool et al. 2008). Kool type C and D tumours are characterized by elevated expression of neuronal differentiation genes, while Kool type D and E tumours are associated with photoreceptor genes expression (Kool et al. 2008). Others such as Northcott et al. had also analyzed gene expression profiles of MB and identified same molecular subgroups, with the exception that Kool type C and D tumours were now categorized as one subgroup called Northcott group D (Northcott et al. 2010). Furthermore, Northcott et al. had identified specific protein markers for each subgroup: CTNNB1 for WNT tumours, GLI1 for SHH tumours, NPR3 for Northcott group C tumours, and KCNA1 for group D tumours, all of these can be used for immunohistochemical assay for high accuracy classification (Northcott et al. 2010). Together, these findings can be linked to clinical follow-up data for prognostication of MB, and be used for developing targeted therapies for each subtype separately.

1.2 MicroRNAs (miRNAs)

1.2.1 Biogenesis

MicroRNAs are a class of single-stranded RNA molecules that range from 17 to 27 nucleotides in length (Visone and Croce 2009). Biogenesis of microRNAs begins in the nucleus where transcription of the primary transcript takes place. The primary microRNA transcripts (pri-miRNAs) are transcribed from the genome by RNA polymerase II (Visone and Croce 2009). Following the transcription, pri-miRNAs fold into a stem-loop structure, and are enzymatically cut by Drosha into smaller fragments that are about 70 nucleotides in length forming the hairpin structure which now called the pre-miRNAs (Visone and Croce 2009). Pre-miRNAs are exported to the cytoplasm by Exportin-5 (Visone and Croce 2009). Subsequently they are cleaved by the Dicer into imperfect double-strand RNAs forming the duplex-designated miRNAs. One of the strands from the duplex is selected to function as a mature microRNA, while the other strand is degraded (Visone and Croce 2009). After series of processing from the primary transcripts and sequential modification steps, the mature microRNAs are incorporated into the RNA-induced silencing complexes (RISC) ready to function as regulators (Orom and Lund 2010).

1.2.2 Functions

MicroRNAs act as gene regulators through incorporating into the RISC, and together as a complex, it binds onto the mRNA sequence of the target genes that are either perfectly or partially complementary to itself (Dalmay 2008). It is suggested that perfect complementarity leads to mRNA degradation, while partial complementarity leads to inhibition of translation (Visone and Croce 2009). Although the degree of homology shared by the microRNA and its targets varies, often a region called the seed region, starting from the 2^{nd} to the 8^{th} nucleotide at the 5' region of the microRNA, shows almost complete complementarity between the two (Dalmay 2008). Not only that microRNAs are found to directly regulate target gene expression by transcriptional degradation or post-translational repression, they are also suggested to be involved in fine-tuning expression of target genes rather than completely switching off their expression (Dalmay 2008).

1.2.3 MicroRNAs & Cancers

Ever since the discovery of human microRNAs, extensive research has focused on revealing their functions and regulations in cancers. Numerous reports have demonstrated the involvement of microRNA-mediated regulation in proliferation,

apoptosis, differentiation and cellular development (Kloosterman and Plasterk 2006). There are several mechanisms as to how microRNA expression can be altered, which include chromosomal abnormalities, epigenetic changes, mutations and polymorphisms (SNPs), and defects in microRNA biogenesis machinery (Visone and Croce 2009). The first evidence of aberrant microRNA expression profile in human cancers was demonstrated in B-cell chronic lymphocytic leukemia (Calin et al. 2002). Chromosomal deletion at the 13q14 locus resulted in the loss or reduction of miR-15 and miR-16 expression, and led to the discovery of genes linked to the disease (Calin et al. 2002). Another example of miRNA and its oncogenic roles is the overexpression of miR-155 and its link to several types of lymphomas (Eis et al. 2005). Transgenic mice with overexpression of miR-155 in B cells were found to develop preleukemic lymphoproliferative disease, which eventually progressed to B-cell leukemia (Eis et al. 2005). Subsequent microarray study of the malignant B cells revealed several deregulated protein-coding genes that are identified as potential targets of miR-155, indicating that deregulation of miR-155 could be involved in early events in oncogenesis (Eis et al. 2005). In addition to their oncogenic roles, microRNAs are found to contribute to tumorigenesis by modulating the expression of proteins that control cellular function and cell death decisions (Visone and Croce 2009). For example, the up-regulation of miR-221/222 has been reported to target $p27^{kip}$ and $p57^{kip}$

proteins, which are key regulators binding to Cdk/cyclin complexes responsible for inhibition of the G_1/S phase switch (Visone et al. 2007; Fornari et al. 2008). MicroRNAs are not only found to participate in early events in oncogenesis and intermediate steps in tumorigenesis, they are also found to participate in later steps such as metastases (Visone and Croce 2009). In a recent study, it was found that suppressing miR-21 in metastatic breast cancer cells can significantly reduce the invasiveness and metastatic properties of the cancer cells (Visone and Croce 2009). Collectively, microRNAs are found to be involved in different types of cancers, emerging as important regulatory factors.

1.2.4 Aberrant Expressions of MicroRNAs in Medulloblastoma

As thousands of microRNAs being identified, several reports have shown evidence for a role of microRNA in tumorigenesis of medulloblastoma. It was first reported by Pierson *et al.* that decreased expression of miR-124 was observed in medulloblastoma, and responsible for modulating cell-cycle regulation by targeting CDK6 to slow tumour cell growth (Pierson et al. 2008). Other microRNAs involve in MB tumorigenesis include miR-92, miR-19a, and miR-20, all of which were found to be overexpressed in hedgehog-active medulloblastoma (Turner et al. 2010). These microRNAs are all encoded by the miR-17/92 cluster and their expressions were found

to be associated with a variety of cancers (Turner et al. 2010). The expression of miR-17/92 was most elevated in MB with activated Shh signaling and associated with the elevated c-Myc and n-Myc; in other words, may enhance the growth potential of MB(Turner et al. 2010). Other medulloblastoma-related microRNAs such as miR-31 and miR-153 were found to have direct association between their expression and disease severity (Turner et al. 2010). There are many more examples showing evidence of microRNA being involved in medulloblastoma; altogether, these studies indicate that microRNA-mediated regulations of important cellular pathways are important factors contributing to medulloblastoma pathogenesis.

1.2.5 MiR-106b-25 Cluster in Medulloblastoma

Preliminarily, our team has investigated the involvements of miRNAs in MB by employing miRMAX microarray analysis for quantitatively profiling of 182 miRNAs in MB cell lines (DAOY and D283) and 4 clinical samples, and compared the profiles to age-matched normal cerebellum samples. The data indicated upregulation of 17 miRNAs and downregulation of 9 miRNAs expression in MB (Table 1.1), of which miR-93 had a fold-change of ~6.4, and miR-25 had a fold-change of ~4.6, while a trend of increased level of miR-106b was also found. Hierarchical clustering analysis of these differentially expressed miRNAs demonstrated pattern of association among

these miRNAs (Data not shown). The expression profiles of miR-106b, miR-93, and miR-25 were verified by real-time stem loop PCR assays in an extended panel of MB samples, and results showed strong correlation with the microarray data (Pearson correlation coefficient $R=0.92$, $p<0.03$) (Data not shown). Our preliminary data clearly demonstrated that aberrant expression of miR-106b-25 cluster is found in MB.

Table 1.1 Aberrant miRNA expression in MB

Upregulated miRNAs

Gene symbol	**Normal Cerebellum**	**Medulloblastoma**	**Fold changes**	**Permutation p-value**
Hsa-miR-106a	486.9	5349.8	11.0	0.0022
Hsa-miR-122a	15.4	418.4	27.2	0.0022
Hsa-miR-141	2.9	39.7	13.9	0.0022
Hsa-miR-144	2.3	51.4	22.3	0.0022
Hsa-miR-148a	15.2	113.2	7.4	0.0022
Hsa-miR-155	13.0	288.8	22.3	0.0022
Hsa-miR-17-5p	469.7	5971.5	12.7	0.0022
Hsa-miR-182	12.1	648.5	53.8	0.0022
Hsa-miR-183	3.8	211.1	56.3	0.0022
Hsa-miR-19a	14.3	225.6	15.8	0.0022
Hsa-miR-19b	153.8	1946.6	12.7	0.0022
Hsa-miR-25	561.4	2608.7	4.6	0.0022
Hsa-miR-325	2.7	50.8	18.8	0.0022
Hsa-miR-371	2.4	73.7	30.7	0.0022
Hsa-miR-373	2.0	47.8	23.9	0.0022
Hsa-miR-93	639.3	4105.0	6.4	0.0022
Hsa-miR-96	5.7	73.3	13.0	0.0022

Downregulated miRNAs

Gene symbol	Normal Cerebellum	Medulloblastoma	Fold Changes	Permutation p-value
Hsa-miR-124a	23937.0	2332.6	-10.3	0.0022
Hsa-miR-125a	11262.2	1546.9	-7.3	0.0022
Hsa-miR-128a	5154.7	430.0	-12.0	0.0022
Hsa-miR-128b	2711.4	313.6	-8.6	0.0022
Hsa-miR-29a	6620.3	948.5	-7.0	0.0022
Hsa-miR-31	1216.4	203.7	-6.0	0.0022
Hsa-miR-324-3p	845.9	192.8	-4.4	0.0022
Hsa-miR-324-5p	4707	107.7	-4.4	0.0022
Hsa-miR-368	721.6	77.8	-9.3	0.0022

1.2.6 miR-106b-25 cluster in Regulating Target Genes

MicroRNA genes can occur in clusters, and transcribed as polycistronic transcripts (Li et al. 2009). The miR-106b-25 cluster, which includes miR-106b, miR-93, and miR-25, was found differentially expressed in various human cancers. This cluster of microRNAs is located on human chromosome 7 in the intron 13 of MCM7 (Li et al. 2009). MicroRNAs serve as important regulators of gene expression; they can function as oncogenes or as tumor suppressors. For example, the transcription factor E2F1 was identified as a target gene for miR-106b and miR-93, and possibly have the function to prevent excessively high E2F1 expression in HCC (Li et al. 2009). Inhibition of miR-106b-25 cluster inhibited cell proliferation, as well as suppressed anchorage-independent growth in HCC (Li et al. 2009). In gastric cancers,

miR-106b-25 cluster was found to be able to inhibit transforming growth factor-β (TGFβ)-induced cell cycle arrest (Petrocca et al. 2008). While in mammary epithelial cells, miR-106b promoted cell division (Ivanovska et al. 2008; Li et al. 2009). These data demonstrate that miR-106b-25 cluster plays an important role in tumorigenesis of various cancers. As the mechanisms and pathways targeted by cancer-related microRNAs are being uncovered, these discoveries would shed new light on the application for these regulatory microRNAs in cancer treatments.

1.2.7 Applications of Regulatory MicroRNAs

Extensive analysis showed that aberrant expression of microRNAs contributes to the tumorigenesis of various cancers. In fact, these dysregulations of microRNAs in tumors indicate that microRNAs are promising candidates for distinguishing different tumour subtypes, resolving different tumour origins, as well as predicting differential stages of tumors (Petrocca et al. 2008). In other words, they may act as useful diagnostic tools, prognostic tools, and therapeutic tools. A study conducted by Lu and colleagues showed that microRNA profiling could accurately distinguish tumours reflecting different mechanisms of transformation in acute lymphoblastic leukemia samples (Lu et al. 2005). These microRNA were clustered distinctively in different lineages of leukemia, indicating its potential to serve as diagnostic tool (Lu et al. 2005).

In fact, microRNA expression profiling has been suggested to be more accurate than mRNA expression profiling for resolving the origin of metastasis of unknown primary tumor (Visone and Croce 2009), again demonstrating its potentially important diagnostic properties. Another interesting finding is that microRNAs seem to correlate with cellular differentiation stage. Murakami and colleagues have reported that miR-222, miR-106a, and miR-17-92 clusters have been associated with the degree of the differentiation of hepatocellular carcinomas (Murakami et al. 2006), suggesting a prognostic role of microRNAs. Other proposed microRNA therapeutic strategies such as re-expression of miRNAs, anti-miRNAs, and target protectors also hold great promise. Several reports have shown that microRNAs are related to drug resistance, and re-expressing miRNAs may be used in treatments that have lost efficacy due to drug resistance (Garzon et al. 2008). Anti-miRNAs and miRNA sponges can bind specific microRNA and prevent its interaction with its targets (Ebert et al. 2007), while target protectors bind to the 3'UTR of specific microRNA target genes to prevent access to target sites (Choi et al. 2007). Although these approaches hold great promises, they rely heavily on the identity of microRNA target genes. These proposed therapeutic approaches will become very useful as more and more targets of microRNAs are being identified, yet further studies are necessary to demonstrate their efficiency in *in vivo* models.

1.3 Target Gene Identification

1.3.1 Recent Molecular Advances in Target Gene Identification

As highlighted in previous sections, microRNAs are important regulators of gene expression and thus participate in physiological processes in different cancers. In fact, ever since the discovery of microRNA, scientists have been trying different ways to identify their targets. There are several different approaches to identify target genes of microRNAs. Recall that microRNAs target their target genes through complementary base-pairing mechanism; therefore, many target gene identification programs, such as BLAST, are based on this idea of "complementary-binding" property (Dalmay 2008). However, this may work well in the plant kingdom, but in the animal kingdom microRNAs are not perfectly complementary to their targets (Dalmay 2008). Experimental target identification is another common approach. It often involves either over-expression or down-regulation of microRNAs, then combined with mRNA profiling to identify genes that have changed in expression. This method is generally referred to as transcriptome analysis (Dalmay 2008). The main advantage of using techniques involved with microarrays is the ability to identify a large set of microRNA targets at a time. Another means of experimental target identification is through RISC purification. This method involves using antibodies against the Argonaute-2 protein, a

key component of the RISC, and then followed by subsequent RISC purification (Beitzinger et al. 2007). Extracting the mRNA from the purified RISC complexes, target genes can be identified through either direct sequencing or microarray hybridization (Beitzinger et al. 2007). Ribosomal mRNA profiling is another means of experimental target identification. mRNAs that are targeted by miRNAs were reported to be associated with polysome, while bound by miRNAs, they would show differential polysomal spectrum (Orom and Lund 2010). In fact, Orom and Lund proposed that polysome profiling could in part reflect the degree of translation of these targeted mRNAs (Orom and Lund 2010). Therefore, mRNAs that are regulated by specific endogenous miRNA can be identified by analyzing the shifts in individual mRNA abundance in polysome profiles following miRNA overexpression or inhibition (Nakamoto et al. 2005). There are still many more approaches in miRNA-mediated target identification, and these approaches would help expand the current knowledge of miRNA and their target recognition.

1.3.2 Importance of Target Gene Identification

It is clear that microRNAs participate in key regulatory networks controlling the cell's fate, affecting physiological processes such as differentiation, proliferation, and apoptosis. Aberrant expression of microRNAs has found to be closely associated with

various cancers including medulloblastoma. The identification of their downstream target genes will not only aid in understanding the pathogenesis of medulloblastoma, but also guides the development of more effective treatment strategies. Although there are several different approaches in identifying target genes, the identification of target genes still proves to be rather challenging. It still remains unknown whether one approach is better than the other, perhaps probably a combination of these approaches would offer a reasonable start.

CHAPTER 2: AIMS OF STUDY

Despite tremendous progress in the field of molecular biology of medulloblastoma in the past few decades, much remains to be found out in understanding the pathogenesis, and critical pathways involved in the tumorigenesis of medulloblastoma. As researchers have expanded their focus from morphological classification to molecular stratification, microRNA profiling has shed new light on the classification system for MB. MicroRNAs are known to be important regulators of gene expression responsible for the pathogenesis of many cancers, not surprisingly, medulloblastoma tumours too are found to express distinctive pattern of microRNAs. In addition to microRNA profiling, identifying downstream target genes regulated by these microRNAs is equally important. Taken together that differential microRNA expression is implicated in the tumorigenesis of medulloblastoma likely through the regulation of oncogene or tumour suppressor gene expressions, these target genes regulated by microRNAs are therefore promising candidates useful for potential gene therapy or small molecule drugs. However, identifying target genes has proven to be a bigger challenge than expected. Given that the miR-106b-25 cluster is found to be aberrantly expressed in MB samples and in cell lines, and given the known phenotypic effect on cell-cycle demonstrated by miR-106b-25 cluster in other cancers as

mentioned in previous sections... in this study, our primary objective is to identify putative target genes regulated by the differentially up-regulated miR-106b-25 cluster in medulloblastoma. Two different approaches will be used to identify putative target genes: 1) computational approach; and 2) experimental approach. In the computational approach, seven computational target prediction programs will be used to generate a list of putative target genes. By combining the seven prediction lists generated using different selection criteria; we hope to narrow down the number of target genes by eliminating false positives. In the experimental approach, we will adopt a biochemical method previously used to identify target genes regulated by microRNAs in C.elegans. The method employs the use of endogenous microRNAs as primers to initiate reverse-transcription to generate cDNAs clones that contain partial sequence of the target genes. By sequencing analysis of the library of cDNA clones, we hope to experimentally identify target genes of the miR-106b-25 cluster using endogenous microRNAs in medulloblastoma cell lines. Lastly, in parallel we would like to investigate on the functional roles of miR-106b-25 cluster in medulloblastoma.

CHAPTER 3: COMPUTATIONAL TARGET PREDICTION

3.1 Introduction- Computational Approach

Based on the fact that microRNAs and their targets share partial complementarity and very often complete complementarity in the seed region, many computational target prediction programs have been developed to predicted potential target genes (Dalmay 2008). There are generally three main types of target sites characterized on the basis of the number and position of matching nucleotides between the microRNA and its target: 1) 5'-Dominant canonical target sites; 2) 5'-Dominant seed-only target sites; and 3) 3'-Compensatory target sites (Sethupathy et al. 2006). 5'-Dominant canonical target sites define targets with perfect complementarity to the seed sequence of the microRNA and extensive base-pairing to the rest, while the 5'-Dominant seed-only target sites have limited base-pairing with the rest of the microRNA (Sethupathy et al. 2006). On the other hand, 3'-Compensatory target sites only have extensive base-pairing with the 3' half of the microRNA, but do not have perfect match to the seed sequence (Sethupathy et al. 2006). Many target gene identification programs such as BLAST, and TargetScan etc., predict target genes based on this idea of "complementary-binding" (Dalmay 2008). This may work well in the plant kingdom, however, in the animal kingdom microRNAs are not always perfectly

complementary to their targets (Dalmay 2008). In other words, the concept of using the property of "complementary-binding" would lead to both false positive and false negative predictions. Recall that there are different types of complementary base-pairing mechanisms as mentioned above; it is not surprising that different prediction programs would have their own selection criteria for target genes based on different parameters, such as base pairing between the miRNAs and their targets, thermodynamic of the miRNA-mRNA duplexes, cross-species sequence comparison, and the number of target sites for the miRNA (Watanabe et al. 2007). As a result, it would be expected that target prediction lists are extensive and embedded with many false positives, and at the same time miss out many false negatives.

Although the exact mechanism behind microRNAs and their actions in regulating target genes are not completely well understood, computational identification of target genes is still an invaluable way to generate lists of putative target genes. Therefore, in this chapter, we will be focusing on using the computational approach to identify potential target genes regulated by miR-106b-25 cluster in medulloblastoma. Seven prediction programs were used to generate the target gene lists for the miR-106b-25 cluster: 1) EIMMo2; 2) miRDB; 3) miR-Tar-miRanda; 4) miR-Tar-RNAhybrid; 5) Diana-microT; 6) Pic-Tar; and 7) TargetScan 4.2. By comparing the lists of target genes predicted by all of the seven programs, we hope to select out common target

genes that appeared in all of the programs, and ultimately narrowing down the target gene lists to a manageable size for experimental validation. The general scheme for this chapter is shown as a flowchart in Figure 3.1.

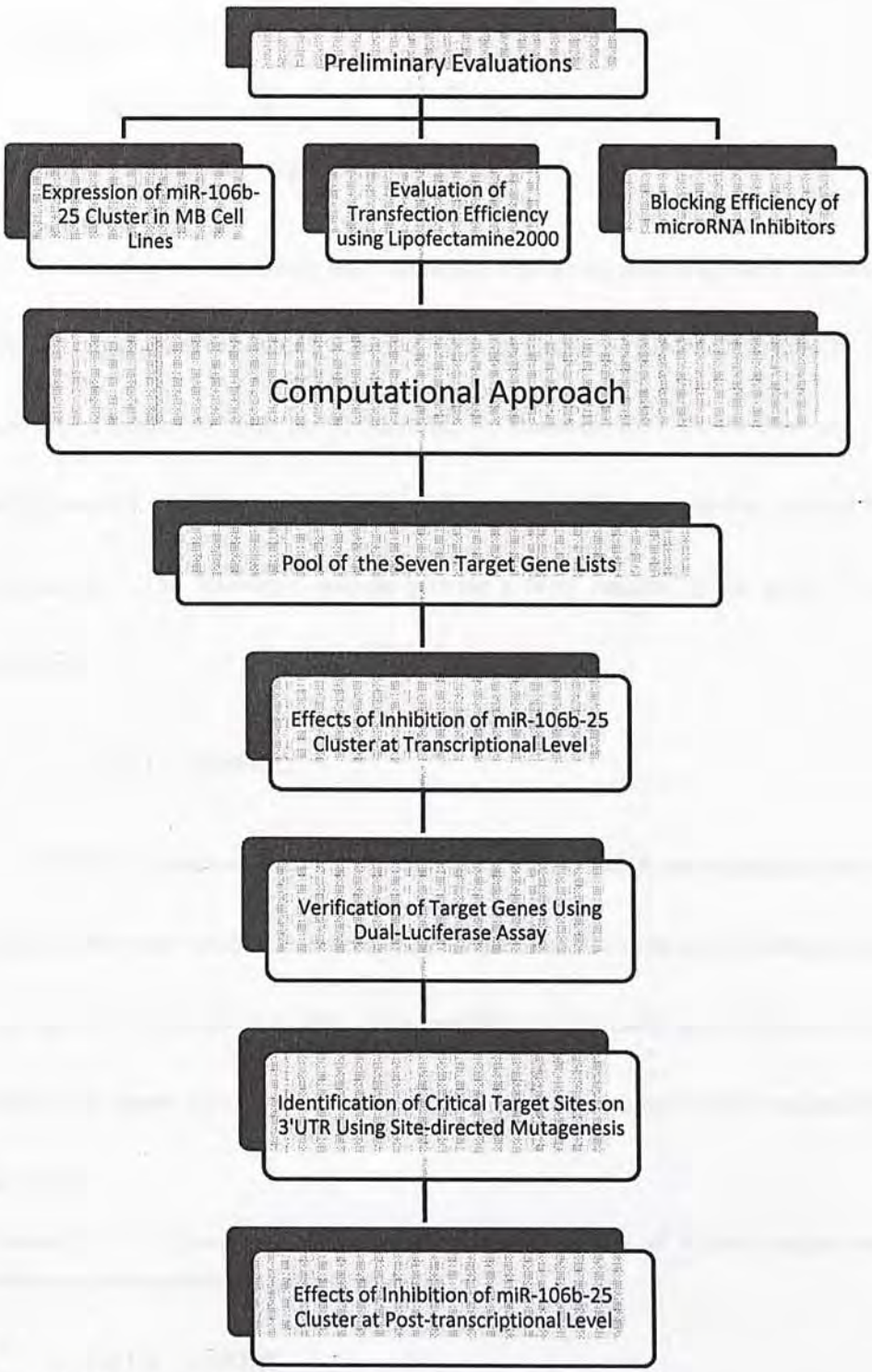

Figure 3.1 Schematic flowchart for the computational approach.

The flowchart summarizes the major steps used to identify potential target genes using the computational approach in this chapter.

3.2 Methods

3.2.1 Prediction Algorithms

A total of seven commonly used prediction algorithms were employed to predict common target genes regulated by the miR-106b-25 cluster: 1) EIMMo2; 2) miRDB; 3) miR-Tar-miRanda; 4) miR-Tar-RNAhybrid; 5) Diana-microT; 6) Pic-Tar; and 7) TargetScan 4.2. Different prediction algorithms have different selection criteria for their targets. The following sections provide a brief description for each of the algorithm.

3.2.1.1 EIMMo2

EIMMo2 focuses on studying the specificity in microRNA-dependent regulation. A general Bayesian method was developed for the inference of microRNA target sites, and together with explicit models for microRNAs to represent the evolution of the orthologous target sites, it allows the program to infer species-specific microRNA targeting.

(Gaidatzis D, van Nimwegen E, Hausser J, Zavolan M: **Inference of miRNA targets using evolutionary conservation and pathway analysis.)**

3.2.1.2 miRDB

miRDB is an online database used for predicting microRNA targets. This

prediction program is based on support vector machines (SVMs) and high-throughput training datasets. By employing the SVMs, which are universal constructive machine learning procedures based on statistical learning theory, the goal is to reduce the training error and while achieving better generalization on unseen data.

(Griffiths-Jones S, Grocock RJ, van Dongen S, Bateman A, Enright AJ: **miRBase: microRNA sequences, targets and gene nomenclature.)**

3.2.1.3 miRTar-miRanda

miRTar is a web server that identifies microRNA targets in the 3'UTR of mRNA of mammalian genes for a given input of microRNA. It is generally faster than the other search tools. Because of its efficient performance, it is often incorporated with powerful microRNA target search tool, such as miRanda and RNAhybrid. miRanda is an algorithm for finding genomic targets for microRNAs. It provides a ranked list of gene targets, as well as detail analyses of each conserved target gene/sites.

John B, Enright AJ, Aravin A, Tuschl T, Sander C, Marks DS. Human MicroRNA targets. *PLoS Biol.* 2004;2(11):e363

3.2.1.4 miRTar-RNAhybrid

RNAhybrid predicts microRNA targets by finding the minimum free energy hybridization for a long and a short RNA. The hybridization takes place in a domain mode where the short sequence is hybridized to the best fitting part of the target.

Marc Rehmsmeier *, Peter Steffen, Matthias Höchsmann, Robert Giegerich Fast and effective prediction of microRNA/target duplexes RNA, 10:1507-1517, 2004

3.2.1.5 Diana-microT

Diana-microT is another web-based program based on several parameters calculated individually for each of the microRNA, and provides a final prediction score by combining conserved and non-conserved microRNA recognition elements. This program also reports a signal to noise ratio and a precision score to address the significance of the predicted targets.

http://www.diana.pcbi.upenn.edu/cgi-bin/micro_t.cgi

3.2.1.6 Pic-Tar

Pic-Tar is an algorithm developed for the purpose of identification of microRNA targets. It provides detailed 3'UTR alignment for microRNA and the mRNA with predicted sites regarding on different vertebrates, *Drosophila* species, nematode species, and as well as targets that are not conserved but co-expressed in the same tissue.

http://pictar.mdc-berlin.de/

3.2.1.7 TargetScan 4.2

TargetScan searches for the presence of conserved 8mer and 7mer sites. 8mer sites are defined as showing complementarity between the mature microRNA to their

target(s) with exact match to position 2-8 followed by an "A", while 7mer sites are defined as showing exact match to positions 2-8 or 2-7 followed by an "A" of the mature microRNA. Predictions are primarily based on complementarity of the seed region, it also identifies sites with mismatches in the seed region yet compensated by conserved 3' pairing.

(Lewis BP, Shih I, Jones-Rhoades MW, Bartel DP, Burge CB: **Prediction of mammalian microRNA targets.)**

3.2.2 Cell Culture

3.2.2.1 Cell Lines

Human medulloblastoma cell line (DAOY) was obtained from the American Tissue Culture Collection (Rockville, MD, USA). DAOY cells were cultured using MEMα (Gibco Invitrogen Corporation) medium supplemented with 10% of fetal bovine serum (FBS) (Gibco Invitrogen Corporation). Cell cultures were maintained in a humidified incubator containing 5% CO_2 at 37°C. Culture medium was renewed every 2 to 3 days. For sub-culturing, DAOY cells were washed twice with 1x phosphate buffered saline (1x PBS) (Sigma Chemical Company), then trysinized using trypsin-EDTA (Gibco Invitrogen Corporation) until cells were detached. Trypsinization was terminated with twice volumes of growth medium. Cell pellets

were obtained by centrifugation at 1,000 rpm for 3 min at room temperature. Cell suspension was re-plated to new culture plates according to their concentrations.

3.2.2.2 Cell Counts

10μL of cell suspension was diluted with equal volume of Trypan blue (Gibco Invitrogen Corporation) to distinguish dead cells from viable cells. Then, 10μL of the mixture was injected into hemacytometer, and cells were counted under the microscope. The cell concentration was calculated using the average of the four corners on the grid of the hemocytometer.

3.2.3 Transfections

All transfections were performed using Lipofectamine 2000 according to the manufacturer's recommended concentrations.

3.2.3.1 Transfection of MicroRNA Inhibitors

Specific inhibitions of endogenous miR-106b/miR-93/miR-25 were achieved by transfection of microRNA inhibitors. Single-stranded microRNA inhibitors (anti-miR-106b/anti-miR-93/anti-miR25) and anti-miR negative control#1(negative) were acquired from Ambion. Mock experiments included only transfection reagent (Lipofectamine 2000) (Gibco Invitrogen Corporation).

3.2.3.1.1 Transfection Efficiency of Lipofectamine 2000

The transfection efficiency of Lipofectamine 2000 (Lipo2000) using the manufacturer's recommended concentrations were investigated using FITC-labelled double stranded RNA (BLOCK-iT Fluorescent Oligo) (Gibco Invitrogen Corporation). $1.8x10^5$ DAOY cells were plated onto 6-well culture plates. After 24hr of incubation at 37°C, a total of 100 pmol of BLOCK-iT Oligo were diluted with 250μL of Opti-MEM®I Reduced Serum Medium (OPTI-MEM) (Gibco Invitrogen Corporation), while 5μL of Lipo2000 were diluted in 250μL of OPTI-MEM for 5 min. Then, the two were mixed together and incubated for another 20 min at room temperature. After the incubation, 500μL of the mixture was added in drop-wise manner to appropriate wells that were refreshed with 2mL of culture medium. FITC signals were detected using a fluorescence microscope at 24 hours post-transfection.

3.2.3.1.2 Transfection of MicroRNA Inhibitors for Real-time PCR

DAOY cells were plated onto 6-well culture plates in triplicates at $1.5x10^5$ cells per well, and incubated for 24hr at 37°C. A total of 100 pmol of anti-miR-106b/anti-miR-93/anti-miR-25 inhibitors were diluted in 250μL of OPTI-MEM, while 5μL of Lipo2000 was diluted in 250μL of OPTI-MEM for 5 min. The two were mixed together thoroughly, and incubated for another 20 min. Then,

500μL of the mixture was added in drop-wise to appropriate wells containing 2mL of fresh culture medium. At 24hr post-transfection, the cells were harvested for RNA extraction, reverse transcription, and real-time PCR amplification.

3.2.3.1.3 Transfection of MicroRNA Inhibitors for Western Blotting

$3.0x10^5$ DAOY cells were plated onto 60-mm culture plates for collection of protein lysates after treatment with microRNA inhibitors (anti-miR-106b/anti-miR-93/ anti-miR-25). After 24hr of incubation at 37°C, a total of 200 pmol of each of the microRNA inhibitors were diluted in 500μL of OPTI-MEM, while 10μL of Lipo2000 was similarly diluted in 500μL of OPTI-MEM for 5 min. Then, the two were mixed together and incubated for 20 min at room temperature. After the incubation, 1mL of the mixture was added to appropriate wells that were refreshed with 5mL of culture medium.

3.2.3.2 Co-transfection of Plasmid and MicroRNA Inhibitors

3.2.3.2.1 Blocking Efficiency of MicroRNA Inhibitors

The efficiencies of microRNA inhibitors in inhibiting endogenous microRNAs were assessed by co-transfecting individual microRNA inhibitors and luciferase expression vectors (pMIR) that were cloned with reverse complement sequences of

specific microRNA (pMIR-miR-106b/pMIR-miR-93/pMIR-miR-25). The efficiencies were tested in DAOY. Co-transfection was preformed according to the manufacturers' recommended concentrations. $1.8x10^5$ DAOY cells were plated onto 6-well culture plate and incubated at 37°C for 24hr. A total of 50 pmol of microRNA inhibitors, 1000ng of pMIR (pMIR-miR-106b/pMIR-miR-93/pMIR-miR-25), and 10ng of pRL-CMV Renilla luciferase control (pRL) (Promega) were diluted in 250μL of OPTI-MEM, while 6μL of Lipo2000 was diluted in 250μL of OPTI-MEM for 5 min. The two were mixed together and incubated at room temperature for 20 min. After the incubation, 500μL of the mixture was added drop-wise into each well containing 2mL of fresh culture medium. At 24hr post-transfection, cells were harvested for dual-luciferase assay.

3.2.3.2.2 Co-transfection of Target Gene Expression Vector and MicroRNA Inhibitors

Co-transfection of microRNA inhibitors and luciferase expression vector cloned with the 3'UTR of potential target genes (pMIR) were performed in DAOY according to the manufacturer's recommended concentrations. $1.2x10^4$ cells were plated onto a 24-well plate, and incubated overnight at 37°C. A total of 150ng of pMIR (cloned with 3'UTR of potential target gene), 10ng of pRL, and 5 pmol of microRNA inhibitors (anti-miR-106/anti-miR-93/anti-miR-25) were diluted in 50μL of OPTI-MEM, while

1μL of Lipo 2000 was diluted in 50μL of OPTI-MEM for 5 min. Then the two were mixed together and incubated for 20 min. After the incubation, 100μL of the mixture was added to each well containing 500μL of fresh culture medium. Cells were harvested at 24hr post-transfection for dual-luciferase assay as above.

3.2.4 Real-time PCR Amplification

3.2.4.1 Total RNA Extraction from Cell Lines

Cells were harvested at 80% confluence for RNA extraction. All centrifugations at this section were performed at 4°C. Cells were first rinsed with 1xPBS. 1mL of TRIZOL® Reagent (Gibco Invitrogen Corporation) was added to each of the 100mm culture dish, and incubated for 5 min at room temperature. 0.2mL of chloroform was added to each sample tube and shaked vigorously for 30 sec, and settled for 3 min. Subsequently, the samples were centrifuged at 13,000 rpm for 15 min. After the mixture had separated into different phases, the aqueous phase was collected and precipitated using 0.5mL of isopropanol for 1 hour at -20°C. Following the precipitation, the mixture was centrifuged at 13,000 rpm for 10 min. The RNA pellet was washed with 75% (v/v) ice-cold ethanol, and air-dried for 15 min. Finally, it was re-suspended in 50μL of RNase free-water. The quantity and quality of the extracted

RNA were determined by the NanoDrop Spectrophotometer. The five RNA samples for the normal cerebellum were purchased from ATCC.

3.2.4.2 Stemloop miRNA Taqman qRT-PCR Analysis

The differentially expressed microRNAs (miR-106b, miR-93, and miR-25) were subjected to stemloop miRNA taqman qRT-PCR analysis to check for their expression levels in 7 MB cell lines (ONS-76, DAOY, D425, D458, D384, D341 Med, and D283 Med), and 5 normal cerebellum samples. The stemloop miRNA Taqman qRT-PCR in this section was performed using the TaqMan® Reverse Transcription Reagents, and TaqMan Universal PCR master mix purchase from Applied Biosystems. 10 ng of total RNA from each cell lines was individually subjected to reverse transcription (RT) using the specific stem-loop microRNA primers for miR-106b/miR-93/miR25 and RNU6B (internal reference). 10μL of the reaction mixture (1.5mM dNTP, 5U of Reverse Transcriptase, 1.5x RT Buffer, 0.38U of RNase inhibitor, and 1.5x microRNA primers) was incubated on ice for 5 min. The reaction condition was as follows: 16°C for 30 min; 42°C for 30 min; 85°C for 5 min; and finally terminated at 4°C. Following the RT, 0.66μL of the first strand cDNA was added to the PCR reaction mixture (5μL Taqman® Universal PCR Master Mix, 0.5μL of 20x miRNA Taqman® probe) to make up the total of 10μL reaction volume. The reaction was performed in

96-well optical plate, and the PCR condition was as follows: 95°C for 10 min; and 40 cycles of 95°C for 15 sec and 60°C for 1 min. This step amplifies cDNA using the groove binder probe labeled with the FAM reporter dye linked to the 5'end of the probe and a non-fluorescence quencher at the 3'end of the probe. Samples were prepared in triplicates. The microRNA expressions were normalized using the internal reference gene (RNU6B), and compared relatively to the average of all the normal cerebellum samples.

3.2.4.3 Reverse Transcription

To study the effect of inhibiting miR-106b/miR-93/miR-25 on the mRNA expression level of the potential target genes, RNA collected from DAOY cells previously treated with microRNA inhibitors were subjected to reverse transcription to synthesize cDNA for subsequent real-time PCR assays. DAOY cells were first transfected with specific miRNA inhibitors as described in section 3.2.3.1. RNAs were extracted from cells treated with specific microRNA inhibitors (miR-106b/miR-93/miR25) as described in the previous sections. A total of 1μg of RNA from each sample was subjected to reverse transcription in a total of 20μL reaction volume (1x AmpliTaq Gold Buffer, 5mM $MgCl_2$, 1mM dNTP, 50ng random hexamer, 10U RNase inhibitor, 50U of MuLV) (Applied Biosystems). The condition

was as follows: 25°C for 10 min; 42°C for 60 min; 95°C for 5 min; and finally terminated at 4°C. The cDNA products were kept at -20°C ready for subsequent real-time PCR reactions.

3.2.4.4 Real-time PCR Target Gene Expression

Real-time PCR assay was used to investigate the gene expression of specific target gene in cell lines, and after treatment with microRNA inhibitors (miR-106b, miR-93, and miR-25). The primer sequences are listed in Table 3.1. cDNAs prepared from the reverse transcription was diluted to 1:44 dilution factor. Using the SYBR Green RT-PCR Kit (Applied Biosystems), 4.5μL of the diluted cDNA was mixed with 2x SYBR pre-mixture, 0.25 μM of paired-up sense and antisense primers to make up a total of 10μL reaction volume. The thermo-profile was as follows: 95°C for 20 sec, 50°C for 2 min, 95°C for 10 min, and 40 cycles of 95°C for 15 sec and 60°C for 1 min. Samples were prepared in triplicates, and evaluation of the expression levels were normalized to the internal control (RPS3). Cycle threshold (Ct) of miRNAs was compared with those of RPS3 to determine relative expression level. Relative fold change between expression of miRNAs in the treated and control samples was determined by the following equation: fold change= $2^{(-\Delta\Delta Ct)}$, where $\Delta\Delta Ct=(Ct_{hsa\text{-}miR} - Ct_{RPS3})_{treated} - (Ct_{miR} - Ct_{RPS3})_{control}$.

Table 3.1 Primers used in real-time PCR amplification for potential target genes

Target Gene	Primers (forward & reverse) 5'→3'
miR-106b targets	
ZNFX1	TCC TGG AAC AGG CAA AAC CTA T
	GCA CAA TGC TGG TCT TCT GAC A
miR-93 targets	
ZNFX1	TCC TGG AAC AGG CAA AAC CTA T
	GCA CAA TGC TGG TCT TCT GAC A
miR-25 targets	
DNAJB12	AGC TGT GAA AAG GGT CAA GCA
	TTG CTG AGT ACC GCA TAT GCT
Reference Gene	
RPS3	AGC CAC CAG AAC ACA GAA TG
	CTA GTG GCC ACC TTT TCA GC

3.2.5 Cloning of Potential Target Genes into pMIR Luciferase Expression Vector

Genomic fragments containing the 3'UTR of potential target genes were PCR amplified using high-fidelity PCR amplification, and then cloned into pMIR luciferase expression vector through specific restriction enzyme digestions and ligation. The pMIR vectors cloned with specific 3'UTR were then ready for co-transfection with microRNA inhibitors and dual luciferase assays. The cloning constructs of the potential target genes can be found in Table 3.2.

Table 3.2 Cloning constructs of the potential target genes

ZNFX1		
ID	NM_021035	
Total Length of 3'UTR	1365bp	
miR-106b		
Conserved Region	Number of sites Location on 3'UTR Location on 3'UTR	2 484-491 1324-1331
Poorly Conserved Region	Number of sites Location on 3'UTR Location on 3'UTR	2 134-140 979-985
miR-93		
Conserved Region	Number of sites Location on 3'UTR	1 483-489
Poorly Conserved Region	Number of sites Location on 3'UTR	1 133-139

DNAJB12		
ID	NM_001002762	
Total Length of 3'UTR	2980bp	
miR-25		
Conserved Region	Number of sites Location	1 2876-2883
Poorly Conserved Region	Number of sites	None

*note that the conserved sites are conserved in Human, Mouse, Rat, Dog and Chicken (TargetScan 4.2)

3.2.5.1 High-Fidelity PCR Amplification of 3'UTR

Genomic fragments containing the 3'UTR of the potential target genes were PCR amplified using FastStart High Fidelity PCR System (Roche). 100ng of genomic DNA was subjected to PCR amplification in a total of 20μL reaction volume (1x FastStart High Fidelity Reaction Buffer; 1.8mM $MgCl_2$; 0.8μM dNTP; 0.4μM of forward primer; 0.4μM of reverse primer; and 2.5U of FastStart High Fidelity Enzyme Blend). The cloning primers and the specific annealing temperature for ZNFX1 and DNAJB12 are listed in Table 3.3. The thermal profile is as follows: 95°C for 2 min; 35 cycles of 95°C for 30 sec, 58°C or 55°C for 30 sec, and 72°C for 50 sec; 72°C for 7 min; and finally terminated at 4°C.

Table 3.3 Primer sequences and specific annealing temperature for 3'UTR cloning

Target Genes	Primer Sequences (Forward & Reverse) 5'→3'	Start Site	Amplicon Size	Annealing Temperature
ZNFX1	GG ACTAGT GGC CAA CAA CCT GAT GAA CT	26896th	1484bp	58°C
	CCC AAGCTT TTT GGC TGA GTT GCT TCT GA	28334th		
DNAJB12	GG ACTAGT GAA ACC ATG GCA ACG AAA GT	17301st	1488bp	55°C
	CCC AAGCTT TCA AGA AAT ACA GCT TCC AGA GG	18777th		

**The underlined sequences are restriction enzyme sequence. ACTAGT is SpeI; AAGCTT is HindIII.

3.2.5.2 PCR Purification of Amplified PCR Product

The amplified PCR products were subject to purification using the PCRquick-spin™ PCR product purification kit (TechDragon Ltd.) according to the manufacturer's protocol. In brief, all of the 20μL from the PCR reaction mixture were added to 500μL of Binding Buffer and incubated for 1 min at room temperature. Then the samples were loaded to the spin column and centrifuge at 13,000 rpm for 1 min. 700μL of Washing Buffer was added to the column and centrifuged at 13,000 rpm for 1 min. Then the column was centrifuged again for another minute to dry the membrane. 50μL of Elution Buffer was added to the column and incubated for 1 min. The samples were collected by centrifugation at 13,000 rpm for 1 min.

3.2.5.3 Restriction Enzyme Digestions

In order to insert the PCR amplified 3'UTR into the pMIR luciferase expression vector, both the amplified fragments and the pMIR vectors were subjected to restriction enzyme digestions. 1μg of pMIR vectors and 1μg of the purified PCR products were separately added to the reaction mixture to make up a total of 20μL (1x NEB Buffer 2; 1μL of HindIII (NEB); and 1μL of SpeI (NEB)). The enzymatic reaction was allowed to incubate overnight at 37°C.

3.2.5.4 Ligation of 3'UTR to Expression Vector

The digested 3'UTRs and pMIR vectors were subjected to another round of purification as described in section 3.2.5.2. The 3'UTR fragments and the pMIR vector (3:1 ratio) together were diluted in 1x T4 ligation buffer with 0.5U of T4 ligase (NEB). Ligation was carried for 2 hr at room temperature.

3.2.5.5 Transformation

20μL of the ligation products were added to 50μL of competent cells (DH5α *Escherichia. coli* competent cells) (Invitrogen) and put on ice for 15 min. The mixture was subjected to heat-shock procedures (42°C for 90 sec; 4°C for 3 min), following by incubation with 200μL of SOC medium (Invitrogen) for 1hr a 37°C. After the incubation, the mixture was spread onto agar plates containing 100mg/mL of ampicillin (USB Corporation) and incubated at 37°C overnight for colony formation.

3.2.5.6 Preparation of the Cloned Plasmid

Single bacterial clones were picked and inoculated overnight at 37°C with vigorous shaking in 100mL of LB broth (Invitrogen) to prepare for purification on the next day. Purification of plasmid was performed using the DNA-midi^{TM} Plasmid DNA Purification Kit (TechDragon Ltd.) according to the manufacturer's protocol. In

brief, bacterial cells were harvested by centrifugation at 13,000 rpm for 5 min at 4°C. The bacterial pellet was re-suspended in 3 mL of M1 buffer, 3 mL of M2 buffer for 5 min, and 4.2mL of M3 buffer for 15 min on ice. After the incubation, the mixture was centrifuged at 13,000 rpm for 10 min at 4°C, and the supernatant was transferred to 500μL of midi-Bead solution. Through centrifugation at 13,000 rpm, a midi-bead pellet was obtained. The pellet was washed with 700μL of Washing buffer A before transferring to the filter column. After spinning down the column, 700μL of Washing buffer B was added and the spin-down was repeated. The sample was finally eluted with 300μL of Elution buffer.

3.2.5.7 Sequencing of the Cloned Plasmid

The purified plasmid was subjected to sequencing analysis for verification of the 3'UTR sequence cloned into the pMIR expression vector. 50ng/μL of the purified plasmid was sent to TechDragon Ltd. for sequencing analysis using the pMIR FW primer (5'- AGGCGATTAAGTTGGGTA-3').

3.2.6 Site-Directed Mutagenesis

Seed regions were mutated to remove complementarity to the miRNA seed region by using the QuickChange® II Site-Directed Mutagenesis Kit (Stratagene) according to the manufacturer's protocol. The mutation primers and the mutation sites are listed in Table 3.4. In brief, 1μg of the wild-type 3'UTR cloned pMIR vector (ZNFX1-pMIR/ DNAJB12-pMIR) was subjected to PCR amplification in a total of 25μL reaction volume (1x reaction buffer; 10μM of each forward and reverse primer; 0.5μL of the dNTP mix; 0.5μL of PfuUltraII FusionHS). The thermal profile was as follows: 95°C for 2 min; 25 cycles of 95°C for 30 sec, 50°C for 30 sec, 72°C for 3 min; 72°C for 7 min, and finally terminated at 4°C. The PCR amplified plasmids were subjected to DpnI (Stratagene) digestion for 5 hrs at 37°C. Following the digestion with DpnI, the plasmids were transformed, purified, and sequenced in procedures similar to section 3.2.5.5 to section 3.2.5.7.

Table 3.4 Primers for site-directed mutagenesis

Target Genes	Primer Sequence (5'→3')	microRNA Target Site
ZNFX1		
R1	CGC CTG TAA TCC CAG **GTG** TTT GGG AGG CCG AGG	Poorly conserved region at position 134-140
	CCT CGG CCT CCC AAA **CAC** CTG GGA TTA CAG GCG	
R2	TAC CCC TGC GCT AGA GTA AGG **TGT** TTA TCT CCA GAA CTG AGA G	Conserved region at position 483-491
	CTC TCA GTT CTG GAG ATA AAC **ACC** TTA CTC TAG CGC AGG GGT A	
R1R2	Same as above	Double mutation at both R1 & R2
Del-R2	CCC CTG CGC TAG AGT A-------TA TCT CCA GAA CTG AG	Deletion of entire seed region at R2
	CTC AGT TCT GGA GAT A-------TA CTC TAG CGC AGG GG	
DNAJB12		
R1	CCT AGA CGG GCT GAG CCA TGT **CGT** ATA AGA ACA TAG ATC CTA AAG	Conserved region at position 2876-2883
	CTT TAG GAT CTA TGT TCT TAT **ACG** ACA TGG CTC AGC CCG TCT AGG	

** The bold nucleotides were the mutated sites where C replaces G, while A replaces T and vice versa. Dashes indicate deletion of nucleotides.

3.2.7 Dual-Luciferase Assay

Dual-Luciferase Assay (Promega, Madison) was performed at 24hr post-transfection. To measure the firefly/renilla signals, cells were harvested and washed with 1x PBS. 100μL/well of 1x Passive Lysis Buffer (Firefly & Renilla Luciferase Assay Kit, Biotium, Inc.) was added the 24-well culture plate and incubated for 15 min on shaking platforms. Then the lysates were transferred to micro-centrifuge tubes ready for the dual-luciferase assay. 50μL of LARII reagent (Promega, Madison) was added to 20μL of sample lysates, and the luminescence for the firefly signal was measured over a period of 10 seconds. Then 50μL of STOP & GLO reagent (Promega, Madison) was added to the mixture, and luminescence for the renilla signal was measured. Luminescence was integrated over a period of 10 seconds.

3.2.8 Western Blot Analysis

To investigate the effect of inhibiting miR-106b, miR-93, and miR-25 on the protein levels in DAOY, western blotting analysis was performed using protein lysates that were collected 24hr post-transfection of microRNA inhibitors. Cells were first washed with 1x PBS. Protein lysates were collected by adding 800μL/well of Nonidet-P40 (NP40) buffer (150mM sodium chloride, 1% NP-40, 50mM Tris, pH8.0) supplemented with 10mM NaF, 1mM of Na Orthovanadate, and 1mM of PMSF. The

concentrations of the protein lysates were determined using the Bio-Rad Protein Assay (Bio-Rad) according to the standard protocol. Proteins from each lysates (40μg) were separated on 12.5% SDS-PAGE gel and transferred onto nitrocellulose membrane. The nitrocellulose membrane was incubated in blocking buffer (6% non-fat milk) for 1hr at room temperature. Following the incubation, it was incubated with primary antibodies: mouse polyclonal to ZNFX1 antibody (1:1000) (ab69172, abcam), or rabbit polyclonal to β-actin antibody (1:10,000) (ab1801, abcam) overnight at 4°C. After several washes with 1xPBS-Tween (1xPBS with 20% Tween), the membranes were separately incubated with secondary antibodies: goat polyclonal secondary antibody (1:5,000) to mouse IgG-HRP (abcam) for ZNFX1, and goat polyclonal secondary antibody (1:5,000) to rabbit IgG-HRP (abcam) for β-actin. The bound antibodies were visualized by using the ECL plus™ detection kit (GE Healthcare). The chemiluminescence signals were captured by Kodak XAR-5 film at various exposure times depending on the different antibodies used.

3.3 Results

**All statistical comparisons are based on Student *t*-test, where negative controls refer to treatment with anti-miR negative control#1 (Ambion).

3.3.1 Expression Levels of miR-106b-25 cluster in MB Cell Lines

The expression profiles of the selected miR-106b-25 cluster were determined by real-time stem loop PCR amplification in seven MB cell lines (ONS-76, DAOY, D425, D458, D384, D341 Med, and D283 Med) and in five normal cerebellum samples (4 adult & 1 fetal). The profile showed that miR-106b-25 cluster exhibit different degree of increase for most of the MB cell lines compared to the average of the normal cerebellum (Figure 3.2). Of the 7 MB cell lines, ONS-76 and DAOY showed distinctive increase in miR-106b (8.4-fold, 8.3-fold), miR-93 (14.3-fold, 21.8-fold), and miR-25 (12.5-fold, 10-fold) respectively in the two cell lines.

A

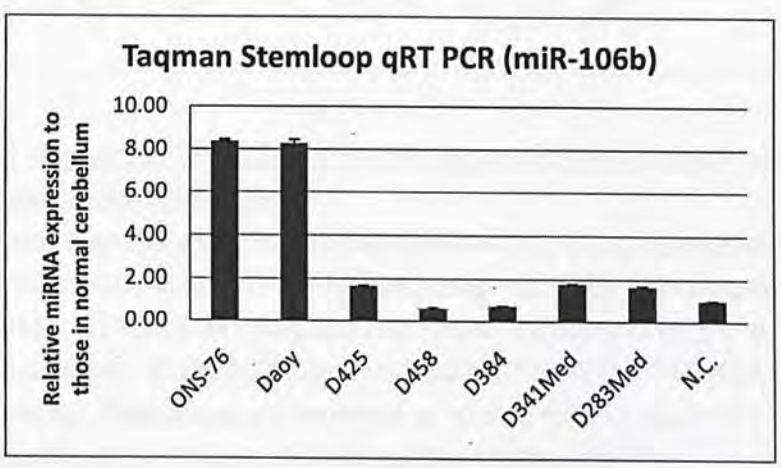

B

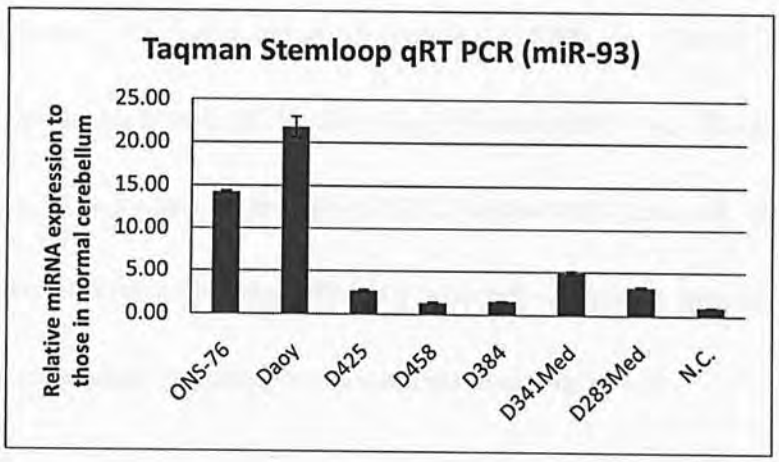

C

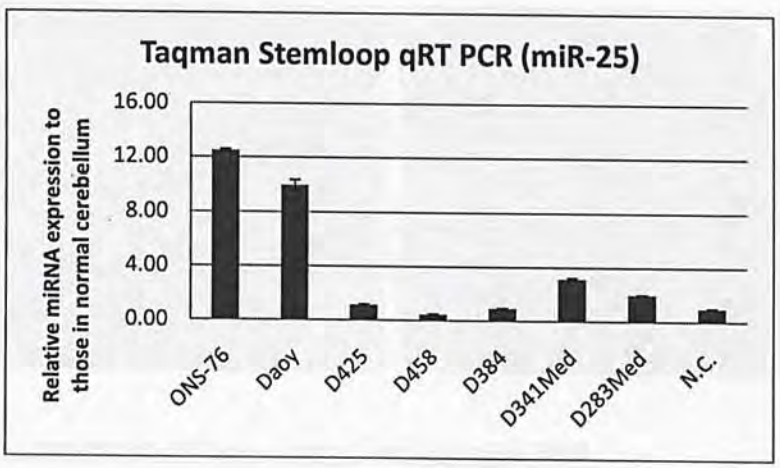

Figure 3.2 Taqman stemloop qRT PCR analyses of miRNA expression levels in MB cell lines and normal cerebellum.

Taqman Stem-loop qRT PCR analyses indicated general trend of up-regulation for this cluster of microRNA in most of the MB cell lines. (A) miR-106b is up-regulated in ONS-76, DAOY, D425, D341 Med, and D283 Med. (B) miR-93 is up-regulated in all cell lines examined. (C) miR-25 is up-regulated in ONS-76, DAOY, D425, D341 Med, and D283 Med. Data shown are expressed as relative miRNA expression level ±SD. Dotted lines denote the value of the average of cerebellum samples.

3.3.2 Evaluation of Transfection Efficiency Using Lipofetamine2000

Transfection efficiency using Lipofectamine 2000 was tested using the FITC-labeled double stranded RNA (BLOCK-iT Fluorescent Oligo). The transfection efficiency was determined by the ratio of FITC-positive cells/ total cell numbers. It was observed that the transfection efficiency achieved ~70% using the recommended reagent concentrations suggested by the manufacturers (Figure 3.3).

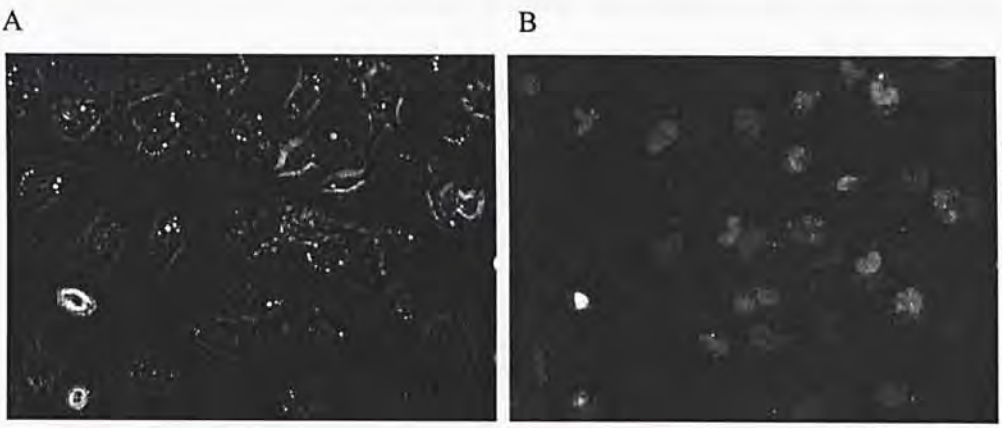

Figure 3.3 Transfection efficiency using Lipofectamine 2000.
Representative images of DAOY cells transfected with FITC-labeled double stranded oligo. FITC signal was examined under a fluorescence microscope at 24hr post-transfection. (A) DAOY cells captured in bright field, while (B) indicates the same area captured using the fluorescence field.

3.3.3 Blocking Efficiency of MicroRNA Inhibitors

The efficiencies for blocking endogenous microRNAs (miR-106b/miR-93 /miR-25) using specific microRNA inhibitors were examined using Dual-luciferase assay. Anti-sense inhibitors of miR-106b (anti-miR-106b), miR-93 (anti-miR-93), and miR-25 (anti-miR-25) were employed to block the activities of their respective endogenous microRNAs. The microRNA inhibitors were co-transfected with a pMIR-REPORT^{TM} vectors that were cloned with the complementary sequence of the corresponding microRNA. Restoration of luciferase activity resulted from inhibiting the endogenous microRNA from targeting the complementary sequence of the reporter construct was observed in all three microRNAs (Figure 3.4). Specifically, luciferase activity was increase after treatment with anti-miR-106b, anti-miR-93, and anti-miR-25 for ~2.2-fold, ~2.0-fold, and ~1.4-fold respectively in DAOY (Figure 3.4).

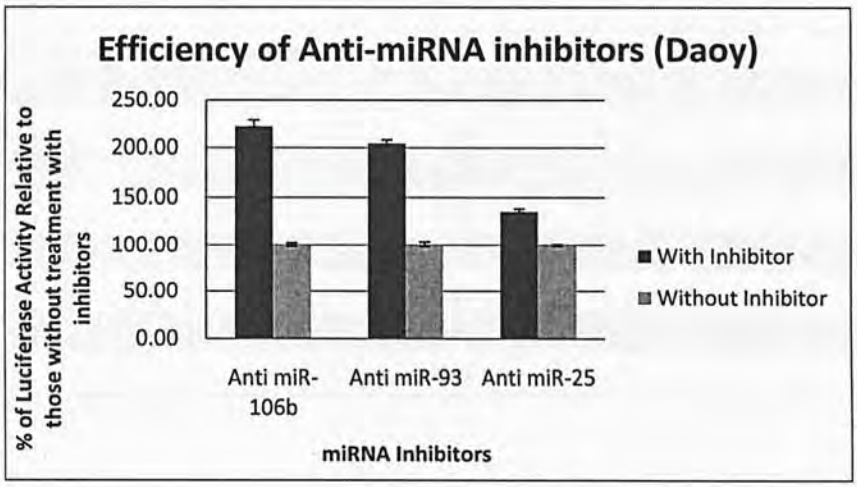

Figure 3.4 Inhibitory effect of anti-miRNAs.

Dual-luciferase assay was used to examine the blocking efficiency of specific microRNA inhibitors with specific complementary sequence of miRNA cloned in the luciferase reporter construct in DAOY. The % of Luciferase activities were normalized with their respective Renilla activities, then compared to the control without treatment with miRNA inhibitors. Data shown are expressed as normalized firefly to renilla relative to the control ±SD. (n=3)

3.3.4 Target Prediction List

Different target prediction programs resulted in different number of predicted target genes for a given microRNA as summarized in Table 3.5. The number of predicted target genes varied from hundreds to several thousands. Among the predicted target genes, ones that were found common in all seven prediction programs are listed in Table 3.6.

Table 3.5 Number of predicted target genes from different prediction programs

hsa-miR-106b predicted targets	
Prediction Programs	**Number of Predicted Targets**
miRanda	178
RNA hybrid	4280
Pic Tar	726
TargetScan 4.2	725
EIMMo2	5280
Diana-microT	843
miRDB	768

hsa-miR-93 predicted targets	
Prediction Programs	**Number of Predicted Targets**
miRanda	473
RNA hybrid	5035
Pic Tar	613
TargetScan 4.2	446
EIMMo2	5706
Diana-microT	9613
miRDB	810

hsa-miR-25 predicted targets	
Prediction Programs	**Number of Predicted Targets**
miRanda	192
RNA hybrid	4531
Pic Tar	3806
TargetScan 4.2	567
EIMMo2	3184
Diana-microT	4713
miRDB	419

Table 3.6 Common predicted targets among the seven prediction programs

hsa-miR-106b common predicted targets	hsa-miR-93 common predicted targets	hsa-miR-25 common predicted targets
CRK	BAHD1	DNAJB12
MAP3K9	MYCN	JOSD1
MYCN	TRIM36	NSMAF
NR4A3	TUSC2	SLC17A6
PCDHA6	UBE2B	
PTPN4	ZNF512B	
SACS	ZNFX1	
TNKS2		
TXNIP		
ZNFX1		

3.3.5 Recognition Sites of Potential Targets

ZNFX1 was predicted to harbor miR-106 and miR-93 recognition sites in its 3'untraslated region (3'UTR); therefore, it was chosen to act as a study model for both miR-106b and miR-93. Of the recognition sites for miR-106b, there were two conserved regions and two poorly conserved regions. For miR-93, there is one conserved and one poorly conserved region; in addition, they share the same recognition sites with miR-106b. The specific location of these recognition sites were summarized in Table 3.2 in the Materials and Methods section. On the other hand, DNAJB12 was chosen to act as a study model for miR-25, and its potential miR-25 recognition site locates at 2876-2883bp on its 3'UTR (Table 3.2).

3.3.6 Expression Levels of ZNFX1 in MB Cell Lines

The mRNA expression level of ZNFX1 was examined in ONS-76 and DAOY by qRT-PCR. Relatively lower expression of the mRNA level of ZNFX1 was observed in both cell lines as compared to the normal cerebellum (Figure 3.5). The down-regulation of mRNA level of ZNFX1 in cell lines is in line with the known up-regulation of the miR-106b, and miR-93.

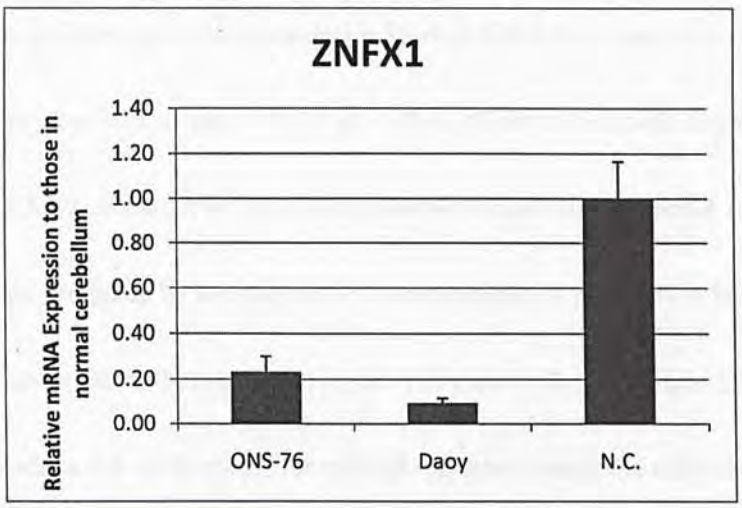

Figure 3.5 Quantitative real-time PCR for candidate genes.
Shown in the figure is the relative mRNA expression level of ZNFX1 compared to the average of normal cerebellum samples expression ±SD. Each expression levels were normalized with the reference gene (RPS3). (n=3)

3.3.7 Transcriptional Regulation of ZNFX1 and DNAJB12

Recall that microRNAs can regulate their target(s) through both transcriptional and translational regulations, therefore, mRNA level of ZNFX1 and DNAJB12 were examined using qRT-PCR in DAOY cells. Statistical analysis suggested that there were distinctive up-regulation of mRNA transcript levels in ZNFX1 upon treatment with anti-miR-106b, and anti-miR-93 inhibitors (Figure 3.6A). On the other hand, distinctive up-regulation of mRNA transcript level in DNAJB12 was also observed when cells were treated with anti-miR-25 as marked by the asterisks in Figure 3.6B. Therefore, ZNFX1 was chosen to be the study model for miR-106b and miR-93 as it is a common target predicted by the programs to be regulated by these two microRNAs, and that it is transcriptionally regulated by miR-106b and miR-93. While DNAJB12 was chosen to act as the study model for miR-25, because among the common targets predicted for miR-25 (data not shown), DNAJB12 was the only that was regulated by miR-25 at the transcriptional level.

A

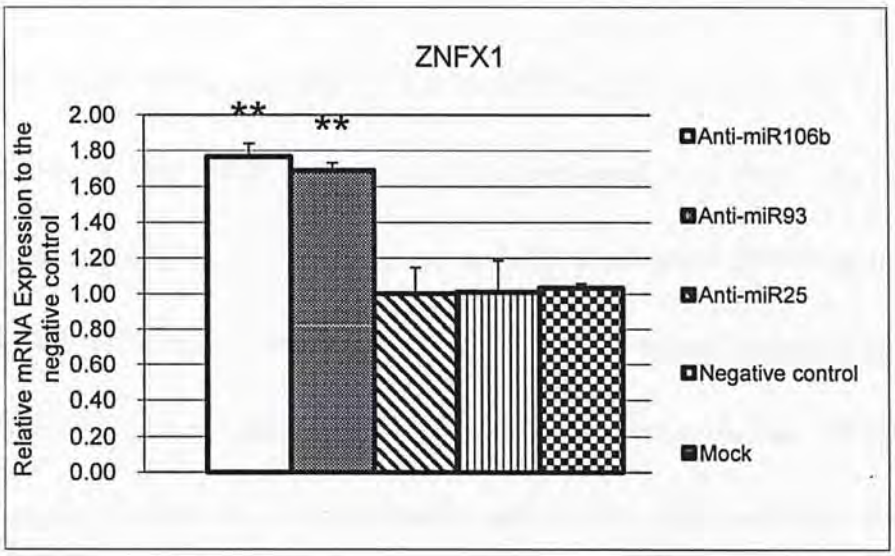

B

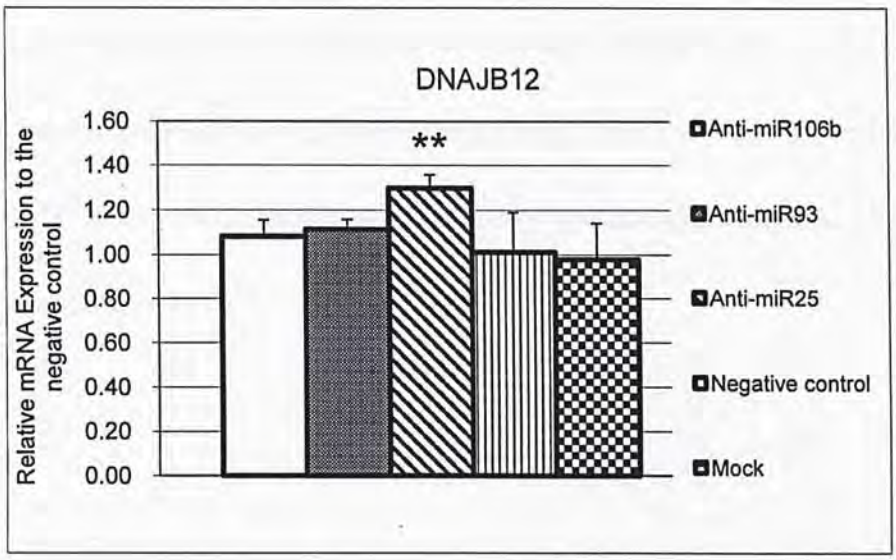

Figure 3.6 Changes in target gene expression in DAOY.

Quantitative real-time PCR was used to examine the temporal changes of mRNA transcripts of ZFNX1 (Fig 3.6A), and DNAJB12 (Fig 3.6B) upon treatment with anti-miRNA inhibitors. Data shown are expressed as relative mRNA to reference gene expression ±SD. (n=3) **denote $p<0.05$

3.3.8 Verification of Potential Target Genes

To further verify whether ZNFX1 and DNAJB12 are target genes regulated by the miR-106b-25 cluster, dual-luciferase assay was performed. Luciferase expression vector cloned with the 3'UTR of the two potential target genes (ZNFX1-pMIR & DNAJB12-pMIR) were co-transfected along with specific microRNA inhibitors into DAOY, and luciferase activities were examined 24-hr post-transfection. Treatment with anti-miR-106b and anti-miR-93 (but not anti-miR-25) could specifically release the endogenous microRNA suppression on the 3'UTR of ZNFX1, which led to the increase in luciferase activity (marked by the asterisks in Figure 3.7A). On the other hand, treatment with anti-miR-25 also released the endogenous miR-25 suppression on the 3'UTR of DNAJB12, leading to an increase in luciferase activity (marked by the asterisks in Figure 3.7B).

A

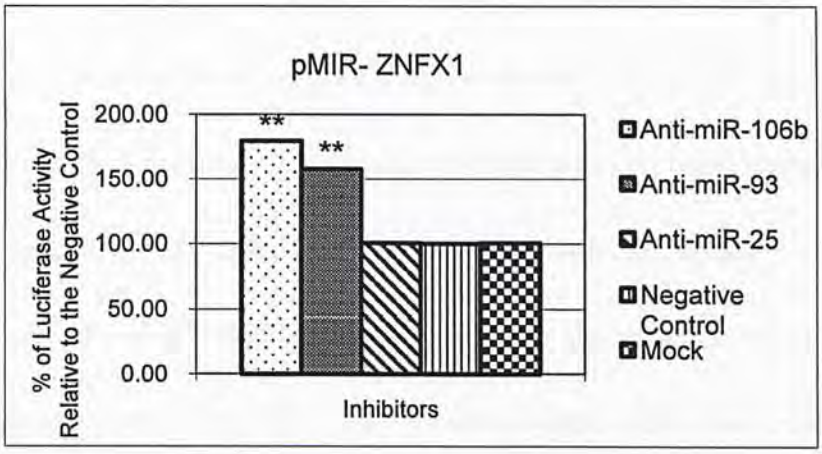

B

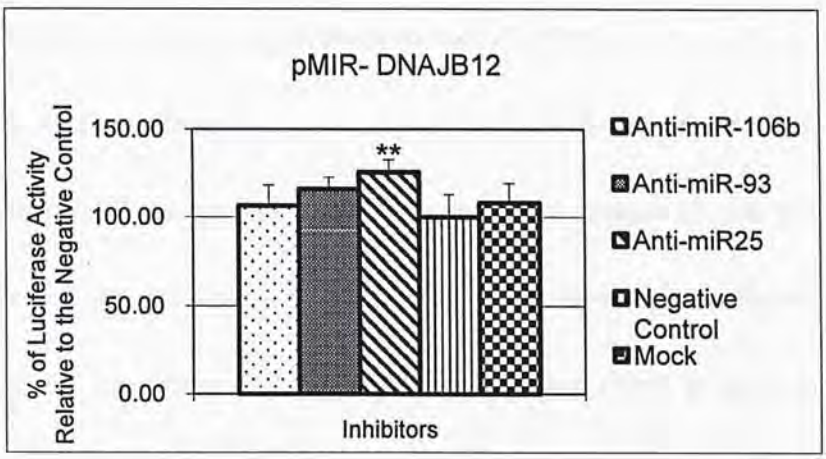

Figure 3.7 Relative luciferase activity of pMIR-ZNFX1 and pMIR-DNAJB12

(A) The levels of luciferase activity of ZNFX1-3'UTR-cloned pMIR after treatment with anti-miR-106b, anti-miR-93, and anti-miR-25 inhibitors are indicated in the histograms (**$p<0.00$ for both anti-miR-106b & anti-miR-93). The SD for anti-miR-106b, anti-miR-93, anti-miR-25, negative control, and mock are ~0.4, ~0.2, ~0.3, ~0.2, and ~0.1 respectively. (n=3) (B) The levels of luciferase activity of DNAJB12-3'UTR-cloned pMIR after treatment with anti-miR-25 show a significant increase (**$p<0.04$). The firefly signals were normalized to the corresponding Renilla signals. Relative luciferase activities were expressed as the ratio of the normalized activity of the treated cells to the negative control. (n=3)

3.3.9 Identification of Critical Target Sites

To narrow down the critical target site(s) recognized by the specific microRNAs, we have induced site-directed mutagenesis at various predicted target regions on the 3'UTR of ZNFX1, and DNAJB12. The constructs with the mutated regions for ZNFX1 are shown in Figure 3.8A. Let's consider the expected results for the wild-type construct. Under the negative control condition (without treatment of miRNA inhibitors), endogenous miRNAs would bind onto the miRNA recognition sites on the wild-type 3'UTR leading to a suppression of luciferase activity. Now, consider the same wild-type construct upon treatment with miRNA inhibitors. Because the endogenous miRNAs are inhibited, the suppressions caused by the endogenous miRNAs are now relieved; therefore, leading to an increase in luciferase activity relative to its negative control. As a result, we should expect to see a significant increase for the change in luciferase activity between the treated sample and its negative control for the wild-type construct. On the other hand, consider the case for the mutated construct. Under the negative control condition, endogenous miRNA would not be able to bind onto the miRNA recognition site due to the induced mutation, thus luciferase activity is not suppressed. Upon treatment with miRNA inhibitors for the same mutated construct, similar luciferase activity is expected because endogenous

miRNAs could not bind on to the mutated miRNA recognition site regardless of the treatment with miRNA inhibitors. As a result, we should expect either minimal or no change in luciferase activity between the treated sample and its negative control for the mutated construct. From our data, the wild-type ZNFX1 3'UTR, as expected, showed an increase in luciferase activity upon treatment with anti-miR-106b, and anti-miR-93 inhibitors. The relative change in the percentage of luciferase activity reached ~55% for anti-miR-106b, and ~56% for anti-miR-93 compared to the negative control (Figure 3.9A), suggesting that it carries the potential target sites for the two miRNAs. Mutation at the poorly conserved recognition site (R1) showed similar change in relative luciferase activity as the wild-type construct (~58% for anti-miR-106b, and ~57% for anti-miR-93) (Figure 3.9A), indicating that R1 do not carry the critical miRNA recognition site. Mutation at R2 resulted a decrease in change of relative luciferase activity (~31% for anti-miR-106b, and ~29% for anti-miR-93) (asterisks in Figure 3.9A), which indicate that R2 contains the critical recognition site for both miR-106b and miR-93. Subsequent double mutation at both target sites (R1R2), and total deletion of the seed region at R2 (Del-R2) both showed similar decrease in the change in relative luciferase activity as the single mutation at R2 (Figure 3.9A), which further confirms the importance of R2 for the specific microRNA suppressions. The consistent decrease in change in relative luciferase activity observed for R2, R1R2, and

Del-R2 constructs demonstrated that R2 is the critical miRNA recognition site for miR-106b and miR-93. When R2 is mutated, regardless whether the microRNA inhibitors or the random oligonucleotides (negative control) were added, the change in relative luciferase activity was minimal as compare to the change observed for the wild-type construct.

The mutation construct for the 3'UTR of DNAJB12 is depicted in Figure 3.7B. For the wild-type DNAJB12 3'UTR, as expected, there was an increase of ~14% in the luciferase activity upon treatment with anti-miR-25 inhibitor compared to the negative control (Figure 3.9B). This suggests that the 3'UTR of DNAJB12 carries the miR-25 recognition site(s). However, mutation at the conserved region (R1) showed a similar increase of ~10% in luciferase activity as the wild-type construct (Figure 3.9B). This suggests that R1 may not be the critical miRNA recognition site for miR-25. The critical recognition site(s) for miR-25 remain to be determined.

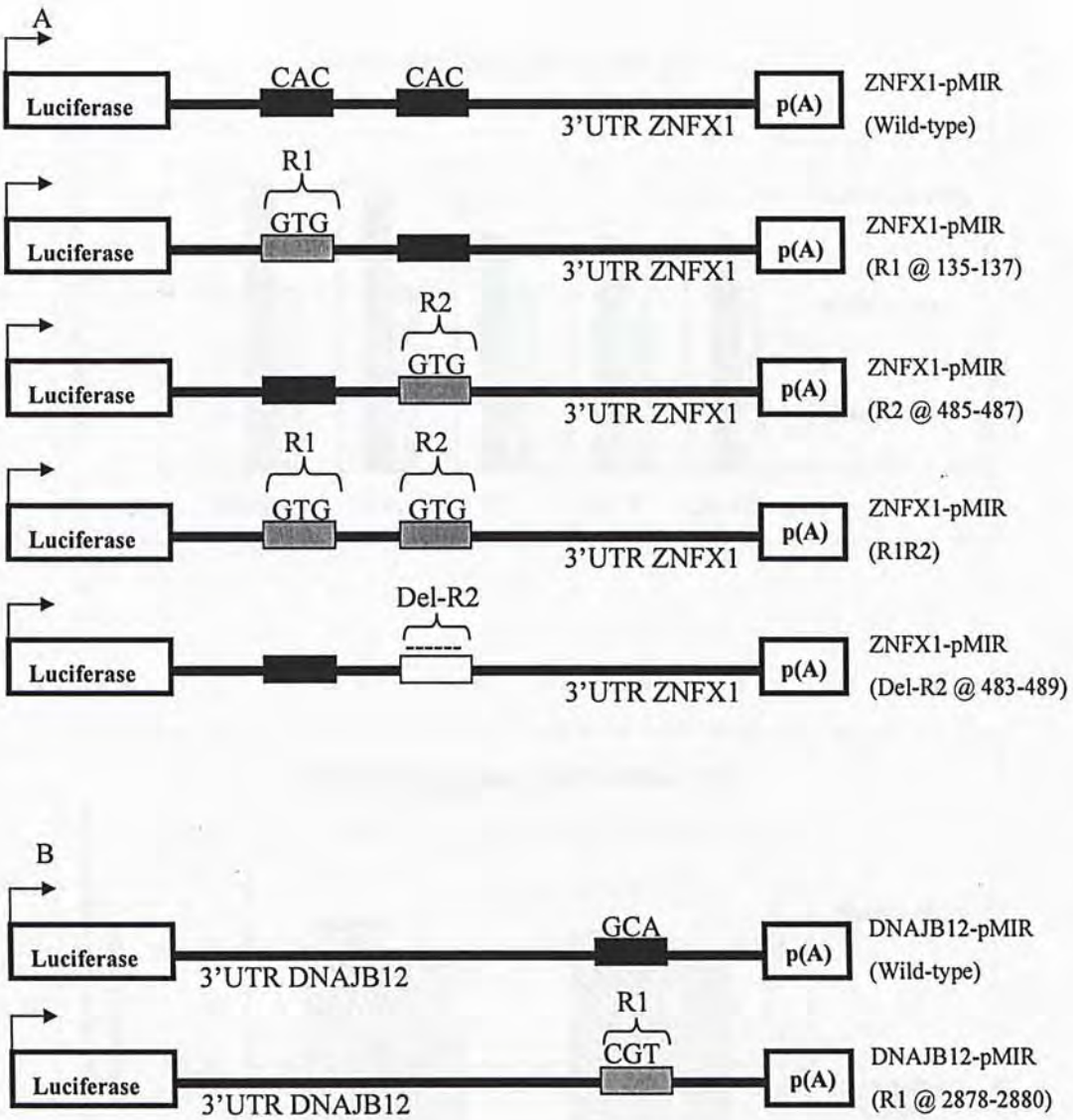

Figure 3.8 Luciferase constructs with mutations at microRNA target sites.
Shown in (A) are the luciferase constructs carrying specific mutations for ZNFX1, while shown in (B) are the luciferase constructs for DNAJB12.

A

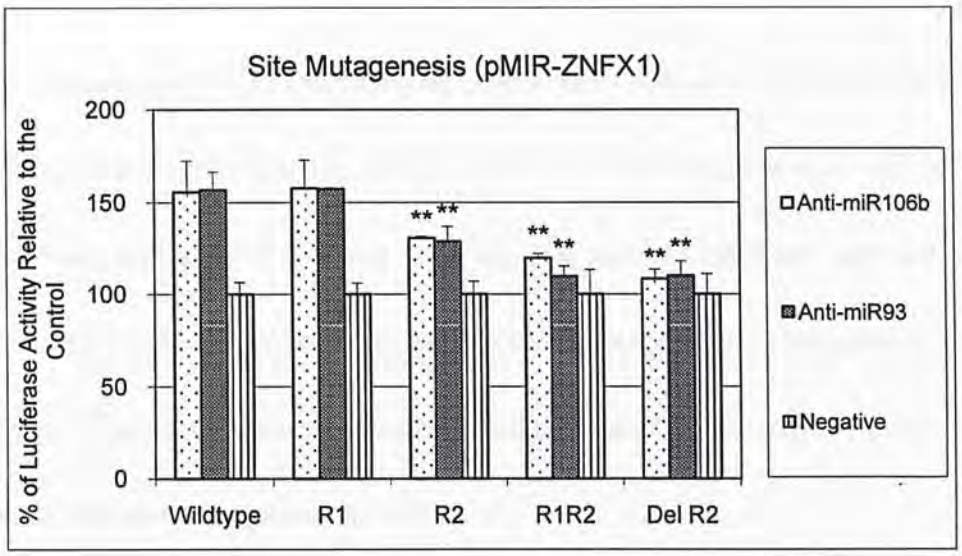

B

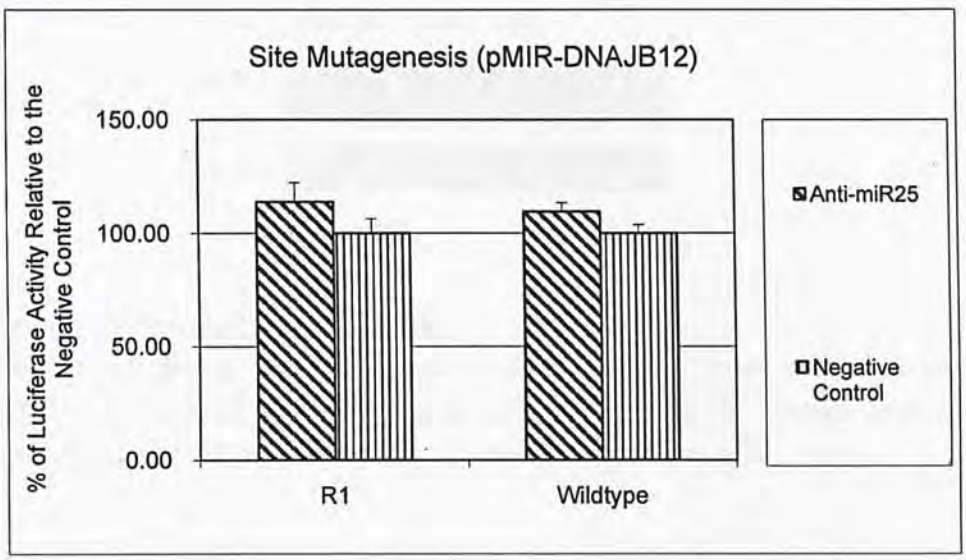

Figure 3.9 Site-directed mutagenesis of 3'UTR.

Relative luciferase activity of (A) ZNFX1-pMIR, and (B) DNAJB12-pMIR harboring various specific mutation(s). Specific expression vector was co-transfected along with miRNA inhibitors (anti-miR-106b/miR93/miR25) in DAOY. The luciferase activities were normalized with Renilla, and compared to their relative negative controls ±SD.

3.3.10 Effects of Anti-microRNA Inhibitor on ZNFX1 Protein Levels

Considering ZNFX1 as a promising target of miR-106b and miR-93, western blot analysis was performed to test whether the protein levels fluctuate upon inhibiting miR-106b and miR-93. It was observed that anti-miR-106b and anti-miR-93 increased ZNFX1 protein level (Figure 3.10), consistent with ZNFX1 being their direct target. Together with the real-time data, it is likely that miR-106b and miR-93 exhibit post-transcriptional regulation on ZNFX1.

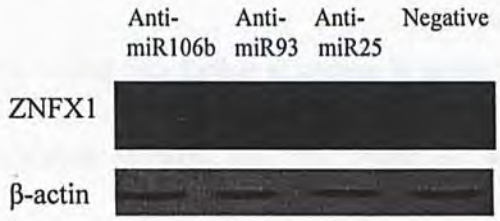

Figure 3.10 Western Blotting of ZNFX1.
There was a general trend of increase in ZNFX1 protein levels when miR-106b, miR-93, and miR-25 were inhibited in DAOY. Shown is the Western blot with anti-ZNFX1 and anti-actin antibodies. β-actin was used as a loading control.

3.4 Discussion

Increasing data support the value of microRNA expression profiling to unravel the role of microRNA in contributing to the pathogenesis of different human malignancies. In a study conducted previously by our group, up-regulation of the miR-106b-25 cluster was observed in primary MB samples compared to the normal cerebellum samples. The up-regulation of this cluster of microRNA was also reported in Ferretti *et al.*'s microRNA profiling study in human medulloblastoma (Ferretti et al. 2009). Thus, it raises the possibility that the differential expression of this cluster of microRNA may be linked to the oncogenic properties of MB. Focusing on the miR-106b-25 cluster, the expression of this cluster was further examined in seven MB cell lines. Stem-loop qRT-PCR amplification revealed that this cluster of microRNA is differentially expressed in different MB cell lines, and with remarkable up-regulation in ONS-76 and DAOY. With these preliminary data, our main goal in this chapter was to identify target genes regulated by miR-106b-25 cluster using the computational approach. By employing seven target prediction algorithms, altogether ~75,000 potential target genes were generated for this cluster of microRNA (Table 3.5). By combining the seven prediction lists and selecting only the common ones, we were able to successfully cut down the number of potential target gene to ten or less (Table 3.6). Although

microRNAs are known to regulate their targets mainly through translational repression, others have also reported that they achieve silencing of cellular messages through mRNA cleavage (Li et al. 2009). Therefore, as a preliminary screen for transcriptional regulation, qRT-PCR was used to examine the effects of inhibiting the miR-106b-25 cluster on the selected potential target genes (ZNFX1 as the potential target gene for miR-106b & miR-93, while DNAJB12 as the potential target gene for miR-25). From the qRT-PCR analysis of ZNFX1 mRNA expression level in DAOY, it was found that upon inhibition of miR-106b and miR-93, the mRNA level of ZNFX1 was increased (Figure 3.6A). Similar result was also observed for the DNAJB12 mRNA expression level when miR-25 was inhibited (Figure 3.6B). These data suggest the presence of miRNA: target mRNA interactions. For further verification using in-vitro models, luciferase reporter assay was carried out to determine if there was direct interaction of miR-106b and miR-93 at the 3'UTR of ZNFX1, as well as miR-25 at the 3'UTR of DNAJB12. Upon treatment with anti-miR-106b and anti-miR-93, there was significant increase in luciferase activity observed for ZNFX1 (Figure 3.7A). Similarly, upon miR-25 inhibition, there was also a statistically significant increase in luciferase activity observed for DNAJB12 (Figure 3.7B). These data suggest that their 3'UTRs exert direct interactions with the miR-106b-25 cluster. Consistently, the increase in luciferase activity was only observed in specific microRNA that was chosen

for its own model. For instance, ZNFX1 was predicted as the target gene for miR-106b and miR-93 only, increase in luciferase activity was only observed when miR-106b and miR-93 were inhibited, but not for miR-25. Similarly for DNAJB12, which was predicted to be a target gene for miR-25, significant increase in luciferase activity was observed only when miR-25 was inhibited. These data suggest that miRNA:mRNA interactions are indeed very specific, and that subtle differences between homologue microRNA may have meaningfully purpose leading to different functional importance (Petrocca et al. 2008). In an effort to narrow down the specific recognition site(s) on the 3'UTR, site-directed mutagenesis was used to induce mutation on the predicted target sites. There were two conserved regions and two poorly conserved regions for miR-106b, while there was only one conserved region and one poorly conserved region predicted for miR-93 (Table 3.2). The two predicted target regions for miR-93 (both conserved (R2) and poorly conserved (R1)) share the same locations on the 3'UTR of ZNFX1 as miR-106b; therefore, they were chosen for site-directed mutagenesis study. Of the two regions examined, only the conserved region at 484^{th}-491 (R2) resulted in a decrease in the relative change in luciferase activity, while mutation on the poorly conserved region showed similar change in relative luciferase activity as compared to the change observed for the wild-type construct (Figure 3.9). This observation re-enforces the idea that microRNAs are

normally highly conserved in the genomes of related species (Yoon and De Micheli 2006), and perhaps more emphasis may be put onto testing conserved regions prior to testing poorly conserved regions when performing verification tests. Also, double mutation at both target sites (R1R2) showed a similar decrease in the change in relative luciferase activity as the single mutation at the conserved site (R2), which again showed that the poorly conserved site have little contribution in miR-106b and miR-93 target regulation. Deletion of the entire seed region at the conserved site (Del-R2) showed further decrease in the change in luciferase activity as compared to mutating only three consecutive nucleotides at the seed region (R2). This observation suggests that complementarity has significant impact on microRNA regulation and that the degree in complementarity is directly related to the degree of regulation. As proposed in section 3.3.9, if the mutated region were the true critical recognition site for the specific miRNA, we would expect no change or very minimal change in the relative luciferase activity between the treatment with inhibitors and its negative control because the suppression effects of endogenous miRNAs on the recognition site(s) were abolished by the induced mutation. However, in our ZNFX1 model, although the change in relative luciferase activity for the R2 mutated constructs was clearly reduced by approximately half fold compared to the change observed for the wild-type construct, but it was not as ideally expected to be totally abolished. This observation

could be explained by the fact that R2 is only one of the critical recognition sites targeted by miR-106b and miR-93 on the 3'UTR of ZNFX1. Another critical recognition site may exist along the 3'UTR of ZNFX1; therefore, when endogenous miRNAs were inhibited using miRNA inhibitors, the miRNA suppression at this unknown recognition site was relieved. As a consequence, the change in relative luciferase activity was not totally abolished. In fact, there are still one conserved region (located at 1324^{th}-1331^{st}), and one poorly conserved region (located at 979^{th}-985^{th}) on the 3'UTR of ZNFX1 predicted by TargetScan 4.2 remained to be verified. Now, let's consider the other predicted target gene, DNAJB12. Previous luciferase reporter assay had demonstrated a significant increase in luciferase activity for DNAJB12 upon inhibition of miR-25. However, site-directed mutagenesis at the predicted conserved region resulted in similar change in relative luciferase activity as the wild-type construct (Figure 3.9B). In other words, mutation at this site has no effect on the regulation mediated by miR-25, and thus not a critical recognition site for miR-25. There is still hope that somewhere along the 3'UTR of DNAJB12 may harbor a target site for miR-25; however, it is definite that this particular region is a false positive indicating that there are potential flaws embedded in the prediction programs. It is still too early to tell whether DNAJB12 is truly a false positive, but discouragingly we are back to the trial and error stage. Shifting back our focus on

ZNFX1, because microRNAs function to regulate gene expression at the post-transcriptional level (Olive et al. 2010), western blot analysis was performed to examine the protein level of ZNFX1 upon inhibition of miR-106b, miR-93, and miR-25. It was observed that upon treatment with anti-miRNA inhibitors (anti-miR-106b, anti-miR-93, and anti-miR-25) the protein level for ZNFX1 was increased. The slight increase in protein level observed for treatment with anti-miR-25 along with the two other treatments may be due to the fact that this cluster of microRNA works in a cooperative manner, affecting other factors that might exert an indirect feedback on miR-25. However, whether the observed increase in protein level is purely through post-transcriptional miRNA regulation or a combination with translational regulation still remain to be determined. Taken altogether, we determined that ZNFX1 is a target regulated by miR-106b and miR-93 in MB. NFX1-type zinc finger-containing protein 1 (ZNFX1) is located on chromosome 20q13.13. It is conserved in dog, cow, mouse, rat, chicken, fruit fly, and mosquito (Ashburner et al. 2000). ZNFX1 is not commonly studied in human; therefore, its exact function is still unknown. However, it is proposed to interact selectively and non-covalently with metal ions (Ashburner et al. 2000). In a study of Atlantic cod conducted by Rise et al., the transcript level of ZNFX1 was found to be upregulated by more than 10 fold in Atlantic cod with high nodavirus carrier state (Rise et al. 2010). Nodavirus is found to target nervous tissue

causing viral nervous necrosis that leads to neurological damage, swimming abnormalities, and morbidity in aquacultures (Rise et al. 2010). This observation suggests that ZNFX1 may be involved in the contribution of nervous necrosis associated with Nodavirus. Although Rise et al. used Atlantic cods as their study model, it is possible that ZNFX1 may be linked to brain abnormality in human too. As a future direction, using MB as a model may help to elucidate the functions of ZNFX1 and its link to human brain diseases.

In this chapter, we see that computational approaches for most time rely on few established principles when predicting targets, such principles include recognition patterns, number of complementarity, and degree of conservation between species etc... However, it cannot reveal novel aspects of microRNA target recognition (Orom and Lund 2010), and despite false positives, it gives no information on false negative targets. Nevertheless, it forms a basic framework and generates lists of putative targets for researchers to start with.

CHAPTER 4:- EXPERIMENTAL APPROACH IN INDENTIFYING POTENTIAL TARGETS

4.1 Introduction- Experimental Approach

As discussed in the previous chapter, identification of microRNA targets using the computational approach proves to be challenging because prediction programs are usually based on a few of the established principles of microRNA regulatory mechanisms, namely, the idea of complementarity. However, microRNAs and their targets often form "imperfect" base-pairing with each other, especially in animals. Therefore, many researchers use the experimental approach to identify potential targets for microRNAs. A number of different experimental approaches are available; some of the commonly used ones are transcriptome analyses, immunoprecipitation of RISC complex, and polysomal distribution analyses (Orom and Lund 2010).

Transcriptome analysis involves examining the shift in mRNA expression profile using microarrays (Lim et al. 2005). As a consequence of over-expressing or inhibiting specific microRNAs, a large set of microRNA targets can be identified (Lim et al. 2005). Although the microarray approach allows one to analyze a large set of target genes at the same time, it is limited to target genes that are regulated at the transcriptional level (Orom and Lund 2010). It gives no information on target genes that are regulated primarily at the translational level.

Perhaps immunoprecipitation of tagged RISC complex may be a better approach to investigate target genes that are translationally regulated by microRNAs. As mentioned before, mature microRNAs are incorporated into RISC, and bound by members of the Argonaute (Ago) family to mediate their regulatory effect as a complex (Karginov et al. 2007). Several reports support the identification of miRNA targets by immunoprecipitating either the tagged or endogenously expressed Ago proteins to analyze the associated mRNAs of specific microRNA. Through subsequent analyses of the immunoprecipitates using the microarrays, targets that are regulated at both the transcriptional and translational level could be identified (Karginov et al. 2007).

It has been reported that microRNA targets exhibit change in the polysomal distribution (Nelson et al. 2004), as such potential targets can be identified by over-expressing or inhibiting specific microRNAs followed by subsequent analyses of their polysomal spectrum and associated mRNA using micro-arrays (Nelson et al. 2004). Assuming that a transcript's position in the polysome profile somewhat reflects the degree of its translation and that shifts into the heavier polysome fraction reflect enhancement of translation, Nakamoto et al. had successfully identified mRNAs that were regulated by specific endogenous miRNA by analyzing the difference in mRNA abundance in the polysome profile followed by miRNA knockdown (Nakamoto et al. 2005). More specifically, they found that the mRNA levels of several genes, such as

CYR61 and CDK6 were significantly increased in the heavy polysome fractions following miR-30a-3p knockdown (Nakamoto et al. 2005). Subsequent analysis of the identified transcripts revealed partial complementarity to miR-30a-3p, yet none of the identified transcripts were predicted by commonly used computational programs (Nakamoto et al. 2005). Their data again re-enforce the importance of experimental approaches in identifying miRNA target genes.

As described, there are several ways to identify miRNA targets experimentally, in this chapter we have employed a biochemical method to identify potential target genes that are regulated by the miR-106b-25 cluster. Using C. elegans as a study model, Andachi had developed a novel method to identify target genes regulated by specific microRNAs by isolating cDNA clones of mRNAs that formed base pairs with the microRNA of interest (Andachi 2008). *C. elegans* is the most intensively studied organism in the field of microRNA research with more than 150 microRNAs identified (Andachi 2008). Using this method, Andachi had successfully isolated cDNA clones of *lin-4* and its known target gene *lin-14*, as well as identified and confirmed new target for *let-7* (Andachi 2008). Adapting from Andachi's method, we aim at identifying target genes regulated by specific microRNA of interest in human cells, specifically in MB cells. The goal is to isolate a library of cDNA clones that contain partial sequence of potential target genes for miR-106b in DAOY. The schematic of the method is

shown in Figure 4.1. The method relies on the base pairing regulatory mechanism of miRNAs and their targets, which allows endogenous miRNAs to act as primers in the reverse-transcription reaction to synthesize cDNAs that contain partial sequence of the target genes. Then, through series of specific enzymatic digestion and ligation to pre-designed adaptors, sequences specific to the miRNA of interest can be amplified and inserted into pCR2.1 vectors creating a library of cDNA clones. Subsequent sequencing of the vectors would reveal partial sequence that shows homology to mRNA transcripts, which may be potential targets of the given miRNA.

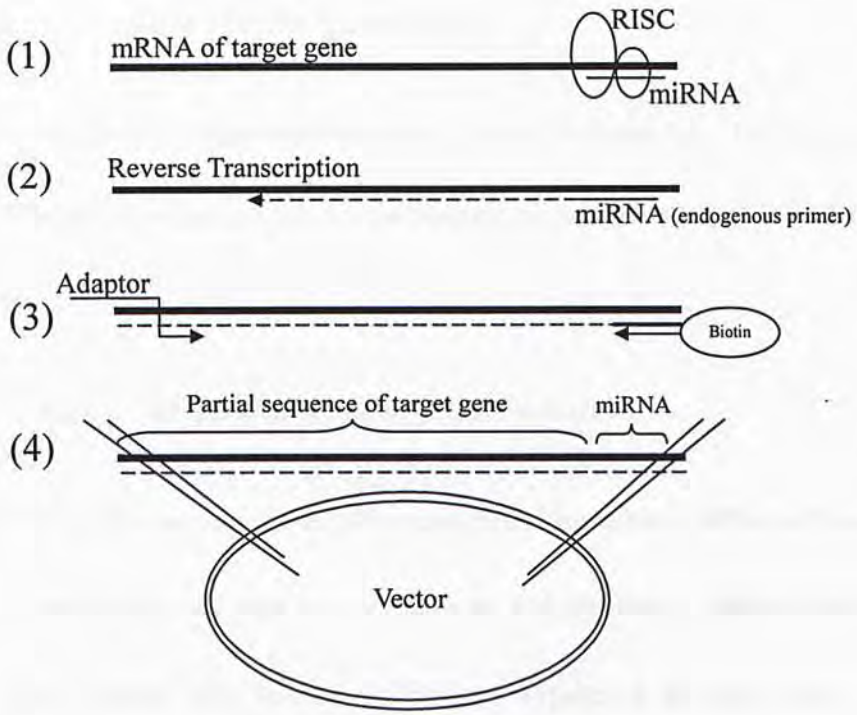

Figure 4.1 Schematic diagram of the biochemical method.

(1) Under normal physiological condition, miRNAs are incorporated into RISC. Together as a complex, it binds onto the mRNA of its target. (2) The endogenously expressed miRNAs would act primers to initiate reverse transcription, enabling the synthesis of first-strand cDNA complementary to the target gene sequence. (3) Amplification of the target gene sequence using the specially designed Adaptor and a miRNA primer labeled with biotin would selectively amplify the desired sequence for the miRNA of interest. (4) Using restriction enzyme digestions, the sequences of the potential target genes are cloned into the vectors for subsequent sequencing analysis.

4.2 Methods

4.2.1 Isolation of cDNA Clone Library

The detailed schematic diagram of the method is shown in Figure 4.1. The step by step description of the procedures will be described in the sections that follow (4.2.1.1 to 4.2.1.15).

4.2.1.1 Preparation of Cytoplasmic Extracts

DAOY cells were cultured in 100mm plates, and harvested at 60% confluence in order to obtain cells that were actively growing and involved in protein synthesis. Cells were washed with ice-cold 1xPBS and trypsinized for cell count. All centrifugations from here on in this section were kept at 4°C. Approximately $1x10^5$ cells were centrifuged at 1000 rpm for 3 min to obtain the cell pellet. After removing the supernatant, the cell pellet was re-suspended in 10 vol of ice-cold cell fractionation buffer (PARIS^{TM} Kit, Ambion). The cell extract was incubated on ice for 5 min, and centrifuged at 500g for 3 min to separate the nuclear and the cytoplasmic cell fractions. While avoiding the nuclear pellet, the supernatant was collected and centrifuged at 13,000rpm for 5 min to precipitate cell debris and the nuclei. The supernatant was mixed with 0.1vol of 10% (w/v) SDS, and incubated on ice for 1 min. The short-term

treatment with SDS at low temperature was included to destabilize the RISC as it may reduce the efficiency of the reverse transcriptase and the efficiency of miRNA priming. The general procedures in this section are depicted in Figure 4.2.

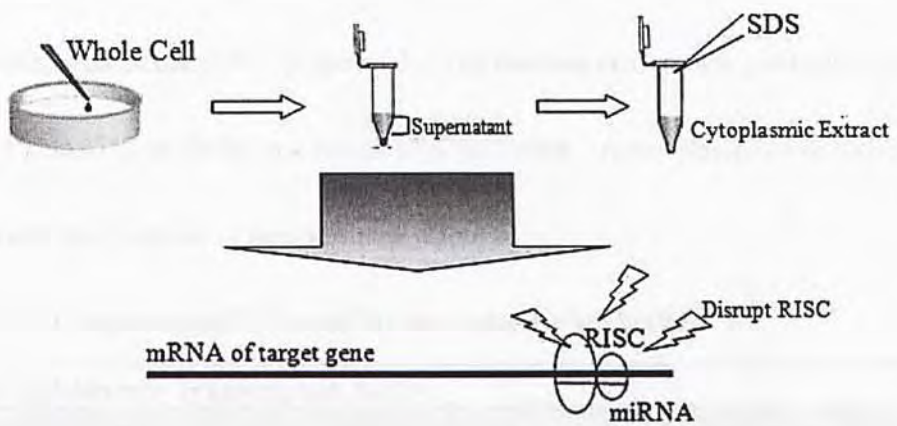

Figure 4.2 Preparation of cell extracts.
DAOY cells were collected using PARIS™ Kit. The cytoplasmic fraction was subjected to SDS treatment to disrupt the RISC complex.

4.2.1.2 Reverse Transcription Using Endogenous miRNA as Primers

After the short-term treatment with detergent, the reaction mixture was immediately diluted to 200 vol using "1st-round"-reverse-transcription buffer. The components of the "1st-round"-reverse-transcription buffer are listed in Table 4.1. In this reverse transcription reaction, endogenous miRNAs would act as primers to synthesize first-strand cDNA (Figure 4.3) The reaction mixture was gradually raised from 4°C to 37°C in 10min, and kept at 37°C for 1 hour. Actinomycin D was included to prevent the synthesis of second-strand cDNA.

Table 4.1 Components of "1st-round"-reverse transcription buffer

1st-Round-Reverse Transcription Buffer	
Reagents	**Concentration**
First-Strand Buffer	1X
DTT	10mM
Actinomycin D	50ng/μL
dNTP	0.5mM
RNasin Plus Ribonuclease Inhibitor (Promega)	1U/μL
Superscript III (Invitrogen)	5U/μL

Figure 4.3 Reverse transcription using endogenous miRNAs as primers.
Endogenous miRNAs ( ) act as primer to start reverse transcription to synthesize a first-strand cDNA ( ).

4.2.1.3 Collection of Polynucleotides

After the 1st round of reverse transcription, the reaction mixture was mixed with 0.02 vol of 10%SDS, and subjected to phenol/chloroform/isoamyl alcohol (25:24:1, pH 8) (Invitrogen) extraction. 1vol of phenol/chloroform/isoamyl alcohol was added, and gently mixed with the reaction mixture. The mixture was then centrifuged at 13,000rpm for 5 min at 4°C. The aqueous layer was transferred to a new tube, and polynucleotides were collected by ethanol precipitation (0.1 vol of 3M sodium acetate and 2 vol of 100% ethanol). After thorough mixing, the mixture was centrifuged at 13,000rpm for 30min at 4°C. Finally, the pellet is air-dried for 15min.

4.2.1.4 Synthesis of Second-strand cDNAs

The collected polynucleotides were incubated in the 2nd-round-reverse transcription buffer (components are listed in Table 4.2) at 25°C for 10 min, followed by 70°C for 30 min. Tth was included in this step because it is a DNA polymerase that catalyzes the polymerization of nucleotides into DNA using an RNA template in the presence of manganese, which allow for synthesis of DNA complementary to both first-strand cDNA and the miRNA (Figure 4.4).

Table 4.2 Components of "2nd-round"-reverse transcription buffer

2nd-Round-Reverse Transcription Buffer	
Reagents	**Concentration**
"1st-Round"-Reverse Transcription Buffer	1X
$MnCl_2$	1mM
dNTP	0.2mM
Tth DNA Polymerase (Promega)	0.2U/μL
RNasin Plus Ribonuclease Inhibitor (Promega)	1U/μL

Second-strand cDNA Synthesis

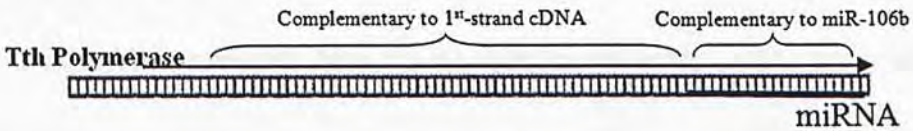

Figure 4.4 Second-strand cDNA synthesis.
Using RNAs as templates, Tth polymerase can synthesize DNA complementary to both the 1st-strand cDNA and the miRNA (as shown with the arrow).

4.2.1.5 PCR Purification of Double-stranded cDNAs

The double-stranded cDNA was purified with the PCRquick-spin™ PCR purification kit (Tech Dragon Ltd.) according to the Manufacture's protocol, and as described in the previous chapter.

4.2.1.6 Restriction Endonuclease Digestion

As a result of the PCR purification step, double-stranded cDNA of various lengths were produced. For the purpose of subsequent cloning, the cDNA fragments were digested with NlaIII (NEB) (Figure 4.5). NlaIII has a recognition sequence (CATG) recognizing four nucleotides consisting of A, T, G, and C, thus it is expected that most of the unknown target sequences would by chance contain at least one recognition site of this endonuclease. 10μL of purified cDNA, and 0.5μL of NlaIII were added into 1x T4 ligation buffer (NEB) to make up a final vol of 15μL. The reaction mixture was incubated at 37°C overnight. Note that the digestion was carried in T4 ligation buffer (NEB) for subsequent ligation reaction without the need for additional purification step to avoid loss of sample.

Endonuclease Digestion with NlaIII

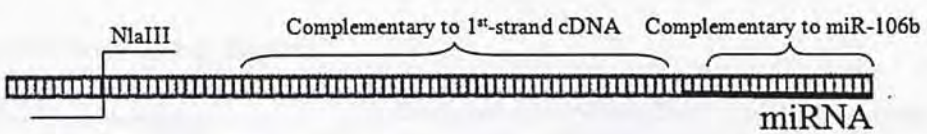

Figure 4.5 Restriction enzyme digestion.
It is expected that the target gene mRNA would by chance contain the recognition sequence of NlaIII (CATG).

4.2.1.7 Ligation to Adaptor

After the enzymatic digestion with NlaIII, the digested fragments were ligated to the specially designed adaptor oligonucleotide (Adaptor) for subsequent PCR amplification. The sequence for the adaptor oligonucleotide can be found in Table 4.3, and the schematic diagram can be found in Figure 4.6. All of the digested products were carried to the ligation reaction (1uL of T4 ligase (NEB), 20μM adaptor oligo, 1mM ATP) to make up a final volume of 25μL. The mixture was incubated for 2 hours at room temperature.

Table 4.3 Sequences of adaptors and primers

Sequences of Adaptors and Primers	
Name	**Sequences (5'→3')**
Adaptor (Adaptor-BamHI-**NlaIII**)	CCTACTGAGGGATCC**CATG**
Biotin-miR106b (Biotin-miR106b)	Biotin-TAAAGTGCTGACAGTGCAGAT
Longer Adp (Longer Adp-BamHI-**NlaIII**)	AAGCAGTTGTCCTACTGAGGGATCC**CATG**
Nested miR-106b (NotI-**miR-106b**)	ATGCGGCCGC**TGCTGACAGTG**

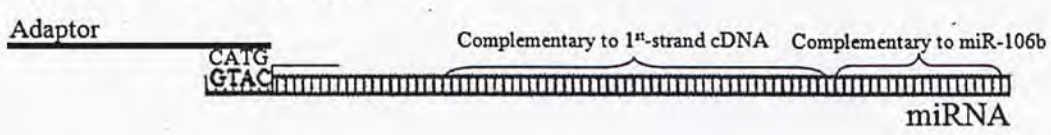

Figure 4.6 Ligation of adaptor
After the NlaIII digestion, the sequences are ligated to the adaptor for subsequent PCR amplification.

4.2.1.8 PCR Amplification with Biotin-labelled miRNA PCR Primers

The cDNA fragments that were successfully ligated to the adaptor were then subjected to PCR amplification with the adaptor primer (Adaptor) and a biotin-labelled miR-106b PCR primer (Biotin-miR-106b). The exact sequence of the primers can be found in Table 4.3. The concentrations for the reagents used in the PCR amplification are summarized in Table 4.4. 1μL of the ligation product was added to the PCR amplification reaction mixture (final vol: 20μL). The PCR amplification conditions are listed in Table 4.5. Note that the annealing temperature was experimentally determined as the highest temperature able to amplify the miRNA genes from genomic DNA. The schematic diagram of this step is shown in Figure 4.7

Table 4.4 Reagents for PCR amplification

PCR Amplification	
Reagents	**Concentration**
Gold Buffer (ABI)	1X
$MgCl_2$	2.5mM
dNTP	0.3mM
Tth DNA Polymerase (Promega)	0.2U/μL
FW primer	0.25μM
RV primer	0.25μM
AmpliTaq Gold® (ABI)	1U/μL

Table 4.5 PCR amplification condition

PCR Amplification			
Stage	**Temperature**	**Time**	**Cycle(s)**
Activation	95°C	10 min	---
Denaturing	95°C	30sec	
Annealing	55°C	30sec	40
Extending	72°C	1 min	
Final Elongation	72°C	10 min	
Hold	4°C	----	

PCR Amplification with Biotin-Labelled miRNA Primer

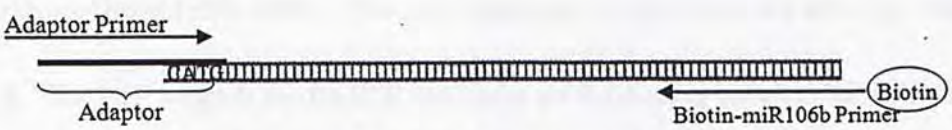

Figure 4.7 PCR amplificaiton with biotin-labelled miRNA primers.

The 2nd-round PCR amplification involves amplifing the polynucleotides by the adaptor primer and the biotin-labelled miR-106b primer

4.2.1.9 Capture of Biotin-labelled PCR Fragments

The amplified products with biotin-labelled PCR primer were captured using the SoftLink™ Soft Release Avidin Resin (Promega). The SoftLink™ Resin was prepared according to the manufacturer's protocol for batch-capture. In brief, the resin was first equilibrated with Gold Buffer (ABI), and then all of the biotinylated products were added to the resin. The capture was incubated overnight at 4°C on rotating platforms. Through series of washing with 1x Gold Buffer, the products were finally eluted by adding 5mM biotin into the buffer. The resin was gently rocked for 1 hour at 4°C. The resin was allowed to settle, and centrifuged at <500g for 5 min at 4°C to obtain the elution fractions.

4.2.1.10 Introducing NotI Recognition Sequence

An aliquot of the collected PCR fragments was amplified with a longer adaptor (Longer-Adp) and a nested miR-106b PCR primer containing the NotI recognition sequence (Nested miR-106b). The exact sequences of the primers are shown in Table 4.3. The PCR reagents and the PCR conditions are the same as shown in Table 4.4 and 4.5. NotI recognition sequence was introduced so that the PCR fragments could be ligated into the expression vector, which contains the NotI site. The schematic diagram is shown in Figure 4.8.

Final-round of PCR Amplification

Figure 4.8 Final round of PCR amplification.
The final-round of PCR amplification involves using the longer-adp primer and the nested miR-106b primer containing the NotI recognition sequence to prepare for cloning into the expression vector.

4.2.1.11 Cloning into the pCR2.1 Vector

Before cloning the PCR fragments into the pCR2.1 vector (Invitrogen), the circular vector was first digested with BamHI (NEB) and NotI (NEB) to cut open the circular vector. The following reaction was prepared in 2 sets: one for the sample reaction, while the other for a negative control to check for self-ligated vector. 2μg of the vector was added to the digestion mixture (1x NEB Buffer 3, 1U NotI, 1U BamHI) making up the total volume of 10μL. The digestion was incubated at 37°C overnight. The digested vector was loaded onto 1% (w/v) agarose gel for gel purification. Gel purification was performed using the standard protocol (Qiagen). On the other hand, the cDNA fragments were similarly digested with BamHI and NotI and then subjected to PCR purification. The schematic diagram can be found in Figure 4.9.

Cloning into pCR2.1

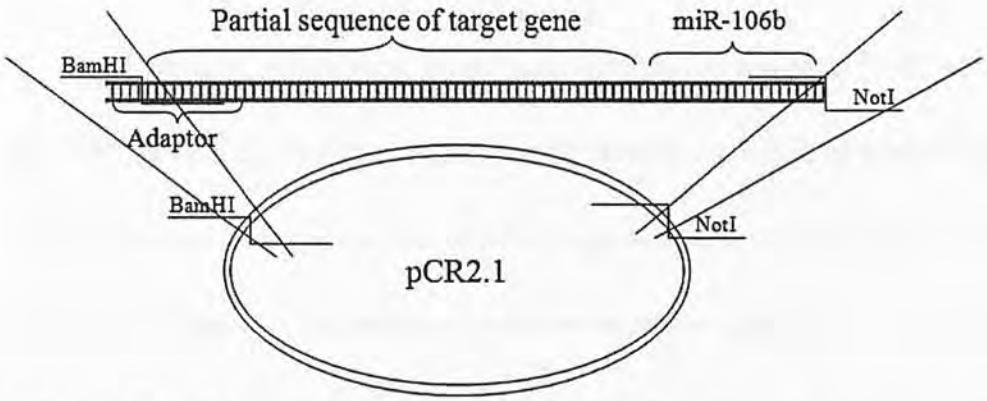

Figure 4.9 Cloning potential sequence into the pCR2.1 vector.
After digesting both the cDNA fragments and the expression vector with the same restriction enzymes (BamHI & NotI), the potential sequences are ready to be cloned into pCR2.1 vector.

4.2.1.12 Ligation of the cDNA Fragments and the pCR2.1 Vector

The (NotI & BamHI) digested cDNA fragments and the pCR2.1 expression vectors were subject to ligation. The reaction condition is similar to those described in section 3.2.5.4 in the previous chapter.

4.2.1.13 Transformation

Transformation is performed using DH5α competent cells as described in the previous sections. One plate was prepared for the negative control to check for self-ligated vectors without insertion of the cDNA fragments, while the other plate contains our ligated samples.

4.2.1.14 Preparation of Purified Plasmids

Single bacterial clones were picked and inoculated overnight at 37°C with vigorous shaking in 2mL of LB broth to prepare for plasmid purification on the next day. 96 individual clones were picked, and subjected to purification using the QIAprep Spin Miniprep Kit (Qiagen). The procedures were carried out using the standard protocol. In brief, the pelleted bacterial cells were re-suspended in 250μL of Buffer P1 and vortexed until no clumps remained. Then 250μL of Buffer P2 were mixed gently with the mixture. Shortly, 350μL of Buffer N3 was added, and centrifuged at 13,000 rpm for 10 min at 4°C. The supernatant was loaded onto the QIAprep spin column, and centrifuged for 1 min at 13,000 rpm. After discarding the flow-though, 750μL of Buffer PE was added to the column and centrifuged again for 1 min. The column was centrifuged for an additional 1 min to remove residual wash buffer. Then the plasmid was eluted by adding 50μL of Buffer EB through centrifugation. After the purification of the plasmids, we have successfully created a library of clones that contain partial sequence of our target gene for miR-106b.

4.2.1.15 Sequencing Analysis of the cDNA Clone Library

The library of cDNA clones were subjected to sequencing analysis for the presence of the potential sequence for the target gene of miR-106b. 50ng/μL of the

purified plasmids were sent to TechDragon Ltd. for sequencing analysis using the M13 FW primer (5'- GTAAAACGACGGCCAG-3').

4.2.2 Real-time PCR Target Gene Expression in Cell Lines

Real-time PCR assay was used to investigate the expression level of ZNF793 and CLN8 in ONS-76 and DAOY. The procedures for total RNA extraction from cell lines, cDNA preparation from reverse transcription, and the real-time PCR amplification were performed similarly to those as described in the previous sections. The sequences for the real-time PCR reaction are listed in Table 4.6. Samples were prepared in triplicates, and evaluation of the expression levels were normalized to the internal control (RPS3).

Table 4.6 Primers used in real-time PCR amplification for ZNF793 & CLN8

Target Gene	Primers (forward & reverse) 5'→3'
miR-106b targets	
ZNF793	CGT CTC AGT GGG TTA TGA AGG CAC C
	TCT TCC CAA CAG TGG CAG CCC
CLN8	GCT GAG TGG CAG CCC AGA TTG A
	AAG CCA GCG ACC ATC AGC GT

4.2.3 Real-time PCR Target Gene Expression Upon Inhibition of miR-106b

Real-time PCR assay was used to investigate the effect of inhibiting miR-106b on the gene expression of ZNF793 and CLN8 in DAOY. The procedures for

transfection of microRNA inhibitor, total RNA extraction, cDNA preparation from reverse transcription, and the real-time PCR amplification were performed similarly to those as described in the previous sections. The sequences for the real-time PCR reaction are listed in Table 4.6. Samples were prepared in triplicate, and evaluation of the expression levels were normalized to the internal control (RPS3).

4.2.4 Cloning of Potential Target Genes into pMIR Luciferase Expression Vector

The cloning of the potential target gene ZNF793 and CLN8 was performed similarly as described in the chapter (section 3.2.5). The sequences of ZNF793 3'UTR, and CLN8 3'UTR were prepared from genomic DNA using PCR amplification as previously mentioned. The PCR primers are listed in Table 4.7.

Table 4.7 PCR primers for 3'UTR cloning

PCR Primers (5'→3')		
ZNF793		**Start Site**
ZNF793-FW	GTCTGCTTCCCTGAGTTCT	16101st
ZNF793-RV	AACTGGTTTGGCATTCTTGG	16983rd
CLN8		
CLN8-FW	GCGAATGATGGCTTTTGAAT	16866th
CLN8-RV	TGGTGGGGGTTAAACTCCAA	17717th

4.2.5 Site-directed Mutagenesis

According to our sequencing analysis, the predicted seed region for miR-106b was mutated in the 3'UTR of CLN8 using the QuickChange®II Site-Directed Mutagenesis Kit (Stratagene). The procedures were performed according to the standard protocol and as in section 3.2.6, and the mutation primers are listed in Table 4.8.

Table 4.8 Primers for site-directed mutagenesis of CLN8

CLN8 Mutation Primer	**Sequence (5'→3')**
CLN8-Mut-FW	CGACGTAATCCCAG**G**A**G**GA**T**GGGAGGCCGAGGC
CLN8-Mut-RV	GCCTCGGCCTCCCA**T**C**C**T**C**CTGGGATTACGTCG

**The bold nucleotides were the mutated sites where G replaces C, while A replaces T and vice versa.

4.2.6 Luciferase Reporter Assay

Luciferase reporter assay was performed for verification of the potential target genes (ZNF-793 & CLN8). The assay was performed similarly as previously mentioned in section 3.2.7.

4.3 Results

4.3.1 Sequencing Analysis of the cDNA Clone-Library

The clones in the cDNA library are expected to contain partial sequence of the target gene; therefore, sequencing analysis can reveal the identity of the target genes. The schematic diagram of the expected construct of our cDNA library is shown in Figure 4.10. The potential sequence of our target gene should be enclosed by the two restriction enzymes that were used for cloning into the expression vector (BamHI & NotI). As depicted in the diagram, the miR-106b sequence should follow immediately after our potential sequence. Notice that the potential sequence should only contain partial sequence of the target gene because it was randomly truncated by NlaIII for the purpose of cloning into the expression vector. However, through sequencing analysis of the partial sequence with the use of the BLAST program, we should be able to find the identity of the potential target genes. Having said that, there are several criteria for analyzing our clones:

1) Clones should contain the full sequence of miR-106b

2) The length of the potential sequence is preferably >10 base-pairs

3) Blast search of the potential sequence falls in the 3'UTR of mRNA of a gene

4) Regions on the mRNA following the potential sequence should preferably show

partial homology to miR-106b recognition sequence

Construct of cDNA Clone

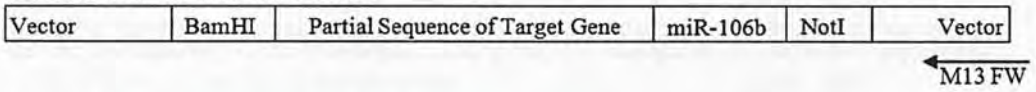

Figure 4.10 Final construct of a cDNA clone.
Shown is the expected final construct of a cDNA clone prepared by series of reverse-transcriptions using miR-106b as an endogenous primer in the experimental approach. M13 FW was used as the sequencing primer.

96 clones were sent for sequencing analysis. The statistical summary is presented in Table 4.9. Of the 96 clones sent for sequencing analysis, 77 showed a clear sequencing result. 3 out of 77 clones were not able to re-locate the full length sequence of miR-106b, suggesting that they were likely to be clones containing random sequences. Of the 74 potential sequences isolated, 10 of them fall on the 3'UTR of a transcript. The exact sequence of the potential sequences and the locations on the corresponding target gene are listed in Table 4.10. After the blast analysis, ZNF793 and CLN8 were selected based on their homology to miR-106b at the seed region. The detailed blast results are shown in Figure 4.11. ZNF793 and CLN8 were selected for further downstream verification because they show extensive homology to the seed region of miR-106b (Figure 4.11 marked by asterisks).

Table 4.9 Statistical summary of the cDNA library

cDNA Library (miR-106b)	
Clear sequencing result	77/96 (80%)
Presence of miR-106b sequence	74/77 (96%)
Potential Sequence <10 base-pairs	19/74 (26%)
Potential sequence falls on a transcript	22/74 (30%)
Potential sequence falls on 3'UTR	10/74 (14%)

Table 4.10 Blast result for potential sequences

cDNA Library (miR-106b)			
Clone#	Potential Sequence	Gene	Location
7	TGCAGAAGTCCGCGGACGAGA AAAGCCGCAGCACGTTGACCA GAGGGAACATGGGATCCGAG	H. sapiens chromosome 20 open reading frame 54	Exon 4
19	GTGAGCCACCCCACCCAGCTGA ACTTTTCTTTTGTACATG	H. sapiens zinc finger protein 793 (ZNF793)	3'UTR
		H. sapiens ceroid-lipofuscinosis, neuronal 8 (epilepsy, progressive with mental retardation) (CLN8)	3'UTR
23	GGTGCATGGGATCCGAGC	H. sapiens protein tyrosine phosphatase, receptor type, S (PTPRS)	5'UTR
		H. sapiens potassium voltage-gated channel, Saw-related subfamily, member 1 (KCNC1)	3'UTR
24	CAGATGTGTAGACGCCCCATGG	H. sapiens protocadherin 20 (PCDH20)	Exon 4
37	AAGGACAACGTGGCATG	Homo sapiens C-type lectin domain family 16, member A (CLEC16A)	3'UTR
38	GATGGGAGGCCATG	H. sapiens protein phosphatase methylesterase 1 (PPME1)	3'UTR
		H. sapiens F-box and leucine-rich repeat protein 7 (FBXL7)	3'UTR
44	GAAGCAATGGGCCATG	H. sapiens hypothetical protein LOC100291302 Chemokine XC receptor 1	3'UTR

61	TAAGCGTGATGACACATG	Homo sapiens solute carrier family 7 (cationic amino acid transporter, y+ system, member1 (SLC7A1)	3'UTR
86	CGTGCTGATGGAACTGTTGTACCATG	H. sapiens c-ros oncogene 1, receptor tyrosine kinase (ROS1)	Exon 20
		H. sapiens minichromosome maintenance complex component 3 associated protein (MCM3Ap)	Exon 9
96	GAACAACAGAGTAGGGAAACGCATG	H. sapiens complement component 3 (C3)	Exon 20
104	GAGGCTCTTAAGCAGGGAGAACATG	H. sapiens phosphodiesterase 6A, cGMP-specific, rod, alpha (PDE6A)	Exon 13
108	GGACAGGGCGGTCATG	H. sapiens v-yes-1 Yamaguchi sarcoma viral related ocogene homolog (LYN)	Exon 13
		H. sapiens purinergic receptor P2Y, G-protein coupled, 8 (P2RY8)	Exon 2
		H. sapiens GATA binding protein 3 (GATA3), transcript variant 1	Exon 3
		H. sapiens serine peptidase inhibitor, Kunitz type, 2 (SPINT2), mRNA	3'UTR
142	GGAAACAGGGCATCTCAGATGGCCCCAAACATG	H. sapiens filamin C, gamma (actin binding protein 280) (FLNC), transcript variant 2 & 1	Exon 39
		H. sapiens nemo-like kinase (NLK)	Exon 11
152	CAGGAAGGAGCAGGGGGTGAAATGTTACAAATTCTAGAACTCAGAGAACTGAAGGTAATTACTTCCTTTTCAACTTGTGAAACATG	H. sapiens eukaryotic translation initiation factor 5A-like 1 (EIF5AL1)	3'UTR

ZNF793

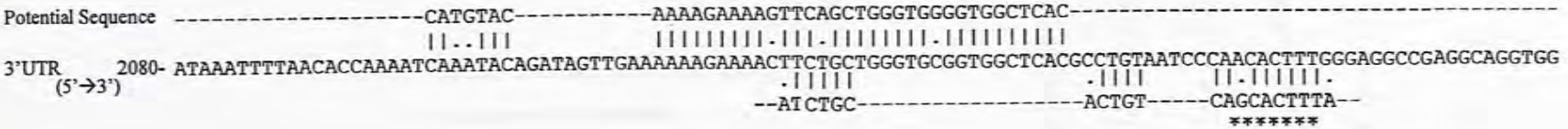

CLN8

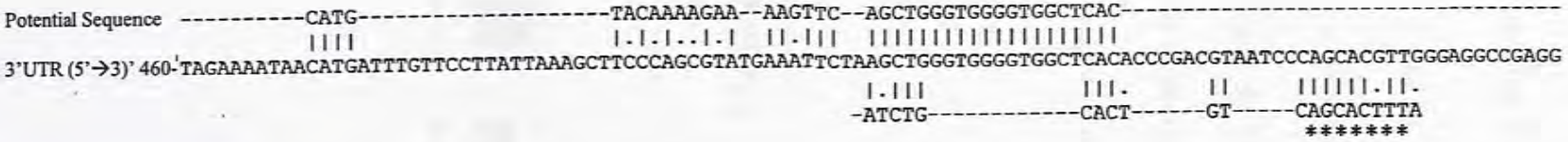

Figure 4.11 Blast result for ZNF793 and CLN8.

Base pairing of miR-106b with the mRNAs corresponding to the potential sequence isolated from the cDNA clones. The alignments in the 3'UTR were based on data in NCBI blast search (http://blast.ncbi.nlm.nih.gov/Blast.cgi), and manually adjusted using EMBOSS Needle_Align (http://www.ebi.ac.uk/Tools/emboss/align/). Identical nucleotides are shown by vertical bars. The miR-106b seed region (2-8th nucleotides) is shown by asterisks. From left to right, both the potential sequence and the 3'UTR of the target genes are in the 5' to 3' direction, while miR-106b sequence is oriented from 3' to 5'.

4.3.2 Expression Levels of Candidate Genes in MB Cell Lines

The expression levels of ZNF793 and CLN8 were first checked in ONS-76 and DAOY by qRT-PCR. Relatively lower expression of the mRNA level for both ZNF793 (Figure 4.12A) and CLN8 (Figure 4.12B) was observed in both cell lines (especially in DAOY) as compared to the normal cerebellum. The down-regulation of mRNA level of ZNF793 and CLN8 in cell lines is in line with the known up-regulation of miR-106b.

A

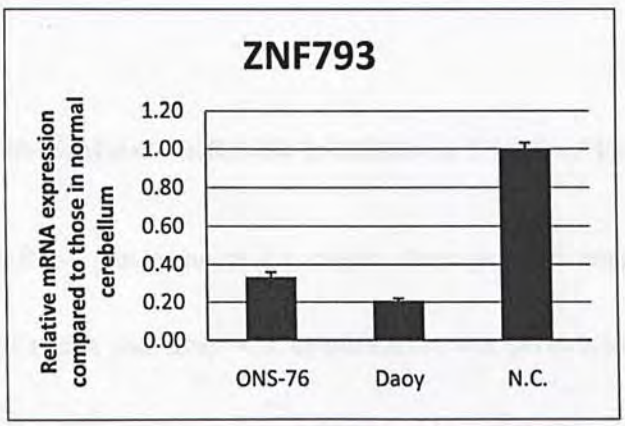

B

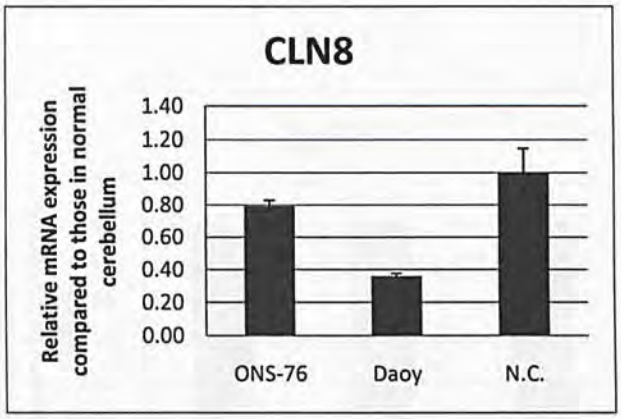

Figure 4.12 Quantitative real-time PCR for candidate genes.
Relative mRNA expression levels of ZNF793 (Figure 4.12A), and CLN8 (Figure 4.12B) compared to those in normal cerebellum. Each expression levels were normalized with their respective reference gene (RPS3) ±SD.

4.3.3 Effects of Anti-miR-106b Inhibitors on 3'UTR of Target Genes

Because miRNA can regulate its targets through both transcriptional and translational regulations, real-time PCR amplification was performed to examine the effect of anti-miR-106b inhibitor on the mRNA level of ZNF793 and CLN8. There was no significant change in mRNA transcript levels for both ZNF793 and CLN8 upon treatment with anti-miR-106b inhibitor in DAOY (Figure 4.13A & B). These data suggest that ZNF793 and CLN8 are likely not transcriptionally regulated by miR-106b.

A.

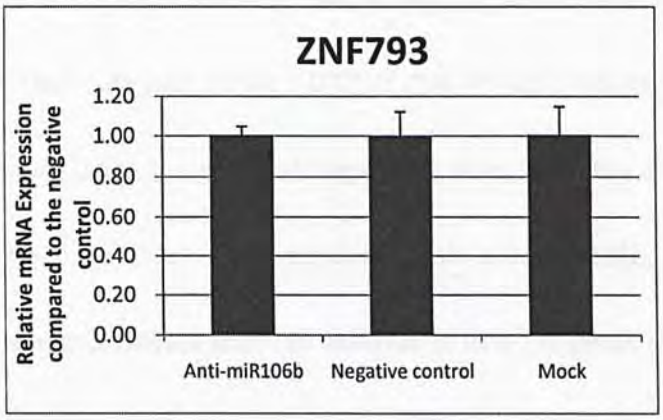

B.

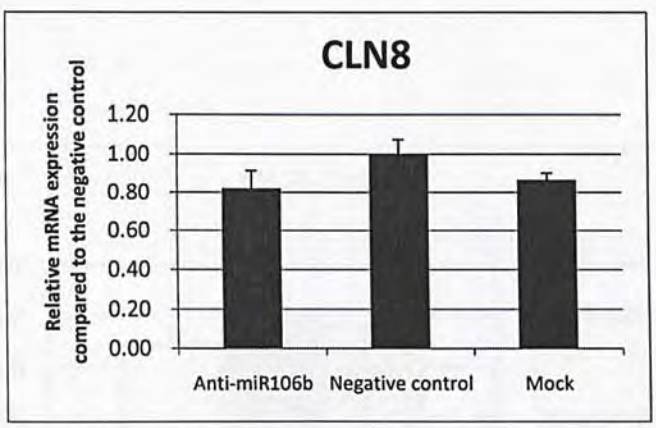

Figure 4.13 Changes in mRNA level upon treatment with miRNA inhibitors.

Quantitative real-time PCR was used to examine the temporal changes of mRNA transcription of ZNF793 (Fig 4.13A), and CLN8 (Fig 4.13B) in DAOY upon treatment with anti-miR-106b inhibitor. The average fold-change was first normalized using the internal reference gene (RPS3), then compared to the negative control ±SD. No significant change in mRNA level is observed.

4.3.4 Verification of Candidate Genes

Dual-luciferase reporter assay was used to verify if ZNF793 and CLN8 are true targets for miR-106b. Regions on the 3'UTR of ZNF793 (ZNF793-pMIR) and CLN8 (CLN8-pMIR) containing the potential target sites were separately cloned into the luciferase expression vector. Upon treatment with anti-miR-106b, there was no significant change in luciferase activities observed in ZNF793-pMIR (Figure 4.14A). On the other hand, significant increase in luciferase activity was observed for CLN8-pMIR upon treatment with miR-106b inhibitors (Figure 4.14B) suggesting that CLN8 may likely be a target gene regulated by miR-106b.

A

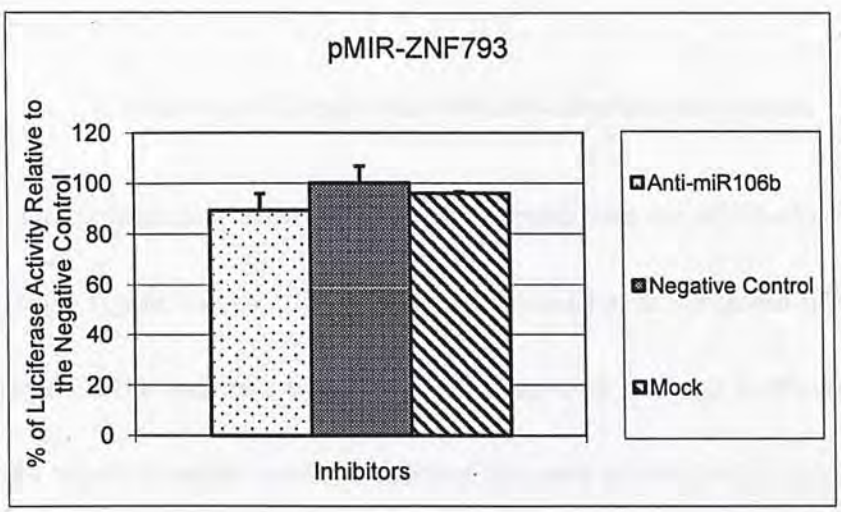

B

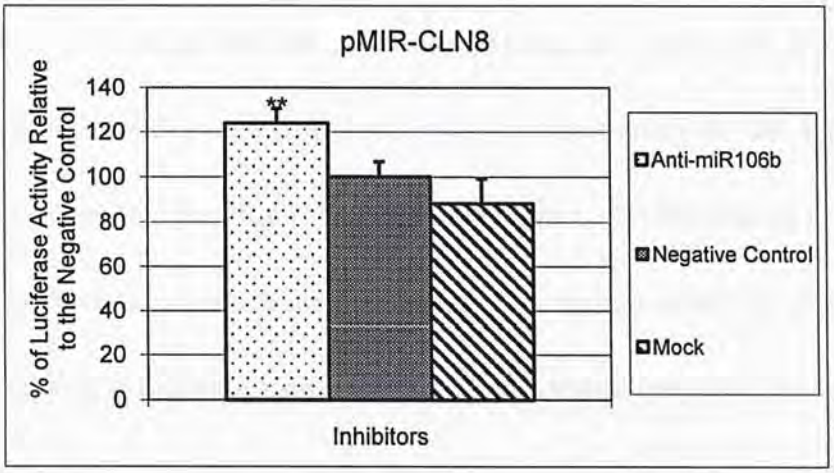

Figure 4.14 Relative luciferase activity of ZNF793-pMIR and CLN8-pMIR.
The histogram in Fig 4.14A shows the levels of luciferase activity of ZNF793-pMIR after treatment with anti-miR-106b in DAOY. The % of luciferase activities were normalized with renilla activity, and compared to their respective negative controls. Statistical comparisons were performed with Student *t*-test. Error bars represented SD. There was no significant change in luciferase activity observed. The histogram in Fig 4.14B shows that there was a significant increase ($p<0.02$) in luciferase activity for CLN8-pMIR after treatment with miR-106b inhibitor (asterisks).

4.3.5 Verification of Target Sites with Site-directed Mutagenesis

To further confirm whether the target site mapped from our cDNA-clone is the critical target region, site-specific mutation was induced at the proposed miR-106b target region. The construct with the mutated region is depicted in Figure 4.15. Under the negative control condition (without treatment of miR-106b), endogenous miR-106b would bind onto the proposed miR-106b recognition site on the wild-type CLN8 3'UTR suppressing the luciferase activity. Upon treatment with miR-106b

inhibitors, the endogenous miR-106b are inhibited, which would lead to a relief of the suppression of luciferase activity on the wild-type construct. As a result, an increase in the change in luciferase activity between the treatment group and the respective negative control is expected for the wild-type construct. On the other hand, if the mutated miR-106b recognition site were the true target region regulated by miR-106b, then the change in luciferase activity between samples treated with miR-106b inhibitor and the respective negative control should be minimal because the miR-106b recognition site is disrupted by the mutation. In other words, no suppression of luciferase activity (no change) is expected regardless if the samples were treated with miR-106b inhibitors or the negative control, because the mutated site is no longer susceptible to miR-106b regulation. From our data, the wild-type CLN8-pMIR, as expected, showed a significant increase in luciferase activity upon treatment with anti-miR-106b (Figure 4.16). After mutating the proposed miR-106b recognition site (R1), the change in luciferase activity was suppressed as compared to the change observed for the wild-type construct, indicating the importance of the recognition site and that it is likely the critical region targeted by miR-106b.

Luciferase 3'UTR CLN8 **CACGT** p(A) CLN8-pMIR (Wild-type)

R1

Luciferase 3'UTR CLN8 **GAGGA** p(A) CLN8-pMIR (R1 @ 483, 485, 487)

Figure 4.15 Mutation construct for CLN8-pMIR.

Shown above are the luciferase construct for the wild-type CLN8-pMIR, and the construct carrying specific mutation at 483rd, 485th, and 487th bp on the 3'UTR of CLN8. Note that the bold nucleotides indicate the mutated nucleotides where they are replaced by their complementary nucleotides.

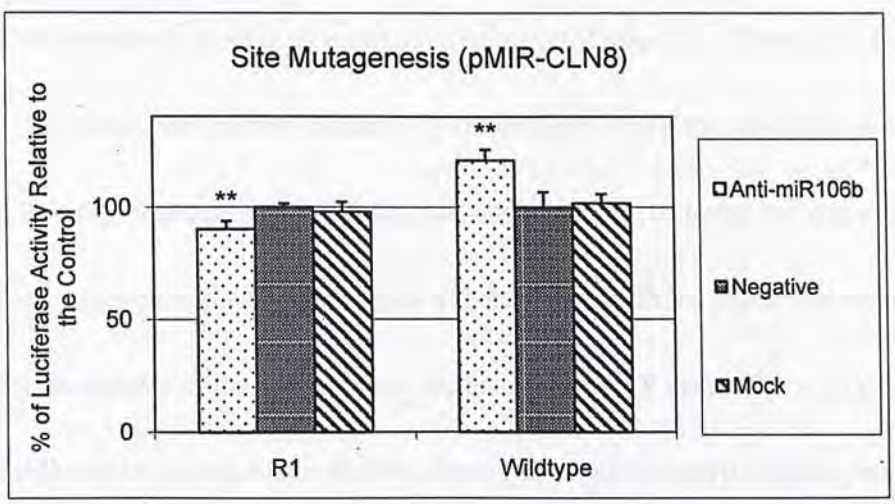

Figure 4.16 Site-directed mutagenesis of CLN8 3'UTR.

Shown is the relative luciferase activity for the wild-type and the mutated CLN8-pMIR. Luciferase activity was normalized with Renilla activity, and compared to their respective negative controls ±SD. Asterisks indicate Student *t*-test $p<0.04$.

4.4 Discussion

The biochemical approach in identifying target genes for specific miRNAs relies on the formation of base pairing between the miRNAs and their target genes; therefore, the miRNAs act as endogenous primers in the reverse-transcription reaction to synthesize first-strand cDNAs. However, to what efficiency can the miRNAs bind to their targets *in vitro* still remains unknown. From the sequencing data of our cDNA-clone library, many of the clones (~26%) carry only very short fragments (≤10bp) of the potential sequence (Table 4.10). This indicates that the initial reverse-transcription using miRNAs as primers may not be too efficient. Also, around 70% of the clones were false positives that do not fall on regions of a transcript (Table 4.9). These clones were likely amplified from random genomic DNA template during the amplification step using the adaptor primer and the biotin miR-106b primer. To lower the rate of false positive, a possible approach is to employ a shorter biotin-miRNA primer that excludes several nucleotides of the miRNA seed sequence from the 3' end. This may act as a screening step to select out false positive clones that do not contain the full sequence of the miRNA. For instance, if the potential sequences were amplified merely using our adaptor primer and the "shortened" biotin-miRNA primers from random genomic DNA templates, the chance of having false positives possessing the exact full length of our

miRNA recognition sequence including the purposely left out nucleotides is very slim. Despite the false positive clones, ZNF793 and CLN8 were isolated and chosen as potential candidates for further verification. Luciferase reporter assays indicated that ZNF793 were not directly involved in the regulation of miR-106b. On the other hand, luciferase reporter assay indicated that the 3'UTR of CLN8 interacts with miR-106b (Figure 4.14B). Site-directed mutagenesis further confirmed the critical target site at 483^{rd} -487^{th} bp on the 3'UTR of CLN8 (Figure 4.16). We determined that CLN8 is a target gene regulated by miR-106b. CLN8, also known as ceroid-lipofuscinosis, neuronal 8, is located on chromosome 8p23. It encodes a transmembrane protein belonging to the TLC domain, which is responsible for lipid synthesis, transport, or sensing (Ashburner et al. 2000). CLN8 is identified as one of the eight causative genes responsible for neuronal ceroid lipofuscinoses (NCL) (Vantaggiato et al. 2009). Patients with NCL usually have progressive ocular and cerebral dysfunction, which leads to cognitive/motor dysfunction and uncontrolled seizures (Wisniewski et al. 2001). More specifically, homozygous mutations in CLN8 are associated with progressive epilepsy and mental retardation (Vantaggiato et al. 2009). Although the physiological function of the protein encoded by CLN8 and the pathogenic mechanism(s) are still unknown, however, a recent study conducted by Vantaggiato et al indicated that CLN8 plays a role in cell proliferation during neuronal differentiation,

as well as in protection against cell death (Vantaggiato et al. 2009). As a future direction, we could study the function of CLN8 in MB through gene silencing approach. Collectively in this chapter, our data suggest that our method not only can identify target genes of specific miRNA, but also able to isolate the critical recognition site on the 3'UTR.

The knowledge on the pairing of mRNA and miRNAs such as Lin-4 and let-7 in C.elegans is well studied (Yoon and De Micheli 2006), and it provides the basic guidelines as to how miRNA interacts with target genes. However, this approach may not be equally efficient in human models as it is not surprising that the complexity of the gene regulatory network increases proportionally as the function of genomic complexity of an organism (Olive et al. 2010). From the top 10 results (~1500 clones) from 34 experiments, Andachi had eventually reached 74% efficient in identifying targets in his lin-14 model. It is still too early to judge whether the experimental approach used in this chapter is efficient or not as there are still other targets remained to be verified (Table 4.10). Perhaps, more trials are needed to improve the overall efficiency. Another factor to be considered in future trials is that some of the potential sequences fall in regions other than the 3'UTR (Table 4.10). Although in our study, we have primarily focused on potential sequences that fall on the 3'UTR, regulations of target genes through 5'UTRs are not rare events. It was demonstrated in Grey et al.'s

study of viral miRNA that miRNA meditates translational repression of multiple cellular genes by targeting their 5'UTR (Grey et al. 2010). Also, a study employed the use of tagging of the miRNA to identify targets of miRNA regulation had found that miR-10a can target mRNAs encoding ribosomal proteins through their 5'UTRs for enhancement of translation (Orom and Lund 2010). These data suggest that the well known complementary binding mechanism of miRNAs and mRNAs may be one of the many mechanisms as to how miRNA regulate their targets, and that targeting through the 5'UTR may be worthwhile to explore.

CHAPTER 5: FUNCTIONAL ASSAYS

5.1 Introduction- Functional Investigation of miR-106b-25 Cluster

The functions of microRNAs were originally described during normal development (Olive et al. 2010). Nowadays, in addition to normal development, miRNAs have emerged as important components of the oncogenic and suppressor network, playing important regulatory roles in cellular processes altered during tumour development (Olive et al. 2010). With the advance in molecular biology in the past decades, many initial studies were conducted to explore the expression patterns of miRNAs. Many miRNA profiling studies have indicated that aberrant expressions of miRNAs are frequently associated with various human cancers. Many reports have further demonstrated that the identified aberrant signatures of miRNAs are associated with distinctive clinical and pathological features that contribute to the phenotypes of the cancers (Calin and Croce 2006), thus these miRNAs are known as oncomiRs processing oncogenic properties or acting like tumor suppressor genes (Ambs et al. 2008). In particular, miR-106b-25 cluster was found to be up-regulated in primary MBs and in various MB cell lines. Up-regulation of miR-106b-25 cluster was also reported in other cancers including breast cancers, colon cancers, prostate cancers, and hepatocellular carcinoma (HCC) (Volinia et al. 2006). The miR-106b-25 cluster has been shown to have functional importance in cancers. For example, it was

demonstrated that the expression of miR-106b-25 cluster is necessary for cell proliferation and for anchorage-independent growth in HCC (Li et al. 2009). In addition, Li et al. have identified the transcription factor E2F1 as a target gene for miR-106b and miR-93, possibly inducing apoptosis by preventing excessively high expression of E2F1 (Li et al. 2009). In a study that attempted to functionally classify specific miRNAs and transcripts known for particular cellular pathways, several members of the miR-106b family were found to correlate with cell cycle-related transcripts (Ivanovska et al. 2008). More specifically, miR-106b was correlated with transcripts involved in DNA replication and mitosis, while miR-93 was correlated with regulator of DNA replication (Ivanovska et al. 2008). These data suggest that the up-regulation of the miR-106b-25 cluster may contribute to the highly proliferative nature of certain tumours (Ivanovska et al. 2008). Therefore, it is important to investigate the functional roles associated with the aberrantly expressed miR-106b-25 cluster. In order to investigate the functional importance of the miR-106b-25 cluster in MB, we have performed several functional assays: 1) MTT Assay, 2) Cell Cycle Profile, 3) BrdU Cell Proliferation Assay, and 4) Wound Healing Assay.

5.2 Methods

5.2.1 Cell Culture

ONS-76 were obtained from American Type Culture Collection (ATCC, Rockville, MD, USA) and maintained in RPMI (Gibco Invitrogen Corporation) supplemented with 10% FBS (Gibco Invitrogen Corporation). Culturing procedures and conditions were performed similarly as described in section 3.2.2.1.

5.2.2 Over-expression of miR-106b Mimic

Over-expression of miR-106b mimic (Ambion) was carried out using Lipo2000 according to the standard protocol provided by the manufacturer. Ectopic expression of miR-106b mimic was assessed by co-transfecting the mimic and the luciferase expression vector cloned with the reverse complement sequence of miR-106b (pMIR-106b). The co-transfection and the luciferase reporter assay were performed similarly as described in chapter 3, section 3.2.3.2.1 with the exception of replacing the inhibitor with the miR-106b mimic and its corresponding negative controls.

5.2.3 MTT Assay

Inhibition of the miR-106b-25 cluster:

The effect of inhibiting the miR-106b-25 cluster on cell growth for adherent cell lines was studied using MTT assay. $1.2x10^3$ ONS-76 cells, and $1.4x10^3$ DAOY cells were separately seeded into each well in a total volume of 100μL culture medium. Transient transfections of 5 pmol of each of the microRNA inhibitors (anti-miR-106b/anti-miR-93/anti-miR-25, negative, and mock (DEPC-H_2O) were transfected into the cells by Lipo2000 according to the suggested concentration for 96-well culture vessel. Each treatment was prepared in 8 replicates. The cell growth was assessed at day 4 by the MTT assay (Cayman Chemical, USA). 1/10 volume of the tetrazolium salt (MTT) was added into each well, and incubated for 4 hours at 37°C incubator. Residuals were removed, and an equal volume of dimethyl sulfoxide (DMSO) was added to each well to solubilize the formazan dye. The absorbance of the mixture was measured at 570nm, and normalized using the reference wavelength at 630nm.

Over-expression with miR-106b mimic:

The effect of over-expressing miR-106b on cell growth in DAOY was examined similarly as described above for the exception of using miR-106b mimic instead of inhibitors.

5.2.4 IC_{50} of Cisplatin

The half maximal inhibitory concentration (IC_{50}) was determined before testing the effect of inhibition of the miR-106-25 cluster on the sensitivity of cisplatin (Fluka). Mock transfection for DAOY cells were first performed in 6-well plate as previously mentioned. One day post-transfection, $1.2x10^4$ cells were re-plated into 96-well plate ready for treatment with various concentration of cisplatin. The tested concentrations of cisplatin were as follows: 8μg/mL, 6μg/mL, 4μg/mL, 3μg/mL, 2μg/mL, 1μg/mL, 500ng/mL, and 250ng/mL. At day 4, cells were subjected to MTT assay as mentioned above.

5.2.5 MTT Assay with Cisplatin Treatment

The sensitivity to cisplatin upon inhibition of the miR-106b-25 cluster in DAOY was examined using MTT assay. Transfection of microRNA inhibitors and the negative control were first performed in 6-well plate as described previously. One day post-transfection, the treated cells ($1.2x10^4$ cells/well) were re-plated into 96-well plate ready for treatment with cisplatin. 0.25μg/mL of cisplatin was added to each well too make up the total of 150μL volume. At day 4, cells were collected for MTT assay as described above.

5.2.6 Cell Cycle

Propidium iodide (PI (P4710), Sigma Aldrich) staining and flow cytometry were used to examine the stage of the cell cycle for DAOY cells upon inhibition of the miR-106b-25 cluster. Transfection of the microRNA inhibitors (anti-miR-106b/ anti-miR-93/anti-miR-25/negative control) and mock transfections were performed in 6-well plates similarly as described earlier. Samples were prepared in triplicates. At 24hr post-transfection, cells were harvested for flow cytometry analysis. In brief, cells were first washed with 1x PBS, and then trypsinized. After centrifugation, the cell pellets were re-suspended in 1mL of 1xPBS. Then 4 mL of absolute ethanol at -20°C were added in dropwise to the cell suspension for fixation of the cells for 15 min. Then cells were pellet, and ethanol was discarded. Cells were subjected to rehydration using 5mL of 1xPBS. After centrifugation, the cell pellets were re-suspended in a total of 200μL of TE buffer (1mL Tris-EDTA, 8μL of PI, and 4μL RNase). Then they were aliquot onto 96-well plate and incubated in the dark for 30 min for subsequent analysis using the BD FACSArray Bioanalyzer. A total of 10,000 events were counted for each sample. Data were analyzed with FlowJo software (Tree Star).

5.2.7 BrdU Cell Proliferation Assay

Cell proliferation was evaluated by bromodeoxyuridine (BrdU) incorporation analysis. (BD Pharmingen^{TM}). Transfection of microRNA inhibitors for DAOY in 6-well plate was performed similarly as described earlier. After 24 hours of transfection, DAOY cells were pulsed with 10μM of BrdU for 1 hour. After the incorporation, cells were fixed in 2mL of ice-cold 80% ethanol for 4 hours. After the fixation, cell pellets were collected, and re-suspended in 2mL of 2M HCl for 10 min. Subsequently, cells were subjected to several washes with 1xPBS with 1mM EDTA. Finally, cell pellets were re-suspended in 50μL of fluorescein isothiocyanate-conjugated anti-BrdU antibody in 1:4 ratio with the supplied incubation buffer, and incubated for 1 hr at 37°C. The percentage of cells labeled with BrdU was determined using flow cytometry.

5.2.8 Wound Healing Assay

The effect of inhibiting the miR-106b-25 cluster on cell migration was examined using the wound healing assay. DAOY cells were first transfected with microRNA inhibitors, negative controls, and mock controls in 60mm culture dishes according to the recommended concentration suggested by the manufacturers. In brief, 200 pmol of each of the microRNA inhibitors or the negative control were diluted in 500μL of

OPTI-MEM, while 10μL of Lipo2000 was diluted in 500μL of OPTI-MEM for 5 min. Then the two were mixed together and incubated for another 20 min. 1mL of the mixture was added to each of the appropriate wells containing 5mL of fresh medium. At 24 hours post-transfection, $2.2x10^5$ cells were re-plated into 6-well plate, and let settled overnight. The next day, the monolayer was scratched with sterile tips, briefly washed with 1x PBS. The cells were maintained in fresh medium, and the wound sizes were observed under microscope and photographed at different time points (0 and 24 hours). The percentage of area for the wound sizes were calculated using the ImageJ program.

5.3 Results

5.3.1 Effects of Inhibition of miR-106b-25 Cluster on Cell Growth

The effects of inhibition of miR-106b-25 cluster on cell growth were examined in two MB cell lines (ONS-76, and DAOY) using MTT assay. Inhibiting miR-106b and miR-25 resulted in significant reductions in cell growth for ONS-76 (Figure 5.1A), and inhibiting miR-106b resulted in significant reduction in cell growth for DAOY (Figure 5.1B).

A

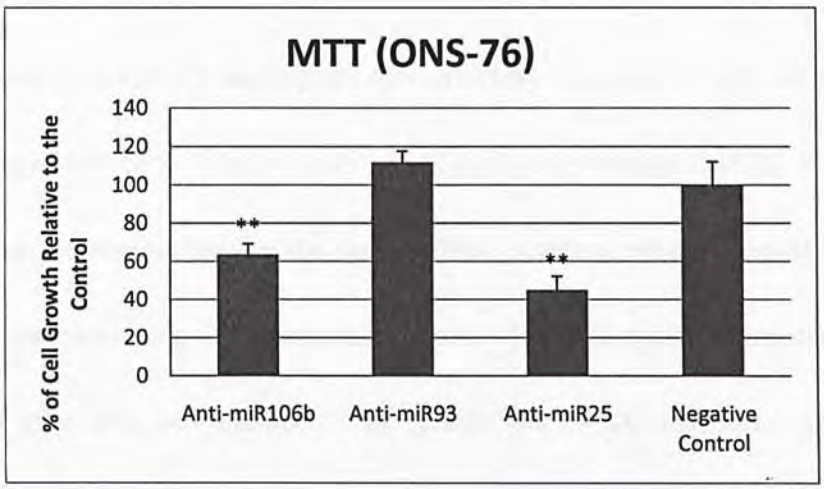

B

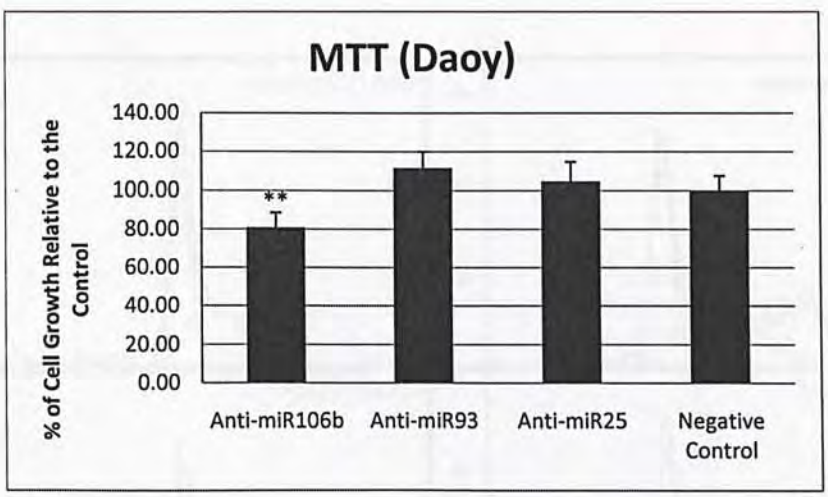

Figure 5.1 Effects of inhibition of miR-106b-25 cluster on cell growth.
Examination of cell growth was achieved using the MTT assay ONS-76 and DAOY. Measurements were taken at Day 4. The relative cell growth for each treatment was compared to the average of their respective negative controls (anti-miR negative control) ±SD. All assays were performed in 8 replicates. Asterisks indicate Student *t*-test with $p<0.00$.

5.3.2 Cell Cycle Distribution Analysis

Propidium iodide (PI) staining and flow cytometry were used to study the effects of inhibition of the miR-106b-25 cluster on cell cycle progression in DAOY. PI binds to DNA by intercalating between the bases of DNA; therefore, cell cycle profile can be deduced by monitoring its fluorescent signals. The cell cycle progression was analyzed after 24hr post-transfection of specific microRNA inhibitors. Overall, inhibiting miR-106-25 cluster did not result in significant change in the distribution of the cell cycle profile (Figure 5.2A &B).

A

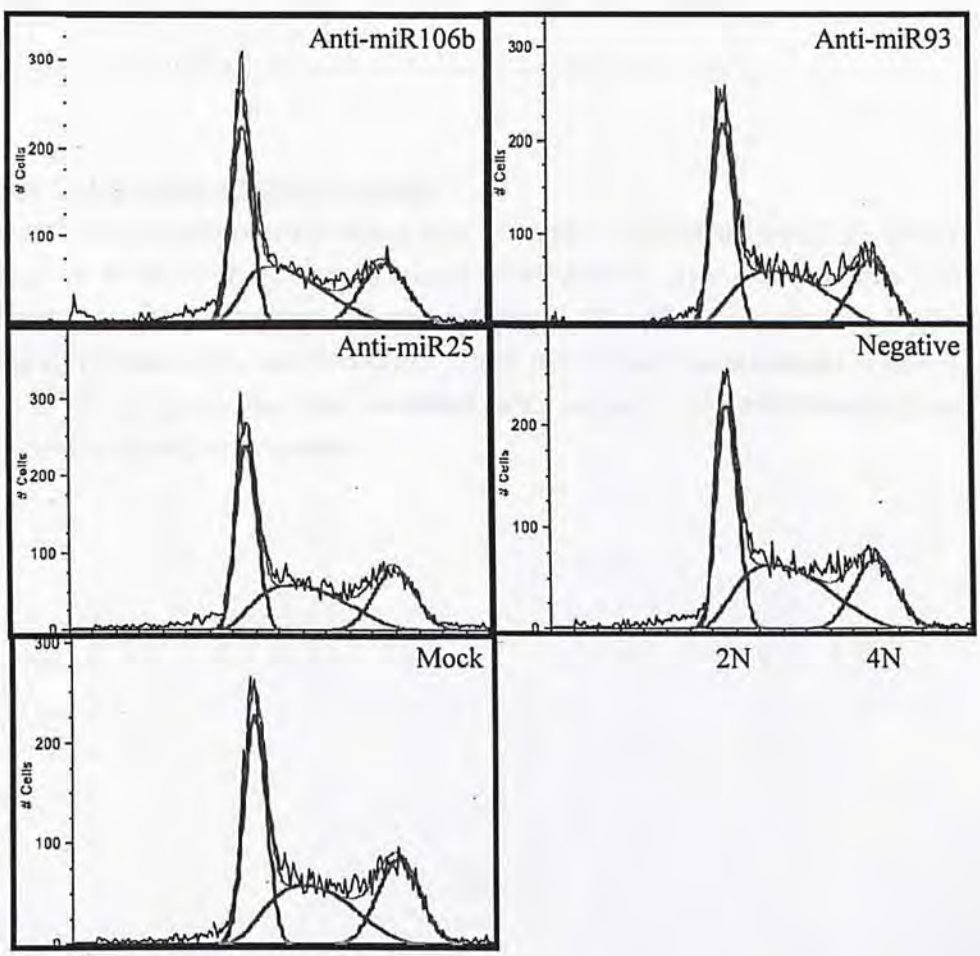

B

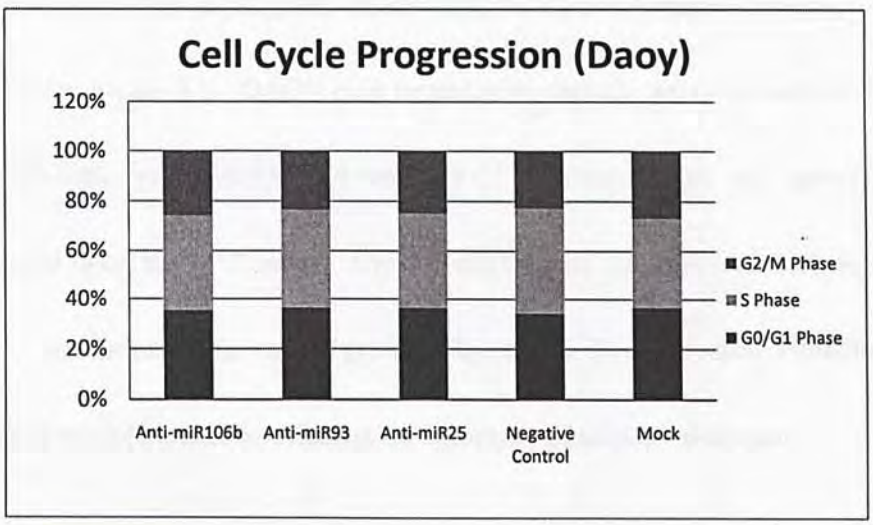

Figure 5.2 Cell cycle progression profile.

Cell cycle profiles were analyzed using flow cytometry. Shown in Figure 5.2A are the histograms of cell numbers (y-axis) against DNA content (x axis) for treatments with different microRNA inhibitors. Shown in Figure 5.2B is the summary chart for the cell cycle distribution for each treatment. There were no significant changes or shift in the cell cycle distribution upon treatment with anti-miR-106b/miR-93/miR-25 as compared to the negative controls.

5.3.3 Sensitivity to Cisplatin

As an anti-cancer drug that can cross-link DNA, cisplatin was used to examine the effect of inhibition of the miR-106b-25 cluster on cell growth. First, the 50% inhibition concentration (IC_{50}) for cisplatin on DAOY was determined to be 0.25μg/mL as shown in Figure 5.3. DAOY cells treated with cisplatin were co-transfected with anti-miR-106b, anti-miR-93, and anti-miR-25 inhibitors, and cell growth was monitored using the MTT assay. Upon treatment with the miRNA inhibitors, there were no significant changes in cell growth (Figure 5.4). In order words, inhibiting this cluster of microRNA has no effect on the sensitivity to cisplatin treatment.

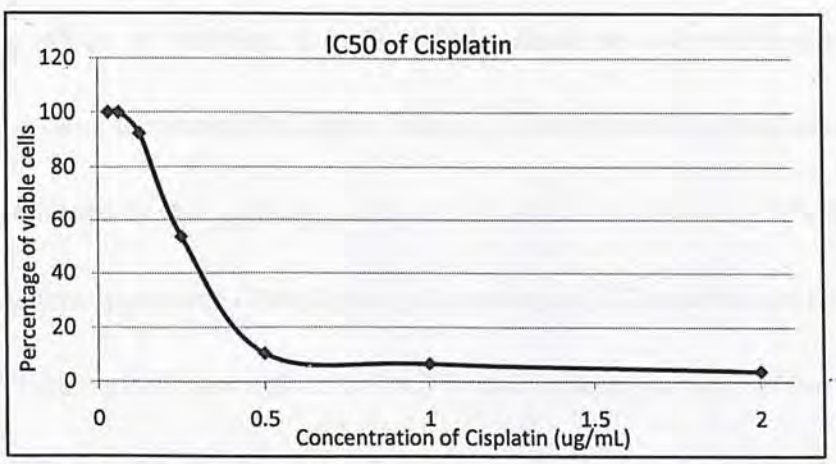

Figure 5.3 IC_{50} for cisplatin in DAOY.
The graph shows the percentage of viable cells after treatment with different concentration of cisplatin. The data points were shown as an average of 8 replicates. The IC_{50} is shown in the dashed lines, and it's approximated to be 0.25μg/mL.

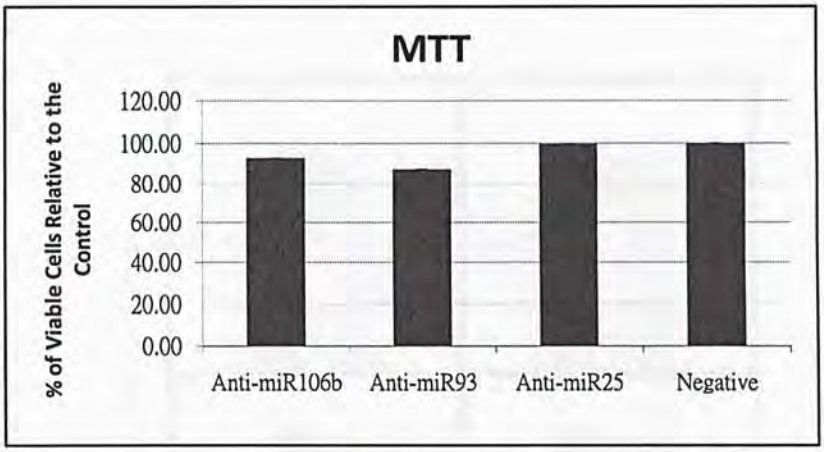

Figure 5.4 Cell growth after treatment with cisplatin in DAOY.

Upon treatment with 0.25μg/mL of cisplatin and various microRNA inhibitors (anti-miR106b, anti-miR93, and anti-miR25), there was no significant change in the percentage of viable cells observed compared to the negative control (treatment with anti-miR negative#1). Samples were taken from the average of 8 replicates, and expressed as % of viable cells relative to the control ±SD.

5.3.4 Cell Proliferation Assay

The effects of inhibiting the miR-106b-25 cluster on cell proliferation were examined using the immunofluorescent staining of incorporated bromodeoxyuridine (BrdU) followed by flow cytometry analysis to determine the frequency of individual cells that have synthesized DNA (S phase of the cell cycle). Treatment with inhibitors of miR-106b, miR-93, and miR-25 in DAOY cells resulted in a trend of decrease in cells in S Phase. Specifically, anti-miR-25 decreased up to approximately 10% of the cells in S phase (Figure 5.5B).

A

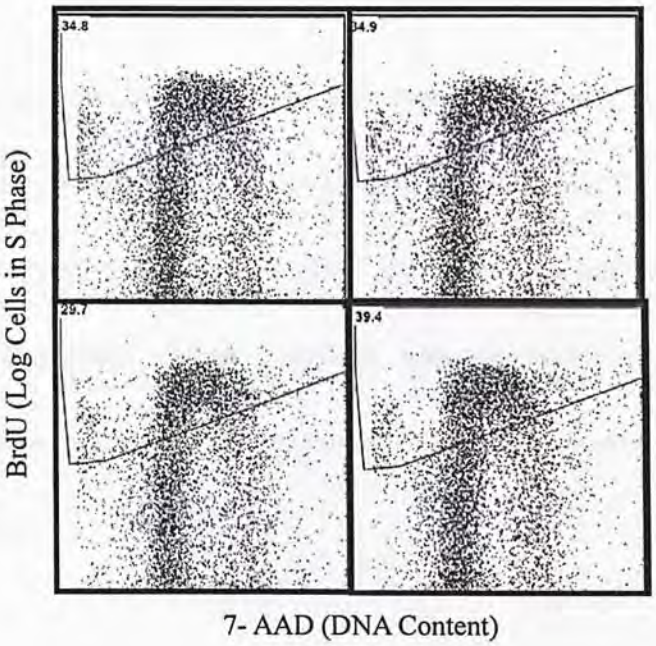

B

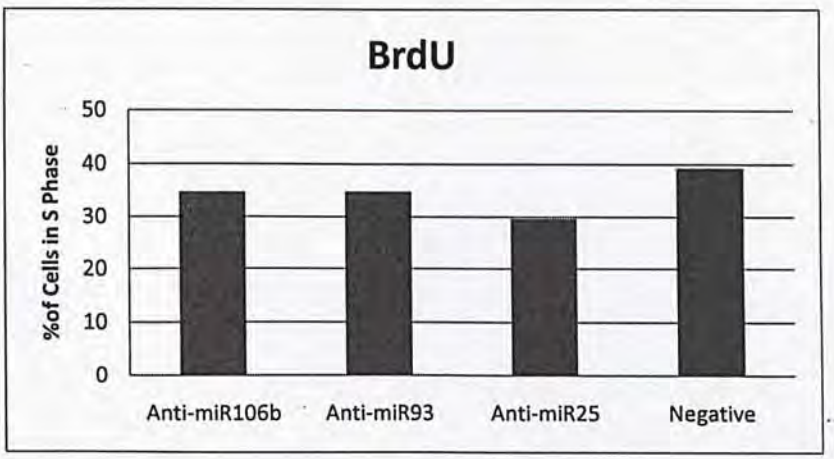

Figure 5.5 Effect of inhibition of miR-106b-25 cluster on cell proliferation.

Shown in Figure 5.5A are the scatter plots of fluorescence intensities of BrdU incorporation in log scale (y-axis) against DNA content (x-axis). The gated regions represent the S-phase populations (positive for BrdU incorporation). Figure 5.5B is the bar chart representing the percentage of cells in S phase.

5.3.5 Cell Motility

Wounds scratched on DAOY monolayer cells were monitored at 0, and 24 hours to investigate the migration properties upon inhibition of miR-106b, miR-93, and miR-25. Upon treatment with anti-miR106b, anti-miR-93, and anti-miR-25, there was a trend of decrease in cell motility. Upon treatments with the inhibitors, there were approximately 20% decreases in the percentage of wound recovered by the cells (Figure 5.6A & B).

A

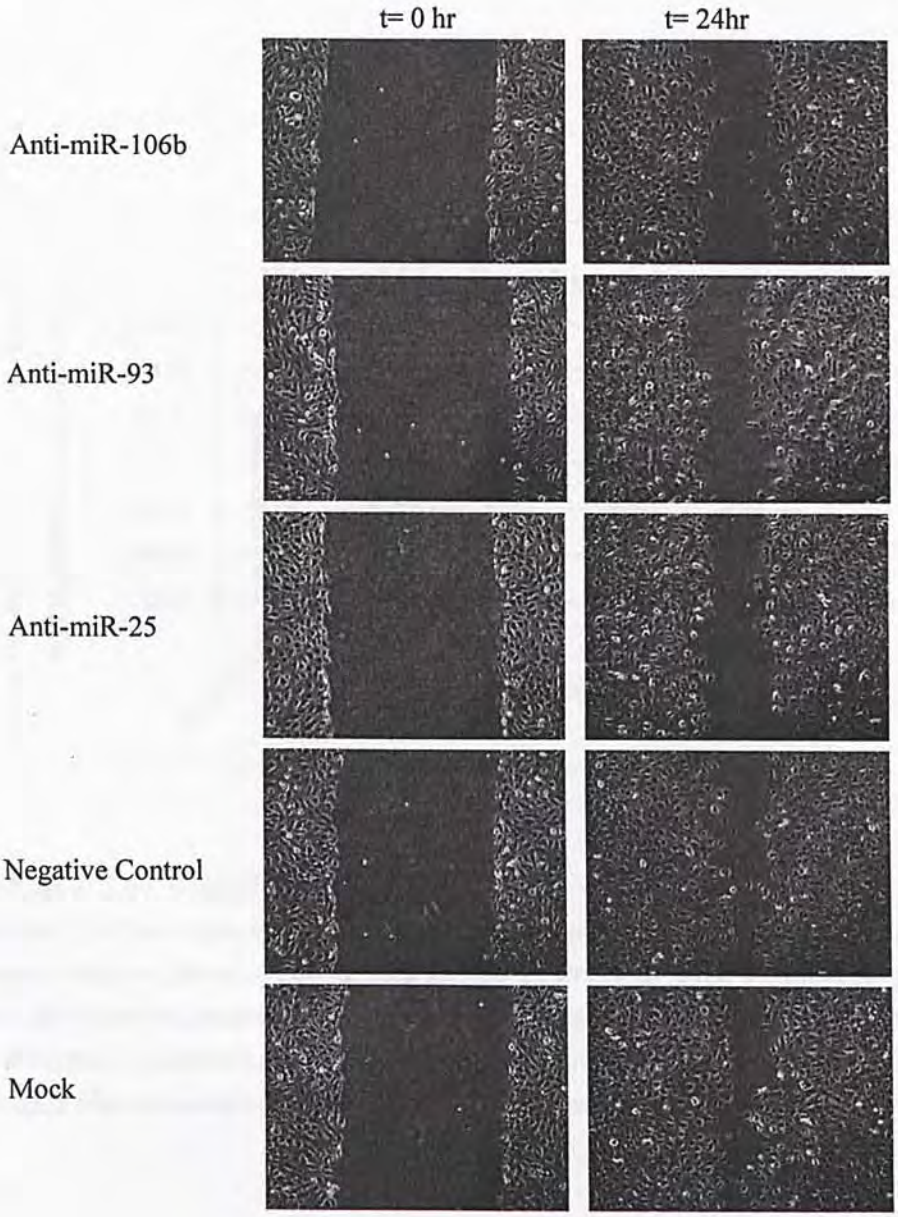
t= 0 hr
t= 24hr
Anti-miR-106b
Anti-miR-93
Anti-miR-25
Negative Control
Mock

B

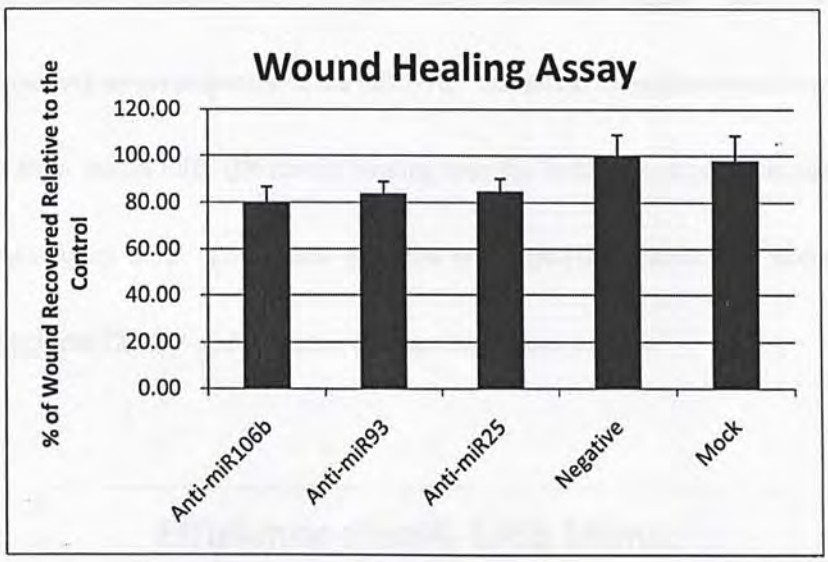

Figure 5.6A & 5.6B Wound healing assays.

Figure 5.6A, the monolayer was scratched with sterile pipette tips, followed by washing to remove cellular debris. Cell migration was observed at 24hr by microscopy. Figure 5.6B shows the relative percentage of wound recovered by cells after treatment with different microRNA inhibitors (miR-106b/miR-93/miR-25) ±SD.. The percentages were calculated from an average of triplicates for each treatment.

5.3.6 Efficiency of Over-expression Using miR-106b Mimic

The efficiency of over-expressing miR-106b was examined using dual luciferase reporter assay. Over-expression of miR-106b in DAOY cells was achieved by transfection of synthetic mature miR-106b (miR-106b mimic). The miR-106b mimic was co-transfected along with the luciferase expression vector cloned with the complementary target sequence of the miRNA. Inhibition of luciferase activity (~97%) resulted from excess miR-106 mimic binding onto the luciferase expression vector was observed (Figure 5.7). These data suggests that miR-106b mimic was successfully transfected into DAOY and mediates its over-expression effects.

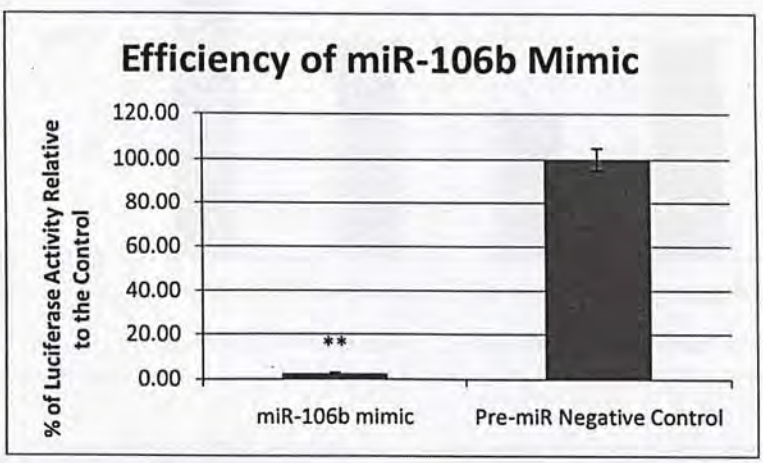

Figure 5.7 Efficiency of over-expression of miR-106b mimic on cell growth.
The suppression of the luciferase activity of the pMIR-reporter cloned with the complementary sequence of miR-106b was used to examine the efficiency of over-expressing miR-106b mimic in DAOY cells. Measurements were taken as an average of triplicates ±SD. Asterisk indicates Student *t*-test with $p<0.00$.

5.3.7 Effects of miR-106b on Cell Growth

The effect of over-expressing miR-106b on the cell growth of DAOY was examined using the MTT assay. By over-expressing miR-106b using the miRNA mimic, cell growth was significantly enhanced. The enhanced growth observed when over-expressing miR-106b is consistent with the decrease in growth when miR-106b was inhibited (Figure 5.8).

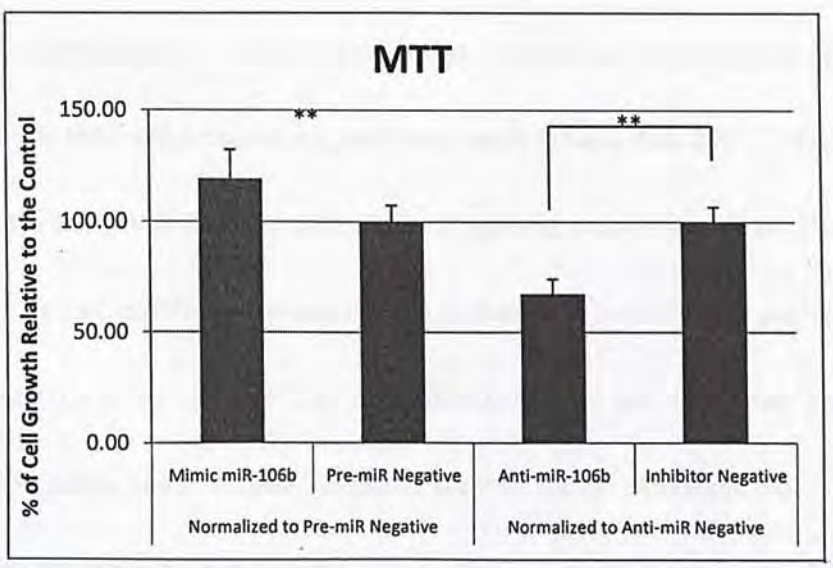

Figure 5.8 Effects of miR-106b inhibition or over-expression on cell growth. Measurements of the MTT assay were taken at Day 4. The relative cell growth for each treatment was compared to the average of their respective negative controls ±SD. All assays were performed in 8 replicates. Asterisks indicate $p<0.00$.

5.4 Discussion

Shifting our gears from the exquisite identification of specific targets involved in one of the many important cellular pathways, in this chapter we have investigated the effects of the dyregulated expression of the miR-106b-25 cluster on some major functional properties in MB cell lines in hope of bringing a broader view on the roles of this cluster of microRNA in MB. As demonstrated in chapter 3, the miR-106b-25 cluster was found to be abberrantly expressed in primary MB, and have confirmed in various MB cell lines as well. Altered expressions of this cluster of microRNA have also been demonstrated in other human cancers including hepatocellular carcinomas, lymphocytic leukemia, lung cancers, and breast cancers (Calin et al. 2002; Takamizawa et al. 2004; Iorio et al. 2005; Li et al. 2009), suggesting crucial roles of this cluster in cancers. In fact, miRNA genes can occur in clusters, and transcribed as polycistronic transcripts (Li et al. 2009). The miR-106b-25 cluster has two other paralogs, miR-17-92 cluster and miR-106a-363 cluster (Li et al. 2009). Among microRNAs, the miR-17-92 cluster is the best characterized and is the most potent oncogenic microRNA (Li et al. 2009). Because the miR-106b-25 cluster is the paralog of the miR-17-92, we speculate that they share similar functional roles. One of the very first functional assays tested was the cell growth assay. Upon inhibition of the miR-106b-25 cluster,

decrease in cell growth was observed for ONS-76 and DAOY. More specifically, there was significant decrease in cell growth when ONS-76 cells were treated with anti-miR-106b, and anti-miR-25. On the other hand, significant decrease in cell growth was observed in DAOY cells that were treated with anti-miR-106b. To deduce the causes responsible for the decrease in cell growth observed, cell cycle profile was examined. However, no shift in cell cycle distribution was observed when cells were treated with miRNA inhibitors of the miR-106b-25 cluster. Then we further investigated whether the inhibition of the miR-106b-25 cluster would be able to further decrease cell growth on top of the cisplatin-induced cell death, however, our data indicated the inhibition of miR-106b-25 cluster did not contribute to the sensitivity of cisplatin. We further examined the cell proliferation using the BrdU cell proliferation assay. It was observed that there was a general trend of decrease in cell proliferation. Cell migration assays also revealed that cells have experienced a slower migration rate upon treatment with the miRNA inhibitors. MTT assays rely on the number of metabolically active (growing) cells, the decrease in cell growth observed after treatment with anti-miR-106b inhibitor may be caused by the hampered cell proliferation and/or cytotoxic effects or non-specific necrosis. To investigate whether cells were dying through apoptosis, we could examine the cleavage of poly-ADP ribose polymerase (PARP), a biochemical hallmark of apoptosis. The trend of decrease in

cell proliferation and cell migration observed may be explained by the fact that the effect of inhibiting indivdiual miRNA separately was not enough to deduce a significant effect in the functional aspects. In fact, it was reported in another study that treatment with a mixture of all three miRNA inhibitors of this cluster led to a more significant inhibiton on proliferation in HCC cell lines than treatment with each of the individual miRNA inhibitors (Li et al. 2009). Also, as mentioned in earlier chapters that miRNA within a cluster may work in a cooperative manner, therefore, it may be the reason as to why the changes observed were subtle. To further confirm the effect of miR-106b-25 cluster in cell growth, we performed the MTT assay followed by overexpression of miR-106b in DAOY. The data were as expected demonstrating a reverse phenotype for over-expression of the miR-106b when contrasted to inhibition of the miR-106b. Although the overall effect of miR-106b-25 cluster on certain functional properties demonstrated in this chapter may be subtle, yet shifting one set of miRNA *in vitro* may be compensated by other systems, as the pathogenesis of cancers is consisted of complex overlapping networks of many pathways. It is unlikely that the observed phenotypes of MB are solely caused by one set of abberantly expressed miRNA, and most of the time, they are accumulatives of series of secondary effects (Ivanovska et al. 2008). It is still too early to draw conclusions on the importance of this cluster of miRNA in the functional properties of MB, as there are still other tests yet

to be investigated. It is possible that the miR-106b-25 cluster act as fine-tuning modulators contributing to the tumorigenesis of MB.

CHAPTER 6: CONCLUSION

It was not until Ferretti et al's microRNA profiling in human MB conducted in 2009 that microRNA expression was first thoroughly studied in MB (Ferretti et al. 2009). In the study, miRNA expression pattern distinguished tumours in a more specific manner, correlating tumour molecular features and disease risk stratification (Ferretti et al. 2009). In addition to the miRNA profiling, more emphasis was put on to the identification of target genes that are regulated by the aberrantly-expressed miRNAs. These targets may be used as novel molecular targets for less toxic and patient-tailored therapeutic strategies (Onvani et al. 2010). In this thesis, we have employed both the computational and experimental approach to identify target for the miR-106b-25 cluster. It is interesting that there were no overlaps between the common targets predicted by the computational method and the target genes that were isolated by the experimental strategy. In fact, in a study of over-expression and inhibition of miR-140, none of the gene discovered were predicted by computational approach (Orom and Lund 2010). Together with our observations, it is suggested that there still exist a significant number of false negatives excluded by the computational approach. Nevertheless, both the computational and experimental strategies have led us to the identification of target genes regulated by the miR-106-25 cluster. It is difficult to judge whether one approach is better than the other as more trials are needed

to conduct to find out their efficiencies. Perhaps, the best route is probably a combination of the two. Also, we have demonstrated that dysregulation of the miR-106-25 cluster exert significant effect on cell growth in DAOY. Although the exact causes responsible for the altered cell growth still remain to be elucidated, but our data suggest that the miR-106b-25 cluster is an integrated component of cellular pathways contributing to the tumorigenesis of MB.

REFERENCE

Ambs, S., R. L. Prueitt, et al. (2008). "Genomic profiling of microRNA and messenger RNA reveals deregulated microRNA expression in prostate cancer." Cancer Res **68**(15): 6162-6170.

Andachi, Y. (2008). "A novel biochemical method to identify target genes of individual microRNAs: identification of a new Caenorhabditis elegans let-7 target." RNA **14**(11): 2440-2451.

Ashburner, M., C. A. Ball, et al. (2000). "Gene ontology: tool for the unification of biology. The Gene Ontology Consortium." Nat Genet **25**(1): 25-29.

Beitzinger, M., L. Peters, et al. (2007). "Identification of human microRNA targets from isolated argonaute protein complexes." RNA Biol **4**(2): 76-84.

Bloom, H. J., E. N. Wallace, et al. (1969). "The treatment and prognosis of medulloblastoma in children. A study of 82 verified cases." Am J Roentgenol Radium Ther Nucl Med **105**(1): 43-62.

Calin, G. A. and C. M. Croce (2006). "MicroRNA signatures in human cancers." Nat Rev Cancer **6**(11): 857-866.

Calin, G. A., C. D. Dumitru, et al. (2002). "Frequent deletions and down-regulation of micro- RNA genes miR15 and miR16 at 13q14 in chronic lymphocytic leukemia." Proc Natl Acad Sci U S A **99**(24): 15524-15529.

Choi, W. Y., A. J. Giraldez, et al. (2007). "Target protectors reveal dampening and balancing of Nodal agonist and antagonist by miR-430." Science **318**(5848): 271-274.

Dalmay, T. (2008). "Identification of genes targeted by microRNAs." Biochem Soc Trans **36**(Pt 6): 1194-1196.

Dhall, G. (2009). "Medulloblastoma." J Child Neurol **24**(11): 1418-1430.

Ebert, M. S., J. R. Neilson, et al. (2007). "MicroRNA sponges: competitive inhibitors of small RNAs in mammalian cells." Nat Methods **4**(9): 721-726.

Eis, P. S., W. Tam, et al. (2005). "Accumulation of miR-155 and BIC RNA in human B cell lymphomas." Proc Natl Acad Sci U S A **102**(10): 3627-3632.

Ellison, D. W. (2010). "Childhood medulloblastoma: novel approaches to the classification of a heterogeneous disease." Acta Neuropathol **120**(3): 305-316.

Ferretti, E., E. De Smaele, et al. (2009). "MicroRNA profiling in human medulloblastoma." Int J Cancer **124**(3): 568-577.

Fornari, F., L. Gramantieri, et al. (2008). "MiR-221 controls CDKN1C/p57 and CDKN1B/p27 expression in human hepatocellular carcinoma." Oncogene **27**(43): 5651-5661.

Fouladi, M., A. Gajjar, et al. (1999). "Comparison of CSF cytology and spinal magnetic resonance imaging in the detection of leptomeningeal disease in pediatric medulloblastoma or primitive neuroectodermal tumor." J Clin Oncol **17**(10): 3234-3237.

Garzon, R., M. Garofalo, et al. (2008). "Distinctive microRNA signature of acute myeloid leukemia bearing cytoplasmic mutated nucleophosmin." Proc Natl Acad Sci U S A **105**(10): 3945-3950.

Gilbertson, R. J. (2004). "Medulloblastoma: signalling a change in treatment." Lancet Oncol **5**(4): 209-218.

Grey, F., R. Tirabassi, et al. (2010). "A viral microRNA down-regulates multiple cell cycle genes through mRNA 5'UTRs." PLoS Pathog **6**(6): e1000967.

Halperin, E. C. (1986). "Pediatric radiation oncology." Invest Radiol **21**(5): 429-436.

Hjalmars, U., M. Kulldorff, et al. (1999). "Increased incidence rates but no space-time clustering of childhood astrocytoma in Sweden, 1973-1992: a population-based study of pediatric brain tumors." Cancer **85**(9): 2077-2090.

Huse, J. T. and E. C. Holland (2010). "Targeting brain cancer: advances in the molecular pathology of malignant glioma and medulloblastoma." Nat Rev Cancer **10**(5): 319-331.

Iorio, M. V., M. Ferracin, et al. (2005). "MicroRNA gene expression deregulation in human breast cancer." Cancer Res **65**(16): 7065-7070.

Ivanovska, I., A. S. Ball, et al. (2008). "MicroRNAs in the miR-106b family regulate p21/CDKN1A and promote cell cycle progression." Mol Cell Biol **28**(7): 2167-2174.

Karginov, F. V., C. Conaco, et al. (2007). "A biochemical approach to identifying microRNA targets." Proc Natl Acad Sci U S A **104**(49): 19291-19296.

Kenney, A. M., M. D. Cole, et al. (2003). "Nmyc upregulation by sonic hedgehog signaling promotes proliferation in developing cerebellar granule neuron precursors." Development **130**(1): 15-28.

Kloosterman, W. P. and R. H. Plasterk (2006). "The diverse functions of microRNAs in animal development and disease." Dev Cell **11**(4): 441-450.

Knoepfler, P. S. and A. M. Kenney (2006). "Neural precursor cycling at sonic speed: N-Myc pedals, GSK-3 brakes." Cell Cycle **5**(1): 47-52.

Kool, M., J. Koster, et al. (2008). "Integrated genomics identifies five medulloblastoma subtypes with distinct genetic profiles, pathway signatures and clinicopathological features." PLoS One **3**(8): e3088.

Lee, S. H., H. S. Kang, et al. (2001). "Growth-inhibitory effect of adenovirus-mediated p53 gene transfer on medulloblastoma cell line, Daoy, harboring mutant p53." Childs Nerv Syst **17**(3): 134-138.

Li, Y., W. Tan, et al. (2009). "Role of the miR-106b-25 microRNA cluster in hepatocellular carcinoma." Cancer Sci **100**(7): 1234-1242.

Lim, L. P., N. C. Lau, et al. (2005). "Microarray analysis shows that some microRNAs downregulate large numbers of target mRNAs." Nature **433**(7027): 769-773.

Lu, J., G. Getz, et al. (2005). "MicroRNA expression profiles classify human cancers." Nature **435**(7043): 834-838.

Marino, S. (2005). "Medulloblastoma: developmental mechanisms out of control." Trends Mol Med **11**(1): 17-22.

Murakami, Y., T. Yasuda, et al. (2006). "Comprehensive analysis of microRNA expression patterns in hepatocellular carcinoma and non-tumorous tissues." Oncogene **25**(17): 2537-2545.

Nakamoto, M., P. Jin, et al. (2005). "Physiological identification of human transcripts translationally regulated by a specific microRNA." Hum Mol Genet **14**(24): 3813-3821.

Nelson, P. T., A. G. Hatzigeorgiou, et al. (2004). "miRNP:mRNA association in polyribosomes in a human neuronal cell line." RNA **10**(3): 387-394.

Northcott, P. A., A. Korshunov, et al. (2010). "Medulloblastoma Comprises Four Distinct Molecular Variants." J Clin Oncol.

Olive, V., I. Jiang, et al. (2010). "mir-17-92, a cluster of miRNAs in the midst of the cancer network." Int J Biochem Cell Biol **42**(8): 1348-1354.

Onvani, S., A. B. Etame, et al. (2010). "Genetics of medulloblastoma: clues for novel therapies." Expert Rev Neurother **10**(5): 811-823.

Orom, U. A. and A. H. Lund (2010). "Experimental identification of microRNA targets." Gene **451**(1-2): 1-5.

Petrocca, F., A. Vecchione, et al. (2008). "Emerging role of miR-106b-25/miR-17-92 clusters in the control of transforming growth factor beta signaling." Cancer Res **68**(20): 8191-8194.

Petrocca, F., R. Visone, et al. (2008). "E2F1-regulated microRNAs impair TGFbeta-dependent cell-cycle arrest and apoptosis in gastric cancer." Cancer Cell **13**(3): 272-286.

Pfister, S. M., A. Korshunov, et al. (2010). "Molecular diagnostics of CNS embryonal tumors." Acta Neuropathol **120**(5): 553-566.

Pierson, J., B. Hostager, et al. (2008). "Regulation of cyclin dependent kinase 6 by microRNA 124 in medulloblastoma." J Neurooncol **90**(1): 1-7.

Polkinghorn, W. R. and N. J. Tarbell (2007). "Medulloblastoma: tumorigenesis, current clinical paradigm, and efforts to improve risk stratification." Nat Clin Pract Oncol **4**(5): 295-304.

Pomeroy, S. L., P. Tamayo, et al. (2002). "Prediction of central nervous system

embryonal tumour outcome based on gene expression." Nature **415**(6870): 436-442.

Rise, M. L., J. R. Hall, et al. (2010). "Impact of asymptomatic nodavirus carrier state and intraperitoneal viral mimic injection on brain transcript expression in Atlantic cod (Gadus morhua)." Physiol Genomics **42**(2): 266-280.

Sethupathy, P., M. Megraw, et al. (2006). "A guide through present computational approaches for the identification of mammalian microRNA targets." Nat Methods **3**(11): 881-886.

Takamizawa, J., H. Konishi, et al. (2004). "Reduced expression of the let-7 microRNAs in human lung cancers in association with shortened postoperative survival." Cancer Res **64**(11): 3753-3756.

Thompson, M. C., C. Fuller, et al. (2006). "Genomics identifies medulloblastoma subgroups that are enriched for specific genetic alterations." J Clin Oncol **24**(12): 1924-1931.

Turner, J. D., R. Williamson, et al. (2010). "The many roles of microRNAs in brain tumor biology." Neurosurg Focus **28**(1): E3.

Vantaggiato, C., F. Redaelli, et al. (2009). "A novel CLN8 mutation in late-infantile-onset neuronal ceroid lipofuscinosis (LINCL) reveals aspects of CLN8 neurobiological function." Hum Mutat **30**(7): 1104-1116.

Visone, R. and C. M. Croce (2009). "MiRNAs and cancer." Am J Pathol **174**(4): 1131-1138.

Visone, R., L. Russo, et al. (2007). "MicroRNAs (miR)-221 and miR-222, both overexpressed in human thyroid papillary carcinomas, regulate p27Kip1 protein levels and cell cycle." Endocr Relat Cancer **14**(3): 791-798.

Volinia, S., G. A. Calin, et al. (2006). "A microRNA expression signature of human solid tumors defines cancer gene targets." Proc Natl Acad Sci U S A **103**(7): 2257-2261.

Watanabe, Y., M. Tomita, et al. (2007). "Computational methods for microRNA target prediction." Methods Enzymol **427**: 65-86.

Wisniewski, K. E., N. Zhong, et al. (2001). "Pheno/genotypic correlations of neuronal ceroid lipofuscinoses." Neurology **57**(4): 576-581.

Yoon, S. and G. De Micheli (2006). "Computational identification of microRNAs and their targets." Birth Defects Res C Embryo Today **78**(2): 118-128.